Sediment Movement in Storm Sewer Systems

by

Yangbo Tang

A thesis submitted in partial fulfillment of the requirements for the degree of

Doctor of Philosophy

in

Water Resources Engineering

Civil and Environmental Engineering

University of Alberta

Abstract

Sediment in storm sewers attracts increasing attentions in recent years due to two major issues including the sewer blockage and the environmental contamination. Pollutants attached to fine sediment surface may adversely affect aquatic life and natural water bodies. Excessive sediment deposition can increase the possibility of urban flooding during storm events. Implement applications of sediment source control, deposition growth prediction, and sewer sediment erosion could help to reduce the severity level of above problems.

A review about sediment in storm sewers was made to identify knowledge gaps about the sediment source control, the deposition growth prediction, and the sewer sediment erosion. Specifically, the review summarized characteristics of storm sewer sediment, studies about sediment removal efficiency in storm sewer inlets, and sediment movement in storm sewers including erosion, transport and deposition processes. In general, knowledge gaps were identified as following: (1) a general prediction method on sediment removal efficiency in storm sewer inlets; (2) the deposition growth in submerged sewer pipes; and (3) the erosion process on storm sewer deposition in the presence of cohesive materials. In this research, one analytical technique, one field investigation and two sets of experimental studies were conducted to extend the knowledge and to fill above gaps.

For the sake of providing a guidance to control sediment source and predict sediment removal efficiency for different source control devices, an analytical technique was developed based on experimental and field studies. In the analytical technique, a comprehensive summary on sediment removal efficiency in different commercial products was conducted, which presented the need to develop a consistent criterion to evaluate the performance of different

devices. Therefore, a general prediction method on sediment removal efficiency considering scaling effects was developed and it approved to be a consistent criterion for different laboratory and field data. The significance of this generalized prediction method was to be used as a preliminary performance indicator for Oil-Grit Separator units that have not yet been subjected to rigorous laboratory testing.

In order to understand deposition growth processes and predict the deposition height, a laboratory experiment was conducted in a submerged pipe under different experimental conditions (i.e., flow rate, pipe slope, particle size, and sediment loading rate). The general process of deposition growth was obtained, which included two stages (rapid growth stage and equilibrium growth stage). The bed shear stress varied from 1.8 to 8.7 N/m^2 under different conditions in this study, which could carry 0.01 to 0.50 kg/m/s sediment loading. The shields diagram and bed load transport equations were proved valid in submerged pipes. A general prediction method on equilibrium height was developed, which could be applied practically in the deposition prediction.

As for erosion processes, a laboratory experiment and a field investigation were implemented to understand erosion patterns, erosion rates, cohesive deposition characteristics, and real deposition characteristics. Deposition erosion patterns were classified as four typical scenarios including: (1) ripple surface deposition, (2) dune surface deposition, (3) flat surface deposition, and (4) rugged surface deposition. Methods to calculate the bed shear stress, the critical shear stress, and the erosion rate were developed and compared to previous studies. The cohesive deposition had more resistance to erosion compared to the non-cohesive deposition, since the critical shear stress was much higher. Real sediment characteristics and the deposition profile were obtained through a field sampling program. Field data validated

the method regarding the calculation on bed shear stress and critical shear stress, which proved its feasibility in practical uses.

Preface

The thesis is an original work by Yangbo Tang and under the supervision from Dr. David Z. Zhu at the University of Alberta. All the published, submitted and to be submitted research works were compiled by myself, my supervisor, collaborators and co-authors.

Chapter 1 is a general introduction about research background, objectives and the scope of this study.

Chapter 2 contains the literature review focusing on sediment movement in storm sewer systems.

Chapter 3 of this thesis was published as Yangbo Tang, David Z. Zhu, and Bert van Duin, "Note on sediment removal efficiency in oil–grit separators" in the journal Water Science and Technology.

Chapter 4 was submitted as Yangbo Tang, David Z. Zhu, N. Rajaratnam, and Bert van Duin in a manuscript "Experimental study of sediment depositions in a submerged storm sewer pipe" to the Journal of Environmental Engineering.

Chapter 5 is currently being prepared as a journal manuscript.

Chapter 6 contains conclusions of this thesis and recommendations for the future research on sediment movement in storm sewer systems.

I was responsible for experimental design, data collection & analysis as well as manuscript composition. Dr. David Z. Zhu was the supervisory author and was involved with concept formation and manuscript composition. Bert van Duin contributed to manuscript edits for

Chapter 3, 4, 5 and assisted with the experimental design for Chapter 4 and 5. Dr. N. Rajaratnam contributed to experimental design and manuscript edits for Chapter 4.

The author also contributed a conference publication:

Tang, Y., Zhu, D. Z., Rajaratnam, N., and van Duin, B. (2017). Experimental study of sediment movement in a submerged pipe. Proceedings of the 14th International Conference on Urban Drainage, 11-15 September 2017, Prague, Czech Republic.

To:

My parents Mr. Keqiang Tang, Mrs. Biyun Yang

And my grandfather

Thanks for your unconditional supports

Acknowledgements

To the beginning, I would like to express my sincere gratitude to my supervisor Dr. David Z. Zhu for his encouragement, support, and guidance. His thoughtful insight and scientific enthusiasm change my understanding to research, which I believe it can be my treasure for my future career and life.

Secondly, I would like to thank Dr. Nallamuthu Rajaratnam. His patience and encouragement support me to understand the difficulties in sediment transport theories. During daily life, he communicated and inspired me to stay optimistic.

Moreover, I would also like to thank Bert Van Duin from the City of Calgary for his collaborative contributions in the experiment design and the paper revision. I wish to thank Perry Fedun who helped to build all experimental setups in the hydraulic lab and helped to solve any issue during experimental tests.

I would also like to acknowledge the funding from China Scholarship Council (CSC) and Department of Civil and Environmental Engineering.

Finally, I would like to express my gratitude to my family and close friends for their support and encouragement during the period of my Ph.D. study.

Table of Contents

List of Tables

List of Figures

List of Symbols

Symbol	Definition
A	Flow area
A_{OGS}	Horizontal flow area of OGS
a, b and c	Coefficients
C	Sediment concentration
$C_{H\text{-}W}$	Hazen Williams coefficient
C_v	Volumetric sediment concentration
C_1 and C_2	Coefficients
D	Pipe diameter
D_M	Modified pipe diameter
D^*	Dimensionless particle size
D_{out}	Outlet pipe diameter
d_{10}	Grain diameter at 10% passing
d_{50}	Grain diameter at 50% passing

d_{60}	Grain diameter at 60% passing
e	Wall relative roughness
E	Erosion rate
f_b	Friction factor of sediment bed
f_c	Composite friction factor
f_w	Friction factor of pipe wall
Fr	Froude number
g	Gravitational acceleration
H	Deposition height
h	Depth of water
Ha	Hazen number
HRF	New scaling parameter
I	Energy slope
L	Length of deposition
l	Depth of water in catch basins
P	Pressure

P_b	Wetted perimeter of sediment bed
P_w	Wetted perimeter of pipe wall
$Pé$	Péclet number
Q	Flow rate
Q_s	Average transport rate
q_s	Sediment transport rate per unit width
R	Hydraulic radius
R_b	Bed hydraulic radius
R_c	Composite hydraulic radius
Re	Reynolds number
Re_p	Particle Reynolds number
R_w	Hydraulic radius related to wall
S	Pipe slope or slope of hydraulic grade line
s	Relative density
T	Hydraulic residence time
T^*	Dimensionless bed shear parameter

u^*	Shear velocity
V	Flow velocity
v	Measured flow velocity
V_0	Nominal velocity
V_c	Critical flow velocity
V_m	Minimum flow velocity for controlling deposition height
V_p	Particle velocity
$V_M=Q/A_{OGS}$	Averaged vertical flow velocity
V_s	Sediment settling velocity
W	Average of initial deposition width and equilibrium deposition width
z	Height above deposition
z_0	Sediment roughness height
α	Angle
η	Removal efficiency

η^*	Rouse number
K	Von Karman's constant
θ_b	Dimensionless bed shear stress
θ_c	Dimensionless bed shear stress corresponding to critical shear stress
ρ	Water density
ρ_s	Sediment density
τ_b	Bed shear stress
τ_c	Critical shear stress
$\tau_c{}^c$	Critical shear stress in the presence of the silt-clay content
τ_w	Wall shear stress
ν	Kinematic viscosity
ϕ	Dimensionless transport parameter
κ	von Karman constant
λ	Particle transport distance

Chapter 1. Introduction

1.1. Background

Storm sewer sediment comes from various sources: the atmosphere, wash-off from catchment surface, sewer pipe deteriorations and construction sites (Ashley and Crabtree, 1992). The practice of winter de-icing sand for road safety can also add a significant amount of sediment in storm sewers. In Edmonton, approximate 50,000 tons of winter de-icing sand enters storm sewer systems every year (The City of Edmonton, 2007). Sediment in storm sewers can settle and form bed deposition, which reduces flow area, cause partial pipe blockage and even lead to surcharged flows and urban flooding (Butler and Davies, 2011). On some occasions, more than 50% of the pipe diameter was found to be filled with sediment (Figure 1-1, The City of Calgary, 2011). The reduction in the level of service is unacceptable, and the costs of pipe cleansing are substantial. In addition, the flow in storm sewers containing sediment discharges into natural water bodies and causes environmental issues. In 2005, for instance, a water quality study found that 90% of sediment that had entered the Bow River, Calgary, Alberta, was from storm sewer system (The City of Calgary, 2011). High levels of sediment concentration contribute to higher turbidity, which limits sunlight penetration thereby prohibiting the growth of aquatic plants (Aryal and Lee, 2009). The sedimentation also can clog fish spawning grounds and reduce the conveyance capability of streams or rivers receiving water from storm sewers. The province of Alberta stipulated that 85% of total suspended solids in storm water should be removed before discharging into a receiving stream or river, through various management systems (Alberta Environment, 1995). In an effort to minimize the above problems caused by storm sewer sediment, many methods have been adopted, e.g. building Best Management Practices (BMPs), optimizing

storm sewer designs, predicting & removing pipe blockage, and implementing flush devices. All methods are related to sediment source control, deposition growth, and sewer sediment erosion.

For the sediment source control, previous studies focused on sediment capture efficiency in catch basins. Studies started from 1977 and continued for decades. Various studies about sediment capture in catch basins were conducted through laboratory studies, field tests and numerical models. Focuses of experimental studies were developing predictive equations on capture efficiency (Lager *et al*., 1977; Wilson *et al*., 2009; Howard *et al*., 2012; Tang *et al*., 2016). Field studies mainly analyzed the performance of existing sediment capture devices (Aronson, 1983; Butler and Karunaratne, 1995). Numerical models were recently used to obtain detailed flow field and test structural revisions (Yang *et al*., 2018). However, catch basins capture relatively large sediment and only have limited capture capacity for fine sediment related to environmental problems. Oil – Grit Separators (OGS) were implemented to storm sewer systems to further remove sediment. Moreover, the application of lager OGSs can be a future trend due to rapid urban development. Thus, scaling effect is of interest, which provides a novel insight into larger OGS applications.

Regarding the deposition growth, previous studies were mainly developed from combined or sanitary sewers (Ab Ghani, 1993). Some field studies recorded deposition profiles in combined sewers (Ashley and Crabtree, 1992; Laplace *et al*., 1992; Bertrand-Krajewski *et al*., 2006). Butler and Davies (2011) summarized the general processes of deposition build-up in combined sewers. Lange and Wichern (2013) produced the sedimentation dynamics in combined sewers. However, the investigation on deposition growth in storm sewers is limited. Understanding deposition growth helps to predict blockage locations, optimize sewer

designs, reduce deposition growth and regulate sewer maintenance activities thus keeping sewer capacity at a good level. In addition, submerged storm sewer outlets were commonly applied in Canada in order to get rid of sewer odor and ice blockage problems (Figure 1-2). Receiving water bodies have a permanently higher water level than the crown of the outlet pipes. In submerged pipes, deposition grew when the flow velocity decreased under dry weather or minor rainfall conditions. Consequently, significant amounts of sediment deposition were found in submerged sewers. Hence, sediment movement and deposition growth in submerged pipes are worth studying prior to any modification of submerged pipe configurations to avoid deposition problems. Moreover, commonly used bed load equations were developed from partially full pipes and were not examined under full pipe flow conditions (May, 1989; Perrusquía and Nalluri, 1995).

For the deposition erosion, flushing devices were applied in storm sewers to erode deposition and transport them downstream, which helped to keep sewer capacity (Pisano *et al*., 2003; Fan, 2004; Campisano *et al*., 2004). From the literature, there are three main categories of flushing devices including automated flushing gate, vacuum flushing system and dosing siphon (Dettmar *et al*., 2002; Dettmar and Staufer, 2005a). The flushing process has two stages: the beginning one is with highly unsteady turbulent wave and the following stage is the one with long-term steady flow. Understanding erosion processes under steady flow could help to regulate sewer maintenance activities.

There are different sediment components including clay, silt, sand, and gravel in storm sewers (Figure 1-3). When the clay content is over 5%, the mixture of sand and clay can be cohesive, which is hard to be flushed away and may form permanent deposition thus further decreasing sewer capacity (Huygens and Tito, 1994; Jain and Kothyari, 2009). Due to

construction activities, clay becomes an important source of storm sewer deposition in some Canadian communities (Figure 1-4). It is important to study the erosion processes on different types of deposition in storm sewers, which could be practically useful when designing or optimizing storm sewers and flushing devices.

In general, knowledge gaps were identified as following: (1) a general prediction method on sediment removal efficiency in storm sewer inlets; (2) the deposition growth in submerged sewer pipes; and (3) the erosion process on storm sewer deposition in the presence of cohesive materials.

1.2. Research objectivities

Based on the importance of this study and the knowledge gaps, the objectivities of this study are as follows:

(1) To develop a general prediction method for sediment removal efficiency in OGSs and identify the scaling effects,

(2) To understand the mechanism of deposition growth, develop a bed load model in full pipe flow conditions, and produce a prediction method on deposition height,

(3) To investigate the erosion processes on deposition in storm sewers and obtain deposition characteristics in real storm sewers.

The research route is developed from the above objectives (see Figure 1-5).

1.3. Thesis outline

This thesis improved the understanding of sediment movement in storm sewer systems. The thesis was written in paper format and could be divided into the following chapters.

Chapter 1 introduced the general background of sediment in storm sewer systems. This chapter also defined the objectives and scope of this research.

Chapter 2 presented the literature review on sediment characteristics, erosion, transport and deposition. Information about sediment removal efficiency in OGS was also introduced. The knowledge gaps were presented.

Chapter 3 was about an analytical technique on sediment removal efficiency among different OGSs. A comprehensive summary about sediment removal efficiency in different OGSs was presented. A general prediction method was developed which can be used to calibrate laboratory and field data. The scale effects were tested based on different dimensionless parameters.

Chapter 4 showed sediment deposition growth in a submerged pipe. The deposition process was described as two stages (rapid growth stage and equilibrium growth stage). The determination method for bed shear stress in submerged pipes was developed. The bed load transport was studied and compared to previous studies. The prediction method on deposition height was produced.

Chapter 5 showed laboratory study about erosion on depositions in storm sewers as well as a field investigation about deposition in a real storm trunk sewer. The erosion pattern was classified as four scenarios (ripple surface deposition, dune surface deposition, flat surface

deposition, and rugged surface deposition). The prediction method on erosion rate was developed. Real sediment characteristics and deposition profile were obtained.

Chapter 6 provided general conclusions of this thesis and recommendations for future studies.

Figure 1-1. Significant amount of deposition in a storm trunk sewer

Figure 1-2. Submerged storm sewer outlet (going to a drained storm water pond)

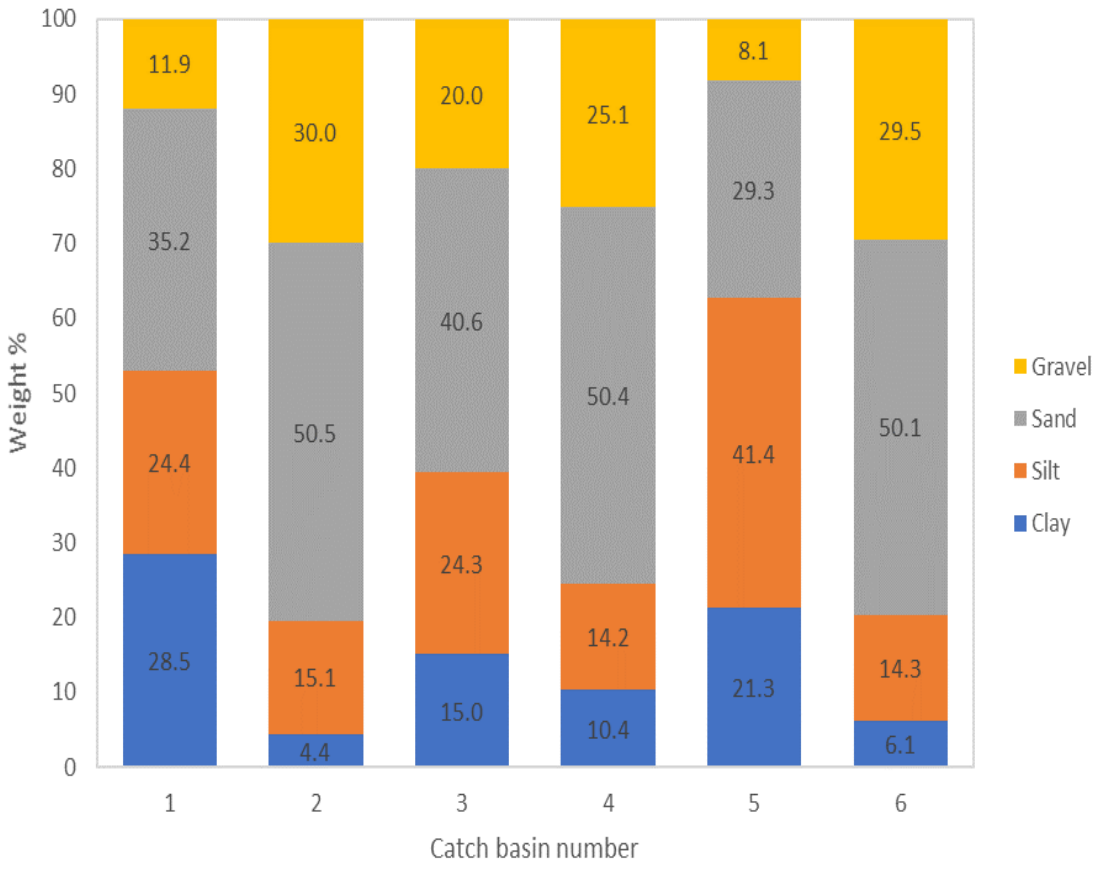

Figure 1-3. Sediment components in catch basins, Calgary, Canada

(a) Sediment sample from a catch basin

(b) Sediment samples from storm sewers

Figure 1-4. Sediment samples

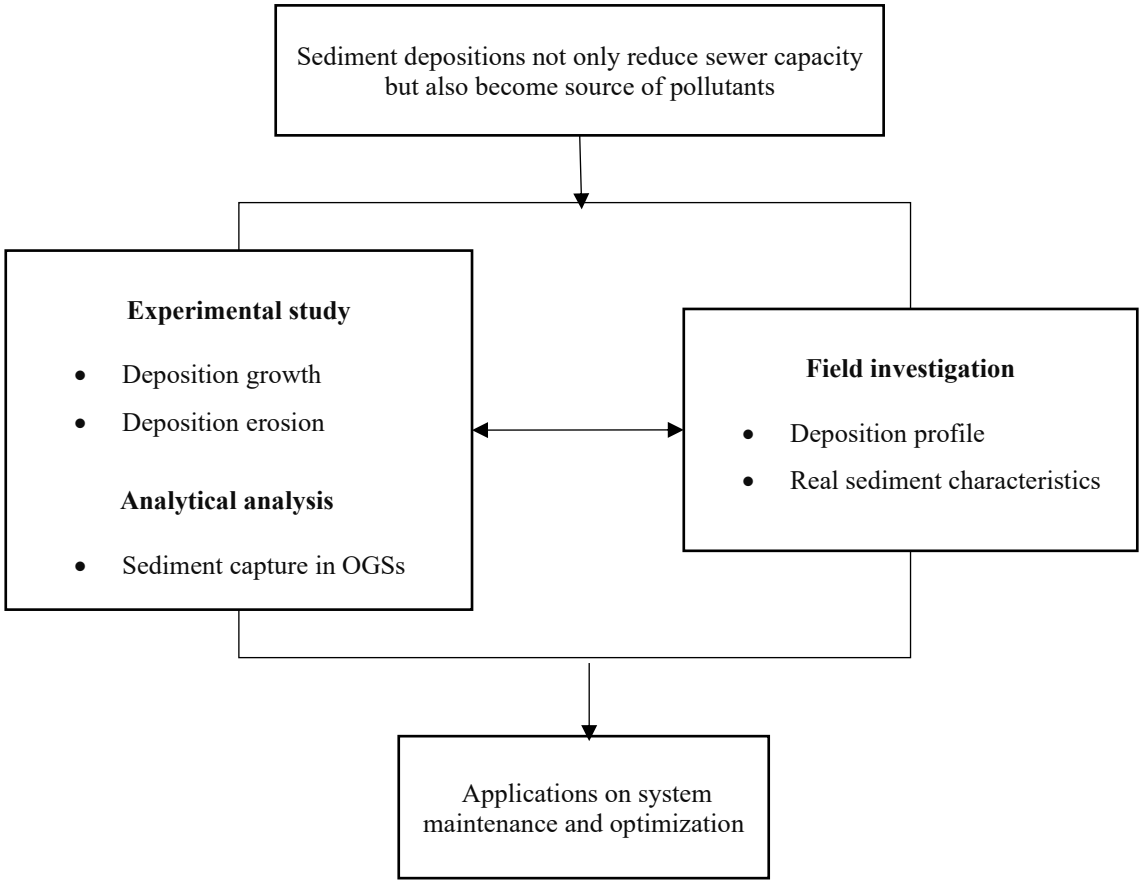

Figure 1-5. Flow chart of research route

Chapter 2. Literature Review

2.1. Sediment characteristics

2.1.1. Sources of sediment

Main sources of sediment in urban storm drainage had been identified as particles from the atmosphere, wash-off from catchment surface, sewer pipe deteriorations and construction sites (Tränckner *et al*., 2008). In addition, winter de-icing sand can be an important source in Canada (The City of Edmonton, 2007). Table 2-1 summarizes the sources of sewer sediment (Ashley and Hvitved-Jacobsen, 2002; Fan, 2004; Butler and Davies, 2011).

2.1.2. Classifications on sediment

Crabtree (1989) classified combined sewer sediment into five categories including:

- Type A: coarse, loose, granular, predominantly mineral, material on the inverts of pipes;
- Type B: a solid mass concreted by coarse mineral, fat, bitumen, etc.;
- Type C: mobile fine sediment always associated with first flush and pollutants;
- Type D: organic wall slimes including biofilms;
- Type E: deposited fine grain and organic sediment.

In storm sewers, sediment was classified according to particle sizes due to its non-cohesive feature. There are two classical standards for grain size classifications for non-cohesive sediment including the American Society for Testing and Materials method (2012) and the International Organization for Standardization method (2002). Roesner and Kidner (2007)

developed a more specific classification for storm sewer sediment. Above three classifications are summarized in Table 2-2. Storm sewer solids vary in size from gravel to clay. The variation in particle size is due to catchment conditions, vehicular activities, surface runoff characteristics and the application of de-icing sanding materials. Investigations about size distributions regarding storm sewer sediment are limited.

2.1.3. Particle size investigations in storm sewer systems

The knowledge of particle size distribution (or median size d_{50}) enables city planner to have better storm management strategies (Butler and Davies, 2011). In Madison, mixed-use land and parking lot areas had the lowest median size d_{50} (42 and 54 μm, respectively), followed street study area (d_{50}=70 μm). Both arterial street and institutional area had similar d_{50} of 95 μm (Selbig and Bannerman, 2011). Goncalves and van Seters (2012) analyzed particle size distributions in Toronto. Two sets of data were obtained in the same city and particle size distributions were different due to site-specific features. Both sets were fine materials (50% of particles were finer than 14 μm in Lawrence at Weston and 90% of particles were finer than 55 μm in Black creek). Twenty-five locations were monitored in Netherlandish storm sewers to determine the particle size distribution (Boogaard *et al*., 2014). According to the research, half of the mass consisted of particles smaller than 70 μm, which meant that particles were predominantly fine (60% of the particles were finer than 100 μm).

Fine sediment (silt or clay) can be easily introduced into storm sewer systems from construction sites by small rainfall events. Fine sediment can coagulate during dry weather, which probably forms a permanent deposition and decreases the sewer capacity. From the literature, when the clay content is over 5%, the mixture of sand and clay can be cohesive

(Huygens and Tito, 1994). Unlike non-cohesive sediment whose main resistance force is submerged weight, cohesive sediment has net attractive inter-particle surface forces, frictional interlocking of grain aggregates, and electrochemical forces (Jain and Kothyari, 2009). Studies about fine sediment characteristics in storm sewers are limited.

2.2. Sediment capture efficiency in storm sewer inlets

Storm sewer inlets have various designs, while in Canada, catch basins and Oil - Grit Separators (OGSs) are commonly used as storm sewer inlets. Catch basins receive surface runoff and can potentially retain sediment, grit and detritus before these are flushed into the storm sewers (Aronson *et al*., 1983). Lager *et al*., (1977) conducted the earliest research about the sediment capture efficiency of catch basins. With respect to the sediment capture efficiency, it was found that catch basins can remove medium to coarse sands very efficiently over a wide range of flow rates (i.e., the capture efficiency can reach 65 to 90%). Aronson *et al*. (1983) collected field data to evaluate the performance of catch basins in controlling pollution. More than 40 sites were investigated showing 60 to 97% capture efficiencies for total suspended solids. Butler and Karunaratne (1995) studied solids trap efficiency in a roadside gully pot and reported capture efficiencies ranging from 15% to 95%. Wilson *et al*. (2009) introduced the use of the Péclet number from reservoirs to storm water treatment facilities. This work provided a fundamental approach to predict the sediment capture efficiency. Tang *et al*. (2016) provided an equation for predicting sediment capture efficiency in catch basins for different particle sizes and flow rates. The proposed equation appears to work well for the data obtained from different studies:

$$\eta = [1 + \frac{1}{(9.23Pe\frac{D_{out}}{l})^{0.69}}]^{-1/0.69} \quad \text{(Equation 2-1)}$$

where, η is the sediment capture efficiency, Pe is the Péclet number, D_{out} is the outlet pipe diameter, l is the depth of water in catch basins.

As can be seen from the above information, studies about catch basins are relatively completed. The capture capacity of catch basins mainly focused on coarse sediment but had limited ability to remove fine sediment. Thus, this research focuses on removal efficiency in OGSs, which not only remove coarse sand but also deposit fine sediment. OGSs are designed to remove oil and grit from storm water runoff that can pose negative impacts on receiving water bodies. Note some OGSs were also installed before the storm sewer outlets. There are three typical OGSs including (1) gravity action type, (2) swirl action type, and (3) screening action type (Malesevic, *et al*., 2014). Various structures in OGSs can pose different impacts on flow regimes thus influencing sediment removal efficiency. There were many separate studies for specific devices. Therefore, introducing a new scaling parameter to summarize not only flow conditions but also sediment removal capacity within various structures can be practically useful.

Cornu *et al*. (2000) examined the removal efficiency of a Downstream Defender unit and found its removal efficiency varied from 70% to 100% at relatively small flow rate decreasing from 25 L/s to 5 L/s (d_{50} of 0.3 mm sediment was used) (see Figure 2-2). In addition, Faram (2000) also tested the removal efficiency of the Downstream Defender unit and created a CFD model to represent the flow regime within the unit. Sturm *et al*. (2007) built a 1:2 scale model to examine the removal efficiency of the Skimpro OGS (gravity action

type). They did several modifications on the device and tested their performance separately (Figure 2-3). CFD has been successfully used in OGSs to simulate hydraulic conditions, however it is difficult to simulate sediment movement (Dufresne *et al*., 2009).

The latest laboratory studies are based on the implementation of the recent Environmental Technology Verification (ETV) Canada protcols (2016, 2017). Performance data for a Downstream Defender Hydro unit (swirl type) (ETV, 2016) as well as a Stormceptor EF4 unit (gravity type) (ETV, 2017) were obtained. The tested flow rates and sediment sizes covered a wide range as per the ETV Canada protocols. They used an identical artificial sediment mixture for all tests.

Numerous field studies have been conducted over the last two decades to obtain removal efficiency data of OGSs under real-world operating conditions. In 2004, two types of OGSs were monitored (i.e., a screening action OGS and a swirl type OGS) in Toronto, Canada (SWAMP, 2004). The sediment in the parking lot runoff contained relatively small sediment with a d_{50} of 20 μm. They found the average removal efficiency of these OGSs to be about 40% to 50%, which was found to be in good agreement with other studies. They suggested that different types of OGSs could be expected to have similar removal capabilities. However, the field data were not accurate as the laboratory data, which presented a need to have a certain method to validate field data prior to field data analyses.

Generally, specific cases of OGSs were studies during recent decades. It is difficult to compare the results from these studies because different experimental approaches and evaluation criteria were used. In addition, a general prediction method on sediment removal

efficiency is not developed. Moreover, the scaling effects were under limited studies especially for special structures in OGSs (e.g. screen or baffle).

2.3. Sediment movement in sewers

After sediment escapes from system inlets (catch basins or OGSs), sediment enters storm sewers. The movement of sediment in storm sewers can be divided into three major categories including erosion, transport and deposition. The following sections contain the literature review on sediment movement in storm sewers.

2.3.1. Erosion

When wet weather flow appears in sewers, existing deposition can be eroded due to large flow rate and high shear stress (Butler and Davies, 2011). Studies of erosion began with alluvial channels using the Shields diagram (Figure 2-4, Ab Ghani, 1993). Two dimensionless parameters were introduced to describe the erosion process (Shields, 1936):

$$\theta_b = \frac{\tau_b}{(s-1)d_{50}\rho g} \quad \text{(Equation 2-2)}$$

$$D^* = d_{50}\sqrt[3]{\frac{(s-1)g}{\nu^2}} \quad \text{(Equation 2-3)}$$

where, θ_b is the dimensionless bed shear stress, τ_b is the bed shear stress, s is the specific density of sand, d_{50} is the median size of particles, ρ is the water density, g is the gravitational acceleration, D^* is the dimension less particle size, ν is the kinematic viscosity.

The dimensionless particle size was commonly used in sediment transport studies which showed the size information of sediment. For certain particle size, sediment could be eroded

by the flow once the dimensionless bed shear stress was above the shields diagram. However, this diagram was developed for alluvial channels and was not examined in sewers. The major differences in sediment movement between open channel flows and pipe flows including: 1) Flow patterns 2) Sediment characteristics; and 3) Effect of armour layer (Butler and Davies, 2011; Wu *et al.*, 2015).

There was a mechanistic model describing the forces on spherical sediment particle at the deposition surface (Yang, 1996). The forces considered the drag force, lift force, submerged weight, and resistance force. At the threshold of erosion, either the lift force is larger than the submerged weight or the drag force is larger than the resistance force (Yang, 1996).

In addition, there were many studies about the threshold of erosion in sewer systems using critical velocity equations. Novak and Nalluri (1975) suggested a fundamental equation for critical velocity:

$$\frac{V_c}{\sqrt{gd_{50}(s\text{-}1)}} a\left(\frac{d_{50}}{R}\right)^b \qquad \text{(Equation 2-4)}$$

where, V_c is the critical mean velocity, R is the hydraulic radius, a and b are coefficients.

There were series of experimental studies adopting the concept of critical velocity but in different test ranges (Ackers, 1984; El-Zaemey, 1991; Ab Ghani, 1993; Safari *et al.*, 2015). They proved the Shields diagram could be used in sewers with limited deposition or under partially full flow conditions. Note that critical shear stress could correspond to the critical velocity, which means the critical shear stress could be obtained through the Shields diagram.

Various researchers had studied erosion rate or pick-up function of sediment particles (Figure 2-5, Van Rijn, 1984). Van Rijn (1984) studied the pick-up process during low flow conditions with a velocity range of 0.5 to 1.5 m/s. The empirical function was:

$$E = 0.00033\rho_s\left((s-1)gd_{50}\right)^{0.5}(D^*)^{0.3}(T^*)^{1.5} \quad \text{(Equation 2-5)}$$

where, E is the pickup rate (kg/m^2/s), ρ_s is the sediment density, T^* is the dimensionless bed shear parameter showing the difference between the bed shear stress and the critical shear stress. As we can see from the above equation, sediment characteristics and the shear stress level determine the pick-up rate. A few studies presented similar equations to describe erosion capacity for different particle sizes (Fernandez-Luque, 1974; Nagakawa and Tsujimoto, 1980). All these studies were conducted in flumes, the erosion processes in storm sewers were not studies yet.

Moreover, in order to maintain good sewer capacity, flushing devices were commonly used to erode deposition in sewers. Flushing devices applied in storm sewers can be generally divide into three categories: automated flushing gate, vacuum flushing system and dosing siphon (Figure 2-6) (Dettmar *et al*., 2002; Dettmar and Staufer, 2005a). Flushing devices usually stores water volumes up to certain level and suddenly releases the stored volumes, in order to obtain sudden increasing flow rates and shear stresses along downstream pipes. The aim is to erode deposited solids in sewers (forming during dry weather) and to transport them towards downstream places with minor deposition problems (Pisano *et al*., 2003; Fan, 2004; Campisano *et al*., 2004). Bertrand-Krajewski *et al.* (2003) mentioned that flushing devices could be necessary in old communities where sewer systems were not appropriately designed and may suffer from bad hydraulic conditions (improperly designed slopes, insufficient

inflow velocities, shallow flow depth, and rough sewer walls). Applying flushing devices is more flexible compared to mechanical cleansing method since some sections are not feasible to cleanse due to complex sewer networks (Bertrand-Krajewski *et al.*, 2006). Note flushing process has two stages: the beginning one is with highly unsteady turbulent wave and the following stage is the one with steady flow rate. This research mainly focuses on the steady stage since the motivation is to quantify erosion rate for different depositions and unsteady waves could be future study topics as an extension.

2.3.2. Transport

Sediment particles may experience continuous exchange between suspended load and bed load in storm sewers determining by different hydraulic conditions. These two transport patterns are introduced in the following sections.

- *Suspended load*

Suspended load sediment is one of important components of sewer solids since it can occupy up to 90% of the total mass of solids transported in combined sewers (Ashley *et al.*, 1994). Dominant particle sizes are about 40 μm (Ashley and Crabtree, 1992). Full suspension occurs when the Rouse number (η^*) is less than three (Ashley and Verbanch, 1996):

$$\eta^* = V_s/\kappa u^* \qquad \text{(Equation 2-6)}$$

where, η^* is the Rouse number, V_s is the particle settling velocity, u^* is the shear velocity, K is the von Karman's constant (around 0.4).

Suspended solids have low settling velocity: 0.6 mm/s for dry weather sewage and 0.2 mm/s for stormwater (Ashley and Verbanch, 1996). Suspended solids concentration profile has a

sharp increase near the sediment bed (Schlutter and Schaarup-Jensen, 1998). Rouse's profile is a traditional way to describe the suspended load profile (Ashley and Verbanck, 1996). Verbanck (2000) developed a two-layer approach, which has a better coincidence in a specific site. Besides profiles, Nalluri *et al.* (1997) introduced three models to describe the suspended load transport by volumetric sediment concentration. Butler and Davies (2011) introduced Macke's equation in no deposition condition and Ackers' equation over sediment bed to describe suspended load. Ebtehaj and Bonakdari (2013) used Artificial Neural Network (ANN) to predict suspended load, which has higher accuracy than those empirical equations. ANN contains a group of interconnected neurons (inputs or variables) and uses them to produce an output. Due to the change of locations or various hydraulic conditions, some sediment can transit from suspended load to bed load (Arthur *et al.*, 1996).

- *Bed load*

Bed load sediment is related to pipe blockage problems since once hydraulic condition turns badly bed load sediment may cease movement and form deposition layer. It is important to understand bed load transport before conducting deposition research. Particles in bed load transport have three different movement patterns including rolling, saltation, and sliding, which depends on sediment characteristics and flow conditions. Lee and Hsu (1994) investigated a continuous sediment saltation process on a rigid boundary and found the particle saltation velocity to be related to bed shear stress and flow velocity:

$$\frac{V_p}{u^*} = a\, D^{*b}\, T^{*c} \qquad \text{(Equation 2-7)}$$

where, V_p is particle traveling velocity, a, b, and c are coefficients.

Many studies were conducted to develop bed load equations and major findings can be divided into two parts: bed load transport over clean pipe and over loose boundary (pipe with small amount of deposition). Once the flow becomes steady and uniform, the sediment supply rate in the upstream is gradually increased until some permanent deposits appear in the pipe. Various studies were conducted to predict the volumetric sediment concentration through testing a wide range of parameters (Table 2-3, Macke, 1982; Mayerle *at al*., 1988; May, 1989; El-Zaemey, 1991; Perrusquia, 1991; Ab Ghani, 1993). Most equations were complicated due to various dimensionless parameters with fitted coefficients. Note that friction factors were important to determine the transport capacity. The most important parameter in bed load transport is bed shear stress, which could be determined through experimental measurement. However, the bed shear stress in the full pipe flow is hard to be obtained experimentally. The direct measurement is based on the vertical velocity profile between 3 times of d_{50} and 1/5 of total water depth (Wilcock, 1996).

A theoretical method about sediment transport capacity was developed based on the method of Graf and Acaroglu (1968). They defined two dimensionless parameters: dimensionless bed shear stress (θ_b) and dimensionless transport parameter (ϕ) to describe sediment transport capacity:

$$\phi = \frac{q_s}{\rho\sqrt{(s-1)g d_{50}^3}} \qquad \text{(Equation 2-8)}$$

$$\phi = a{\theta_b}^b \qquad \text{(Equation 2-9)}$$

where, q_s is the sediment transport rate per unit width (g/m/s).

This method was widely used in predicting sediment transport capacity and there were several prediction equations based on different flow and sediment characteristics (Novak and Nalluri, 1975; Novak and Nalluri, 1984; Ota and Nalluri, 2003; Safari *et al*., 2015). Various bed load transport studies were developed in partially full pipes (May *et al*., 1996; Ackers *et al*., 2001). Note that the area occupied by the transported sediment is assumed negligible. However, different from partially full conditions, there are many submerged storm sewer outlets in Canada in order to prevent ice blockage and odor issues, in which there are huge amounts of depositions. The application of above bed load equations should be examined in full pipe flow conditions in the presence of depositions. Otherwise, a new equation should be developed in full pipe conditions.

2.3.3. Deposition

In the mid 1970's and early 1980's, several experiment studies were firstly carried out to record under what circumstance deposition started to accumulate in sewers (Ab Ghani, 1993). The focus of these studies was to obtain certain design criterion, e.g., self-cleansing sewers.

Simons and Senturk (1977) summarized bed form depositions as different patterns including flat beds, ripples, and dunes. When bed shear stress is small, bed form deposition would keep the flat bed pattern. With the increase of shear stress or sediment transport capacity, bed forms could turn into ripples and dunes. Sand less than 0.7 mm would form ripples. The height of ripples is less than 5 cm and the length is less than 30 cm. Sand larger than 0.7 mm could form sand dunes with relatively large dimensions (Simons and Senturk, 1977).

Fredsoe (1982) used bed shear stress to describe deposition dimensions. Van Rijn's (1984) method assumed that the deposition dimensions are related to bed load transport, which is

related to the theories proposed by Fredsoe (1982). Some flume tests were conducted and results were shown below:

$$\frac{H}{h} = 0.11\left(\frac{d_{50}}{h}\right)^{0.3}(1 - 2.72^{-0.5T^*})(25 - T^*) \quad \text{(Equation 2-10)}$$

$$L = 7.3\,h \quad \text{(Equation 2-11)}$$

where, *H* is the deposition height, h is the water depth in the flume, *L* is the deposition length.

For studies about sediment deposition, the majority of the research had so far focused on sanitary and combined systems. A field study conducted by Laplace *et al*. (1992) showed that the increase of sediment volume had an asymptotic tendency along time in combined sewer system, which meant the slower sediment accumulation was due to the stronger solid transport capacity. For deposit build-up rate, Ashley and Crabtree (1992) showed that, it was possible to predict deposit build-up rate in small sewers for specific sites, whereas estimating the rate in larger sewers was difficult due to changes of hydraulic conditions and site specific sediment characteristics. Butler and Davies (2011) summarized general processes of deposition build-up. Bertrand-Krajewski *et al*. (2006) presented a continuous field experiment during 4 years to monitor deposition accumulation in an egg-shaped combined sewer in Lyon. Deposition depth was found as an important variable to describe deposition profile. In recent years, Lange and Wichern (2013) produced sedimentation dynamics in combined sewer systems (Figure 2-7). However, the research about deposition growth in storm sewer system is limited. In addition, there is no prediction method on sedimentation growth in storm sewers. There were studies about deposition dimensions in flumes, which

could be an important foundation for deposition studies in storm sewers. Moreover, the consolidation effect also plays an important role in sediment deposition (Alvarez-Hernandez, 1990). The erodibility of consolidated deposition decreased with the increase of consolidation duration (Kamphuis and Hall, 1983). According to the literature, fully developed self-weight consolidation for sand and clay mixture can take 10 days (Figure 2-8, Li *et al*., 2013). Studies on consolidated deposition in storm sewers are limited.

Table 2-1. Sediment sources and characteristics

Source	Particle characteristics	Description
Winter de-icing	Particle size range approximately from 0.05 to 20 mm	Sands or grits, around 5,000 tons, enter storm sewer system annually
Catchment surface	Wide size range, primary inorganic	Include grit from road abrasion, particulates from vehicles, and construction materials, etc.
Construction sites	Fine particles < 50 μm and gravels > 2 mm	Form permanent deposition layer
Soil erosion	Typical solids <1 mm	Due to leaks or pipe/manhole/gully failures
Domestic sewage	Up to 50 mm	Organic
Wind-blown from sand/soil/litter	Large organics possible, inorganics <5 mm	Entry via catch basins/inlets, size reduced when discharged into storm sewer

Table 2-2. Classifications for storm sewer sediment

Sediment classification	Size range	Reference
Coarse gravel	19 mm - 75 mm	
Fine gravel	4.75 mm -19 mm	
Coarse sand	2 mm – 4.75 mm	American Society for Testing
Medium sand	0.475 mm -2 mm	and Materials method, 1992
Fine sand	0.075 mm – 0.475 mm	
Clay or silt	< 0.475 mm	
Gravel	> 2 mm	International Organization for Standardization method, 2002
Coarse sand	0.5 mm – 0.5 mm	
Medium sand	0.063 mm – 0.25 mm	
Fine sand	< 0.063 mm	
Mud		
Gross solid	> 5 mm	Roesner and Kidner, 2007
Coarse solid	75 µm – 5 mm	
Fine solid	2 µm - 75 µm	
Dissolved solid	< 2 µm	

Table 2-3. Bed load models

Equation	Condition	Reference	No.
$C_v = \frac{f_w^{0.3} V^5}{30.4(s-1)V_s^{1.5} A}$	Clean pipe	Macke, 1982	2-14
$C_v{}^{0.18} = \frac{0.07V}{\sqrt{g d_{50}(s-1)}} D^{*0.14} (\frac{d_{50}}{R})^{0.56} f_c^{-0.18}$	Clean pipe	Mayerle *et al.*, 1988	2-15
$C_v = 0.0211 \left(\frac{h}{D}\right)^{0.36} (\frac{D^2}{A}) \left(\frac{d_{50}}{R}\right)^{0.6} \left(\frac{V}{g(s-1)D}\right)^{1.5} (1 - \frac{V_c}{V})^4$	Clean pipe	May, 1989	2-16
$C_v{}^{0.165} = \frac{0.52V}{\sqrt{g d_{50}(s-1)}} (\frac{P_b}{h})^{0.4} (\frac{d_{50}}{D})^{0.57} f_b^{-0.1}$	With deposition	El-Zaemey, 1991	2-17
$C_v = 15.3 (\frac{P_b}{D}) \left(\frac{H}{D}\right)^{-0.7} (\frac{D^2}{A}) \left(\frac{h}{D}\right)^{0.19} f_b^{2.6} \left(\frac{d_{50}}{D}\right)^{-0.63} D^{*-0.96} (\frac{V}{g(s-1)D})^{2.1}$	With deposition	Perrusquía, 1991	2-18
$C_v{}^{0.21} = \frac{0.32V}{\sqrt{g d_{50}(s-1)}} D^{*0.09} (\frac{d_{50}}{R})^{0.53} f_c^{0.21}$	Clean pipe	Ab Ghani, 1993	2-19
$C_v{}^{0.16} = 0.85 \frac{V}{\sqrt{g d_{50}(s-1)}} (\frac{P_b}{h})^{0.18} (\frac{d_{50}}{R})^{0.53} f_c^{0.31}$	With deposition	Ab Ghani, 1993	2-20

where C_v is the volumetric sediment concentration, f_w is the pipe wall friction factor, f_c is the composite friction factor, f_b is the bed friction factor, R is the hydraulic radius, A is the flow area, P_b is the deposition width, and D is the pipe diameter.

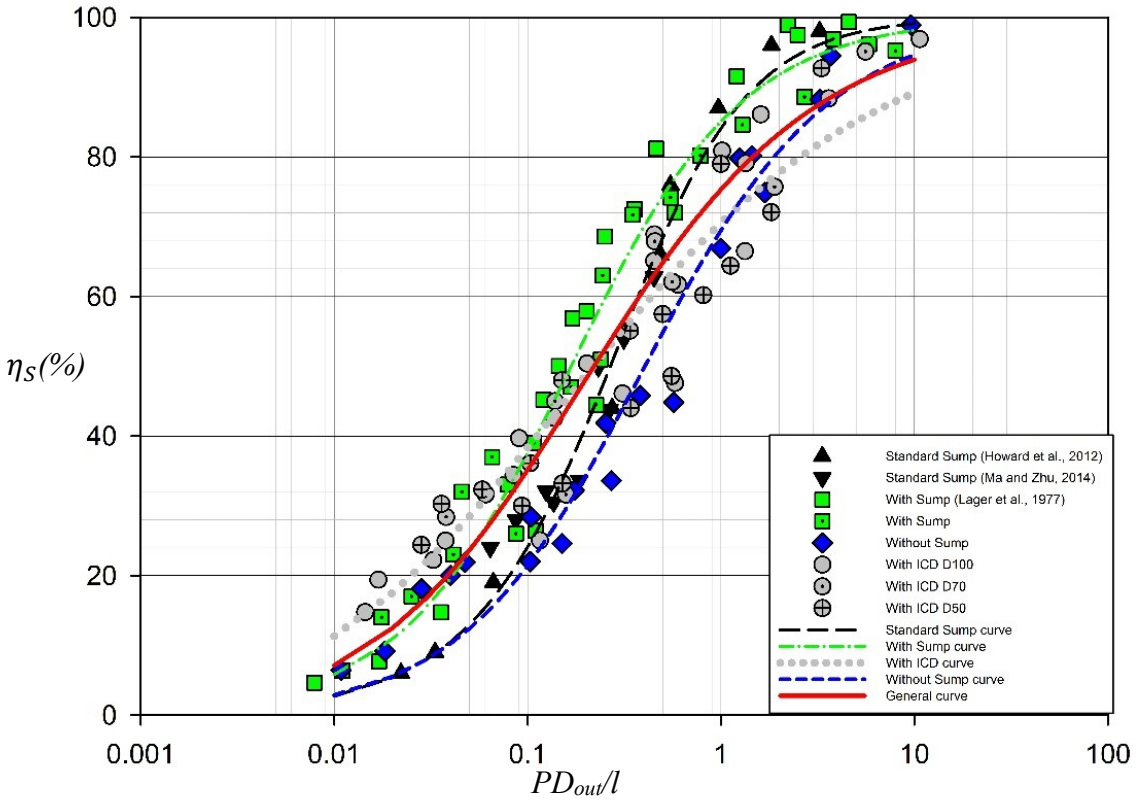

Figure 2-1. Measured and simulated sediment capture efficiency in catch basins (Tang *et al.*, 2016)

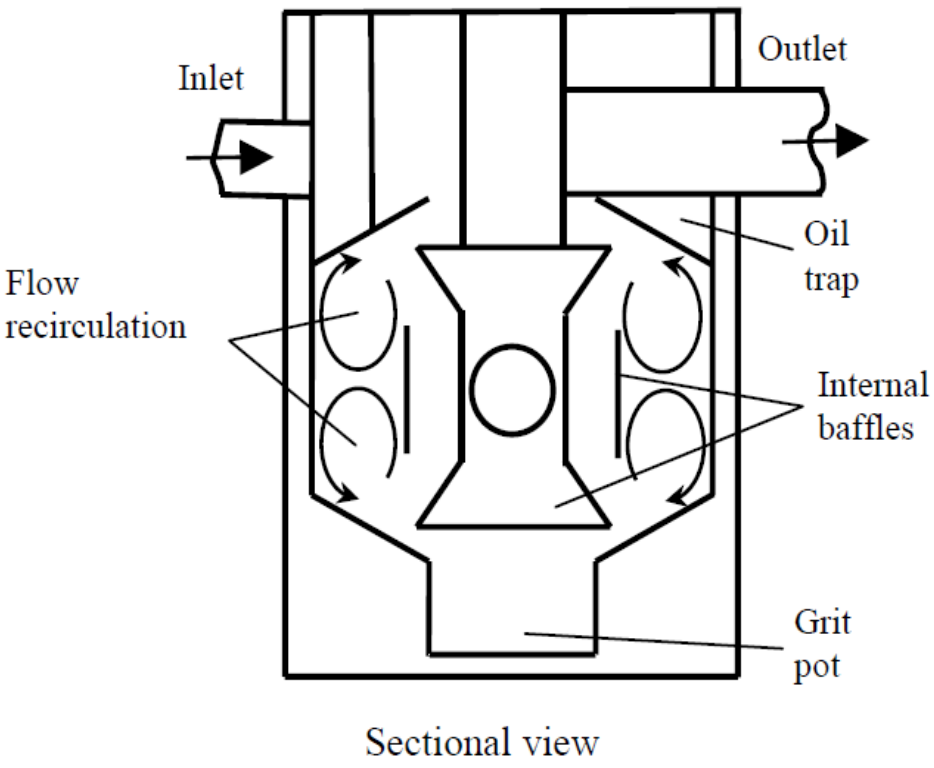

Figure 2-2. Schemetic of Downstream Defender (Cornu *et al*. 2000)

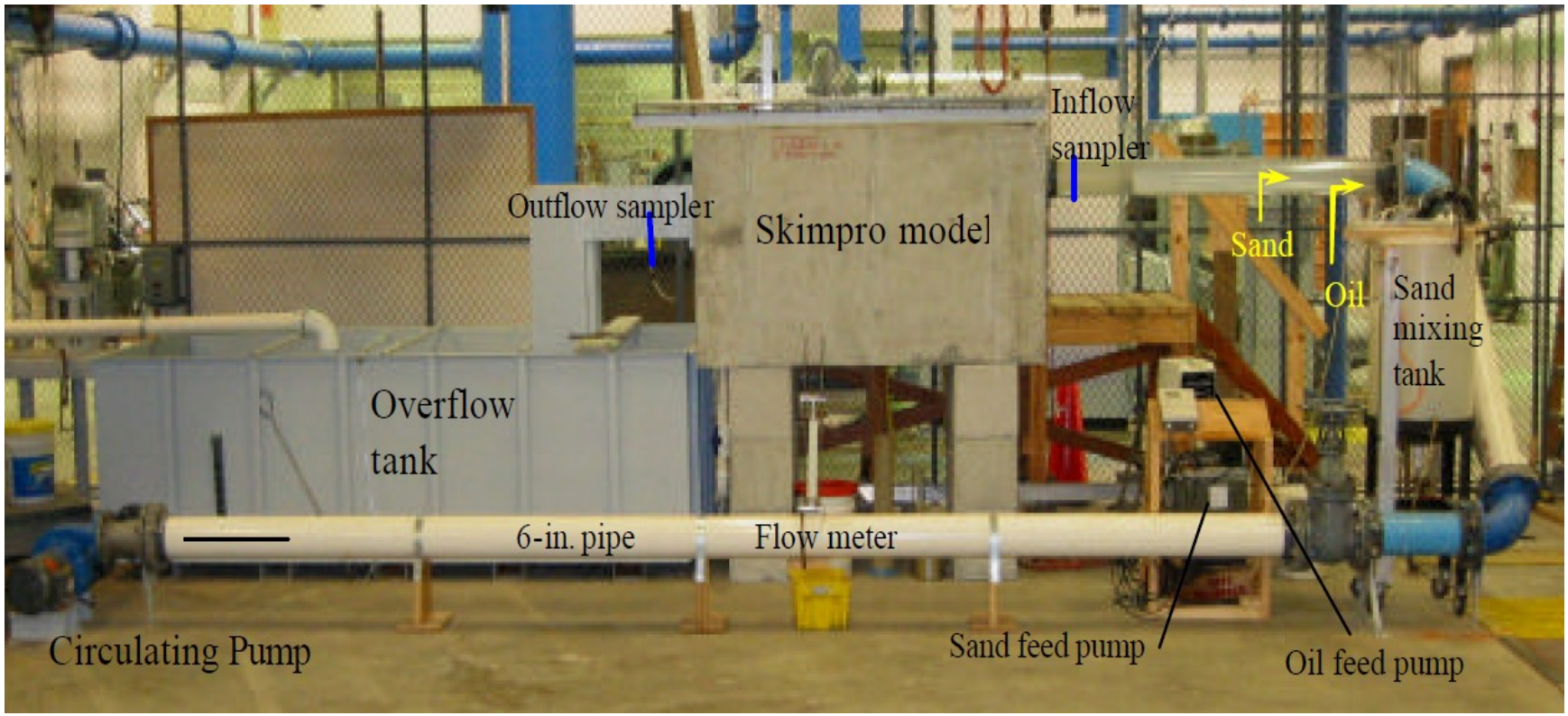

Figure 2-3. Setup of Skimpro OGS (Sturm *et al*. 2007)

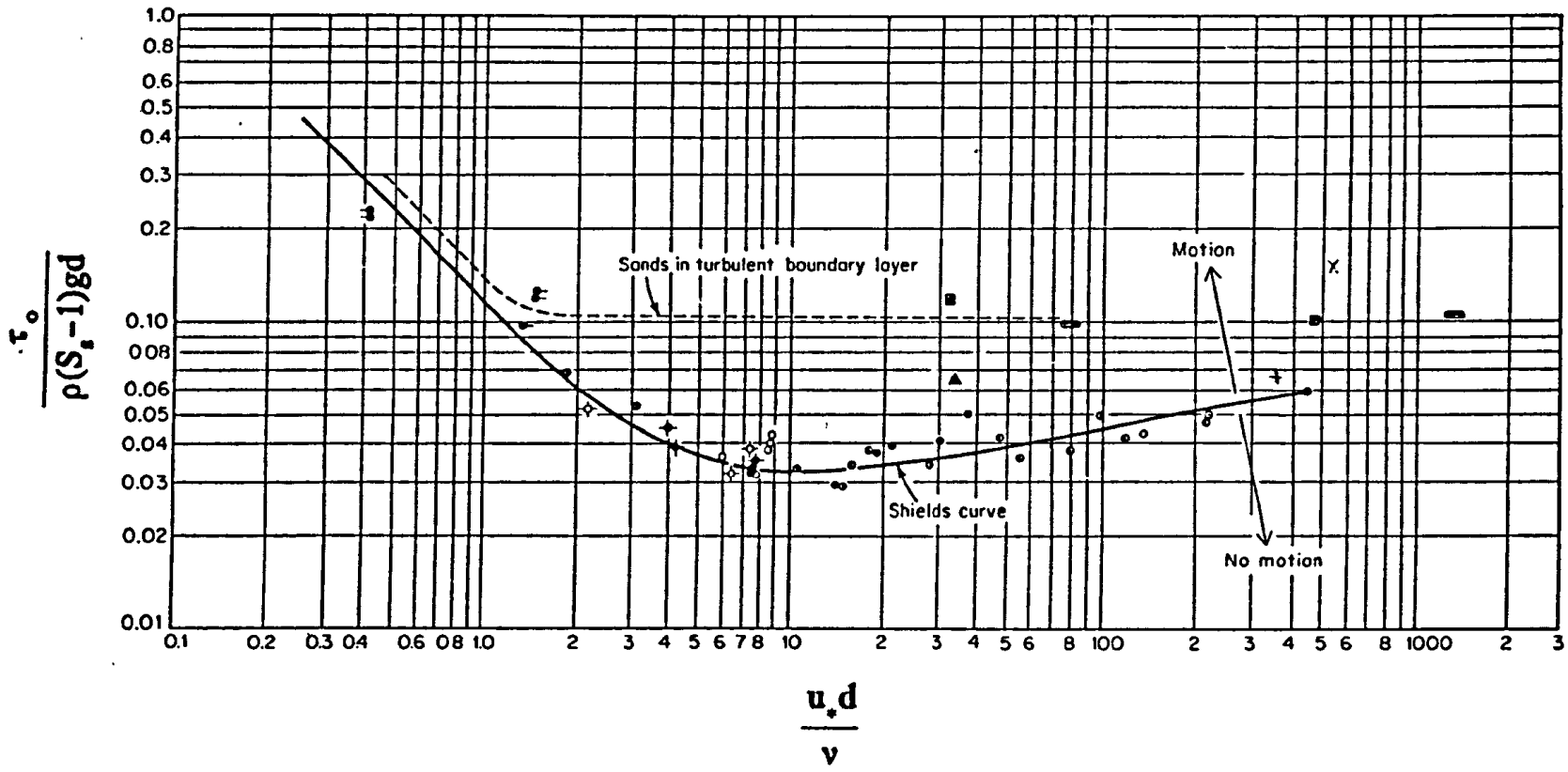

Figure 2-4. Shields diagram (Ab Ghani, 1993)

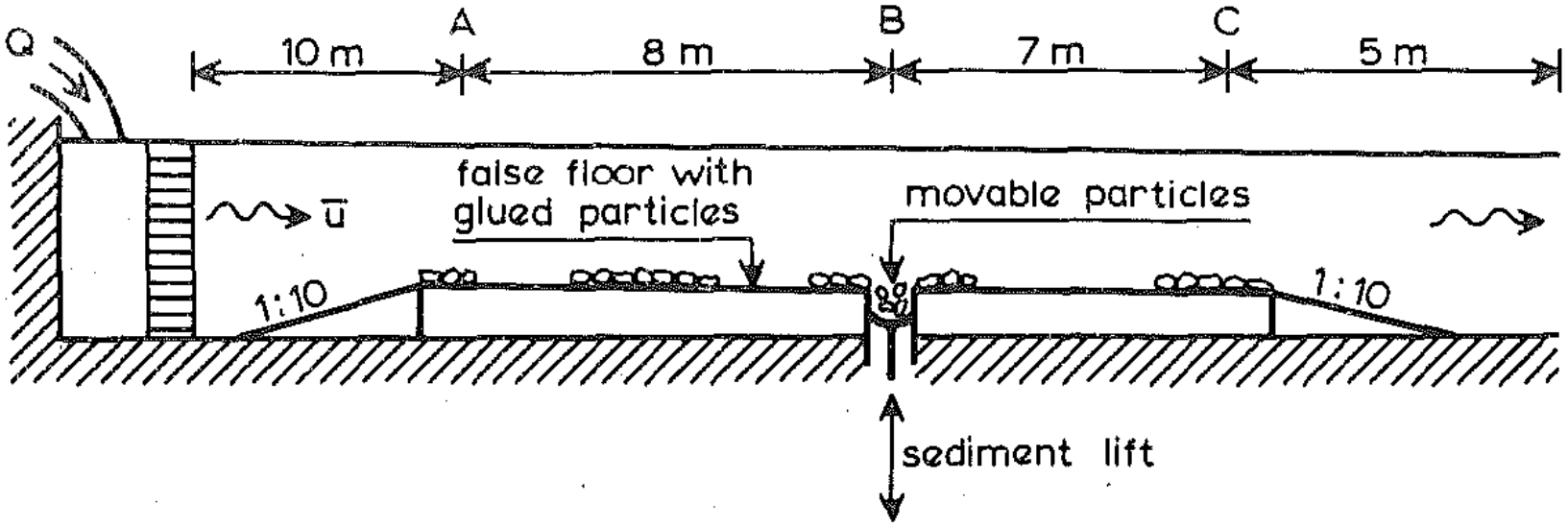

Figure 2-5. Experimental setup for pick-up rate study (Van Rijn, 1984)

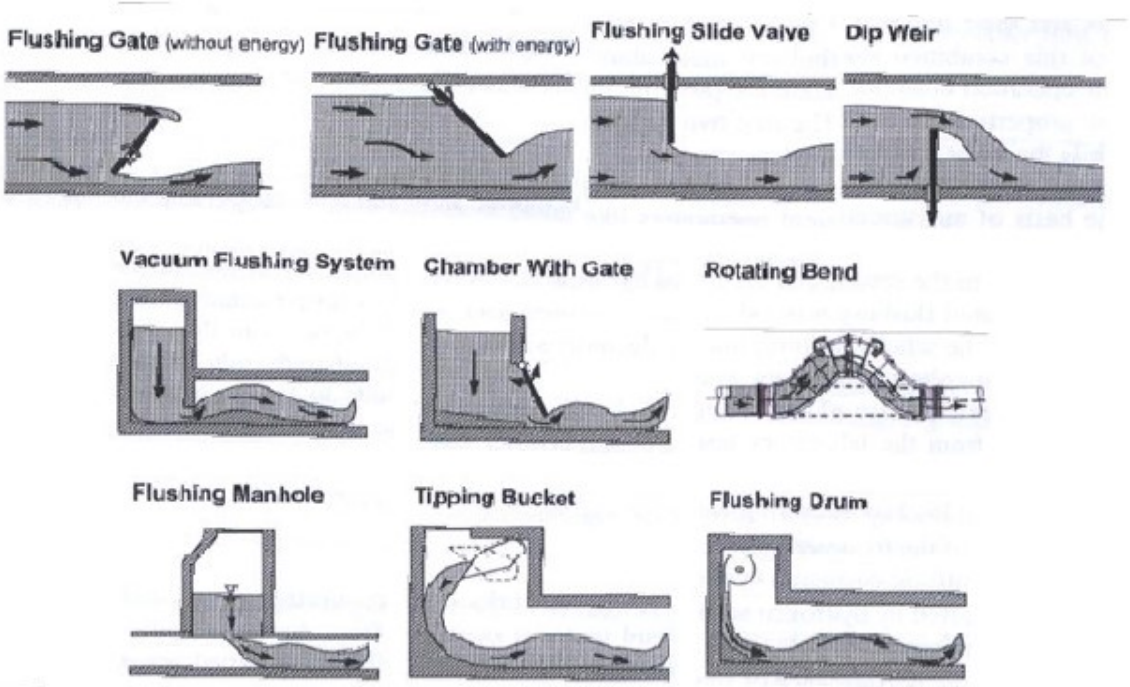

Figure 2-6. Flushing devices (Dettmar *et al*., 2002; Fan, 2004)

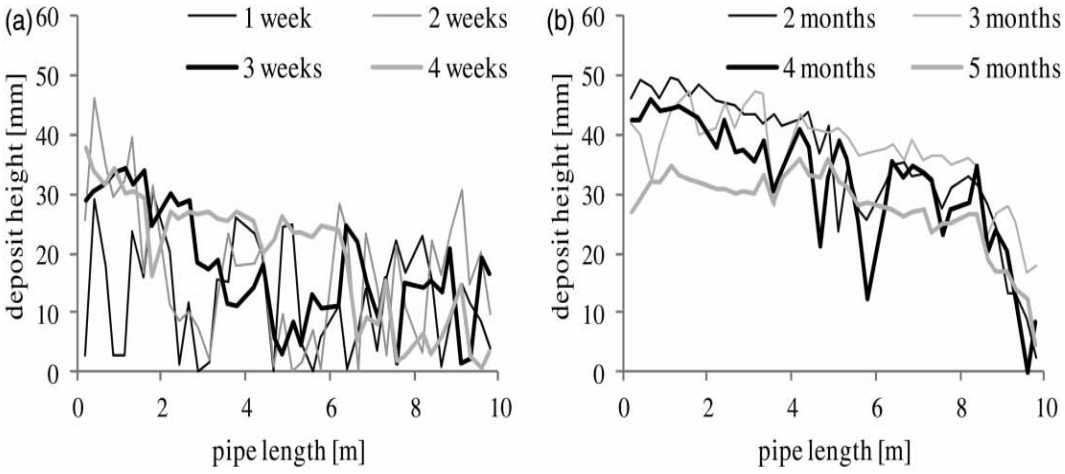

Figure 2-7. Deposition height over pipe length (Lange and Wichern, 2013)

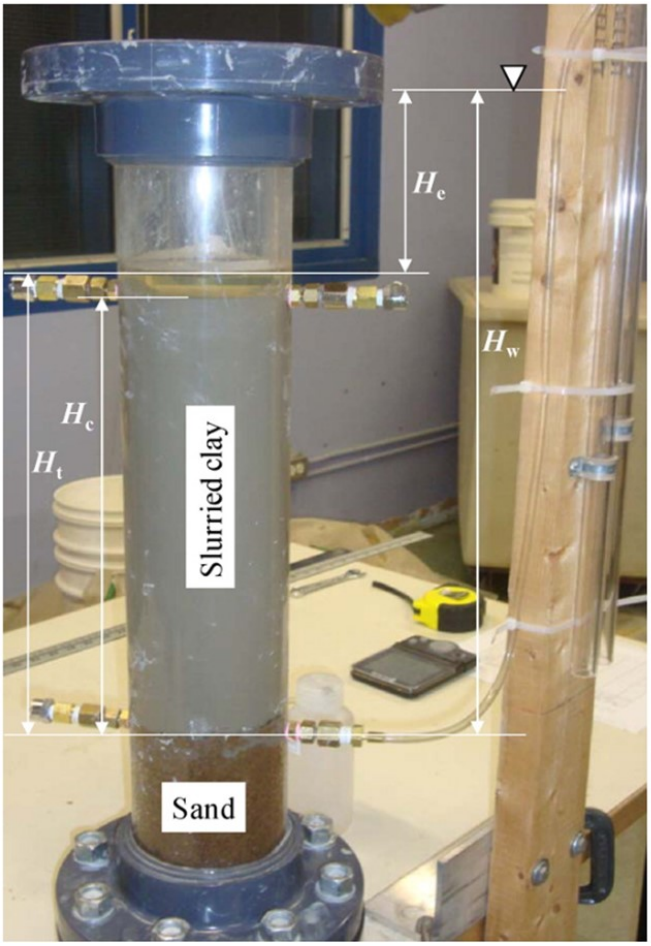

Figure 2-8. Self weight consolidation experiment (Li *et al*., 2013)

Chapter 3. Sediment Removal Efficiency in Oil - Grit Separators[1]

Oil - Grit Separators (OGSs) are one type of Best Management Practices, designed to remove oil and grit from storm water runoff (e.g., from parking lots and paved roads). This chapter examines scaling parameters for OGS removal efficiency. Three dimensionless parameters are chosen as scaling parameters: Hazen number (*Ha*), Reynolds number (*Re*) and Froude number (*Fr*). The Hazen number is a ratio of hydraulic residence time to particle settling. The Reynolds number measures the surrounding turbulence effects on sediment removal efficiency. The Froude number represents the ratio of inertial and gravitational forces, which indicates the influence of gravity on fluid motion. The collected data from the literature on sediment removal in OGSs can be represented by a single curve when the Hazen, Reynolds, and Froude numbers are combined into a new scaling parameter ($HRF=Ha\frac{Re}{Fr}$). A general form is proposed to correlate the sediment removal efficiency with this new parameter. This generalized prediction method can be used as a preliminary performance indicator for OGS units. The obtained curve can also be used to adjust raw laboratory and field measurement data to improve the evaluation of the performance of various OGSs.

3.1. Introduction

Storm water runoff or snowmelt from urban imperious surfaces (e.g., parking lots and paved roads) usually contains oil and grit that can pose negative impacts on receiving water bodies. In order to minimize these negative impacts, Oil - Grit Separators (OGSs) are commonly

[1] A paper based on this chapter has been published on Water Science and Technology.

used to capture oil and grit (Higgins, 2000). The focus of this chapter is only on sediment removal which is the main characteristic used to evaluate the performance of different types of OGSs. OGSs can be divided into three types based on the different removal methods: (1) gravity action type in which sediment is captured by gravity only, (2) swirl action type in which swirling flow directs sediment toward the center of the OGS, and (3) screening action type which uses a screen to capture sediment (Malesevic, *et al*., 2014). Although various OGSs have different configurations and dimensions, they all have two key aspects in common: the primary design function is to separate oil and grit from runoff, and they all rely on gravity to achieve their function. In order to properly apply OGSs, it is important to be able to quantify the removal efficiency under different catchment characteristics (e.g., for various sediment sizes, sediment concentrations, and flow rates).

In order to obtain removal efficiency data needed for sizing purposes, many laboratory evaluations of OGSs were conducted by suppliers, regulatory agencies and municipalities, each with their own specific sediment and for different flow rates. For example, Cornu *et al*. (2000) examined the removal efficiency of a Downstream Defender unit (i.e., a swirl type of OGS) and found its removal efficiency varied from 70% to 100% for relatively small flow rates decreasing from 25 L/s to 5 L/s (d_{50} of 0.3 mm sediment was used). Faram (2000) also tested the removal efficiency of a Downstream Defender unit and created a CFD model to represent the flow regime within the unit. Based on their CFD model, the turbulence level was found to be strong in the unit being evaluated, which might negatively affect the sediment removal efficiency. Sturm *et al*. (2007) built a 1:2 scale model to examine the removal efficiency of the Skimpro OGS (i.e., a gravity action type). They made several

modifications on the device and subsequently tested their performance. A detailed velocity field was obtained in their study, which also indicated the influence of turbulence.

In addition to laboratory investigations, numerous field studies have been conducted over the last two decades to obtain removal efficiency data of OGSs under prototype operating conditions. For instance, in 2004, two types of OGSs were monitored (i.e., a screening action OGS and a swirl type OGS) at a parking lot in Toronto, Canada (SWAMP, 2004). The sediment in the runoff contained relatively small sediment with a d_{50} of 20 μm. The average removal efficiency of these OGSs was found to be about 40% to 50%, which is in good agreement with other studies. They suggested that different types of OGSs can be expected to have similar removal capabilities. However, their field data included some unexpected values, e.g., with a 1.7 L/s flow rate, the sediment removal efficiency was only around half of that with an 8.2 L/s flow rate. There was some concern that the performance results might be biased due to the uncertainty during fieldwork. A second challenge is that the field-testing only cover a fraction of the conditions that the units might be subjected during their operation.

In order to overcome the discrepancies in both the laboratory and field investigations, several jurisdictions adopted various testing protocols in order to provide uniform testing conditions (Howie, 2011; NJDEP, 2013). In Canada, to provide a common procedure for testing and verifying the actual performance of treatment devices under controlled conditions, in an independent, transparent manner, a nation-wide protocol for laboratory testing was adopted under the auspices of the Canadian Environmental Technology Verification (ETV) process (2014). Performance data based on the implementation of the recent ETV Canada protocols was obtained for several OGS units: a Downstream Defender Hydro unit (swirl type) (ETV, 2016) as well as a Stormceptor EF4 unit (gravity type) (ETV, 2017). The tested flow rates

and sediment sizes cover a wide range as per the ETV Canada protocols. An identical, artificial sediment mixture was used for all experiments. The removal efficiency results for the overall sediment removal are believed to be reliable. However, the removal efficiency results for some of the individual particle size fractions appear to be unusual under certain flow rates, see Figure 3-1. The unusual behavior is the result of challenges with being able to properly disintegrate the overall sediment sample retained in the OGS into the original particle size fractions used to create the mixture used in the experiments. In addition, the settled fine sediment can coagulate to relatively coarser sediment, which may significantly increase the sediment removal efficiency for one particle fraction group while decreasing it for other particle size fractions. As a result, the findings for some of the particle size fractions may need to be adjusted which requires a transparent, scientifically defensible procedure.

In this chapter, the general performance of sediment removal efficiency in OGSs is described, which can predict the sediment removal efficiency prior to OGS installation. The significance of this generalized prediction method is that it can be used as a preliminary performance indicator for OGS units that have not yet been subjected to rigorous laboratory testing. In addition, this chapter provides useful information for the interpretation as well as, when needed, adjustment of data obtained following the ETV Canada protocols. A selection of field data as well as experimental laboratory data are compared against the outcome from the general prediction equation to demonstrate the potential use of the general prediction method.

3.2. Scaling parameters for OGS removal efficiency

Before determining scaling parameters, it is important to list all related physical parameters determining the sediment removal efficiency in OGSs. In general, there are three types of

physical parameters: the sediment characteristics, fluid characteristics, and flow conditions. For the sediment characteristics, they are the sediment fractions of interest (using d_{50}: mm), the sediment density (ρ_S: kg/m^3), and the sediment settling velocity (V_S: m/s). The fluid characteristics include the water density (ρ: kg/m^3) as well as the kinematic viscosity (ν: m^2/s). The flow conditions can be described as the average vertical flow velocity (V_M=Q/A_{OGS}: m/s), the depth of water (excluding sediment storage depth, h: m), and the horizontal flow area (A_{OGS}: m^2) of the water column in the OGS. The gravitational acceleration (g: m/s^2) is also important. After Pi theory was applied (Buckingham, 1914), three dimensionless parameters were chosen as scaling parameters to predict the sediment removal efficiency in this chapter (specifically, Hazen number, Froude number and Reynolds number).

In the literature, two parameters are commonly used for hydrodynamic separators including OGS unit: the Froude number ($Fr = \frac{V_M}{\sqrt{gh}}$) and the Hazen number ($Ha = \frac{V_S}{V_M}$) (Fenner and Tyack, 1997; Higgins, 2000; Luyckx, *et al*., 2005). In some studies, the Froude number was examined as a potential scaling parameter for the OGS removal efficiency since gravity plays an important role in removing sediment within OGSs (Fenner and Tyack, 1997; Higgins, 2000). However, Higgins (2000) found that the Froude number has limited applicability for modeling some devices since it is more relevant to free surface gravitational effects and does not strictly hold for swirl flow conditions. However, swirl flow conditions are commonly observed in many OGSs (Malesevic *et al*., 2014), which means only using the Froude number will not be sufficient. Therefore, some researchers (Fenner and Tyack, 1997; Luyckx *et al*., 2005) suggest that the Hazen number has a good applicability to describe swirl action. The Hazen number can be presented as the ratio of the particle settling velocity and the vertically

averaged flow velocity (Luyckx *et al*., 2005). The particle settling velocity can be calculated using the equation developed by Ferguson and Church (2004):

$$V_S = \frac{(\rho_S - \rho) g d_{50}^2 / \rho}{C_1 \nu + (0.75 C_2 (\rho_S - \rho) g d_{50}^3 / \rho)^{0.5}} \quad \text{(Equation 3-1)}$$

where, C_1 = 18 and C_2 = 1.0. In fact, the Hazen number equals to $\frac{(Ah)V_s}{Qh}$ (Q is the flow rate in the OGS), which can be treated as the ratio of the hydraulic residence time ($T = \frac{Ah}{Q}$) to the particle settling time ($\frac{h}{V_s}$). Note that the Péclet number (*Pé*) has also been used to explain sediment removal in hydrodynamic separators (Wilson *et al*., 2009; Tang *et al*., 2016). However, there is no difference between *Pé* and *Ha* in terms of physical meaning (Wilson *et al*., 2009). The only difference between these two parameters is that their averaged velocities have different directions (vertical for *Ha* and horizontal for *Pé*). For devices with horizontal mean flow (e.g. standard sump), *Pé* is recommended (Howard *et al*., 2012). For devices with vertical mean flow (e.g. catch basins and OGSs), *Ha* is normally used (Fenner and Tyack, 1997; Higgins, 2000; Luyckx *et al*., 2005). Besides the Froude and Hazen numbers, the Reynolds number ($Re = \frac{V_M h}{\nu}$) was also considered in this chapter since turbulence plays a significant role in sediment removal. The turbulence caused by the interchange of eddies in a vertical direction can maintain sediment in suspension against the action of the gravitational force (Chien and Wan, 1999; Verstraeten and Poesen, 2000).

A combined parameter ($HRF = Ha\frac{Re}{Fr}$) is selected to develop a general prediction equation to express the removal efficiency of OGS units. The ratio of *Re* to *Fr* representing the ratio of the gravitational forces to the viscous forces has been used in many studies to describe the

turbulence level as well as the hydraulic conditions (Kirkgöz and Ardiçlioğlu 1997; Belfiore 2003; Zhou and Cheng, 2009). The product of *Ha* and the ratio of (*Re/Fr*) is defined as *HRF* and can be written as:

$$HRF = Ha\frac{Re}{Fr} = \left(\frac{V_S T}{h}\right)\frac{\frac{V_M h}{\nu}}{\frac{V_M}{\sqrt{gh}}} = \frac{\sqrt{g}}{\nu}V_S T\sqrt{h} \qquad \text{(Equation 3-2)}$$

The resulting parameter is a function of the sediment settling velocity, the hydraulic residence time, and the water depth. As for the physical meaning of *HRF*, with the increase of particle size, hydraulic residence time and water depth, the sediment removal efficiency increases. This tendency is physically reasonable. Note that the power of V_s, T, and h can be different from Equation 3-2, since *Ha*, *Re*, and *Fr* are dimensionless parameters and can be of different power. However, after several trials, the combined parameter (*HRF*) was found to have the best fit in terms of R^2 and root mean square error (*RMSE*) (see Table 3-1).

3.3. Sediment removal efficiency in OGSs

Data were collected from previous studies including eight laboratory tests. The data covers a relatively wide flow rate range from 0.75 to 166.6 L/s. Different OGSs have different dimensions and designs, but their common purpose is to remove grit in storm water. All removal methods (gravity, swirl, and screening actions) are covered in this chapter. The sediment sizes used cover a relative wide range (d_{50}: 0.05-0.62 mm), representing very fine to coarse particles, and thus reflecting the sediment that is typically found in storm sewer systems. Table 3-2 summarizes key parameters of the eight laboratory studies.

Figure 3-1 shows the sediment removal efficiency as a function of the surface loading rate (Q/A) for the different types of OGSs. In general, the removal efficiency decreases as the surface loading rate increases and the particle size decreases. As can be seen in Figure 3-1, data from the Downstream Defender, Skimpro OGS, Stormceptor STC 900, Stormceptor OSR 250, CDS, and Vortech model 2000 follow this general tendency. They have approximately a 100% removal efficiency when the surface loading rate is low. When the surface loading rate increases, the sediment removal efficiency drops gently from 100% to 80%. After this period, the removal efficiency decreases rapidly all the way to around 20%. However, as mentioned before, in some instances it is hard to properly distinguish between the various particle size fractions that are part of the overall sediment sample that has been retained in the OGS. As a result, some units such as the Downstream Defender Hydro as well as the Stormceptor EF4 display unusual removal efficiency tendencies for some particle size fractions, which therefore needs adjustment. These data are therefore excluded from the data sets used to develop the general prediction model and will be adjusted afterwards.

The relationship between the developed parameter and the sediment removal efficiency is plotted in Figure 3-2 (log x-axis). All data are concentrated in an S shape curve. In general, the sediment removal efficiency for all devices approaches 0% at low values of *HRF* and approaches 100% at high values of *HRF*. With changing values of *HRF*, the sediment removal efficiency slowly approaches 80% and 20% from 100% and 0%, respectively. When the removal efficiency approaches 50%, *HRF* equals 2.6×10^6. Note that the value of *HRF* is always large since the kinematic viscosity is the denominator. A general function is proposed below, which reflects the above features:

$$\eta = [1 + \frac{1}{a(HRF)^b}]^{-1/b} \quad \text{(Equation 3-3)}$$

where η is the removal efficiency, a and b are coefficients. In Figure 3-2, a = 2.32×10^{-7} and b = 1.78 with the R^2 value of 0.93 and the *RMSE* of 5.8%. The removal efficiency prediction works properly since the difference between the various experimental data and the prediction curve is only as high as 10%. This general equation can be used as a preliminary performance indicator for OGS units that have not yet been subjected to rigorous laboratory testing protocols. The values for a and b may be slightly different for each individual OGS device reflecting the specific configuration of the unit in question. As such, where reliable experimental data exist this should be adopted for design purposes. However, the general function can be used to evaluate whether the experimental data reflects the expected behavior and to adjust the raw data where appropriate.

Data from the Downstream Defender Hydro (ETV, 2016), Stormceptor EF4 (ETV, 2017), and field sampling (SWAMP, 2004) were plotted together with the general prediction curve (see Figure 3-3). The data can be easily divided into two groups: a) data fitting within a 20% deviation area and b) data falling outside of this 20% deviation area. The 20% deviation is chosen since it can cover majority of raw data, which not only represents the experimental tendency but also identifies unusual data points. The data falling outside need to be adjusted to fit the general prediction curve. Specifically, for the Downstream Defender unit, the particle size fractions 0.1-0.15 mm and 0.02-0.05 mm data need to be adjusted, while for the Stormceptor EF4 unit, the particle size fractions 0.5-1.0 mm, 0.15-0.25 mm, 0.1-0.15 mm, 0.05-0.075 mm, and 0.02-0.05 mm data need to be adjusted. The field data needs to be adjusted as well. The general prediction concept can be used as a tool to adjust the apparent

scatter so that the processed data mimic the expected removal efficiency behavior. There are several factors may bring uncertainties to the general prediction equation. Firstly, the combined parameter (*HRF*) simplified not only the sedimentation and transport processes but also the various flow conditions in OGSs. Secondly, the inner structure of the OGSs (e.g. screen structure) can impact the accuracy of the equation, however, it was not considered in the scaling analysis part. Moreover, various sediment size distributions, concentration and sediment composition will also affect the prediction results. More future research should be done to quantify the influence of above factors on the prediction equation. The following section contains the application of the prediction equation.

3.4. Adjustment method based on the general prediction equation

The data adjustment method based on the general prediction equation follows the flowing steps. Note this method was used as a data filter which evaluated the performance of OGSs. In this chapter, the field data (SWAMP, 2004), the laboratory data and 0.1-0.15 mm from ETV (2016) are adjusted as examples (Figure 3-4). First, collect all related experimental data for a particular OGS unit and transfer them into *HRF* as per Equation 3-2. Then, superimpose the relationship between *HRF* and the observed sediment removal efficiency on the general *HRF* curve of Figure 3-2. In this plot, the data points that have a deviation greater than 20% from the general curve should be adjusted, i.e., the data points outside of the dashed lines in Figure 3-3. Replace the observed removal efficiency data by the values on the general curve (i.e., the raw data and the adjusted data share the same value of *HRF*). Note that adjusting the data points will affect the total amount of sediment mass. For the Downstream Defender unit (ETV, 2016) at the surface loading rate of 6.7 L/s/m^2 (Figure 3-4), the removal efficiency

of 0.1-0.15 mm sediment is overestimated in the lab study comparing to that on the general *HRF* curve. Under the assumption of mass conservation, the removal efficiencies of other sediment fractions are underestimated. Therefore, removal efficiencies of other sediment fractions at 6.7 L/s/m^2 (in Figure 3-1) have been increased in this chapter. The comparison between the adjusted data (i.e., the solid lines) and the original raw data (i.e., the dashed grey lines) can be found in Figure 3-4. The adjusted removal efficiencies present a more realistic performance of the device for the particle size fraction of interest.

3.5. Chapter summary

OGSs are commonly used to capture oil and grit from storm water runoff or snowmelt on urban imperious surface. There are three different types of OGSs based on different removal methods: (1) gravity action type, (2) swirl action type, and (3) screening action type. The Hazen number, Reynolds number and Froude number are chosen as scaling parameters. A combination of these parameters expressed as HRF is chosen to describe the removal efficiency. This parameter is a function of the sediment settling velocity, the hydraulic residence time, and the water depth. As the settling velocity, hydraulic residence time, and water depth increase, the sediment removal efficiency increases. A general prediction form for the performance of several OGS devices was developed: $\eta = (1 + \frac{1}{2.32\times10^{-7}(HRF)^{1.78}})^{-\frac{1}{1.78}}$. This form has a good fit with R^2 over 0.93 and RSME less than 5.8%. Note that a and b can be different when processing data sets from other studies. The generalized prediction method can be used as a preliminary performance indicator for OGS units that have not yet been subjected to rigorous laboratory testing. In addition, based on the general tendency of the removal efficiency, an adjustment method is developed that can be

applied for test results where the results for the individual particle size fractions needs adjustment.

Table 3-1. Different combined parameters with R^2 and *RMSE*

Combined parameters	R^2	*RMSE*
$Ha^{0.5}\ Re/Fr$	0.77	11.3%
$Ha\ Re^{0.5}/Fr$	0.83	11.2%
$Ha\ Re/Fr^{0.5}$	0.51	11.8%
Ha Re/Fr	**0.93**	**5.8%**
$Ha^2\ Re/Fr$	0.75	13.6%
$Ha\ Re^2/Fr$	0.17	24.8%
$Ha\ Re/Fr^2$	0.83	10.9%

Table 3-2. Laboratory studies on different OGSs

Parameter	Downstream Defender (Faram, 2000)	Stormceptor STC 900 (Imbrium Systems Corporation, 2004)	Stormceptor OSR 250 (Imbrium Systems Corporation, 2007)	Skimpro OGS (Sturm, Costanza, *et al*., 2007)	CDS (FB Environmental Associates, 2010)	Vortech 2000 (Contech Engineered Solutions, 2015)	Downstream Defender Hydro (ETV, 2016)	Stormceptor EF4 (ETV, 2017)
Type	Swirl action	Gravity action	Gravity action	Gravity action	Swirl and screening action	Gravity action	Swirl action	Gravity action
Q (L/s)	2.5-17.5	4.4-22	17.6-88.3	21-86	3.4-50	2.3-21	3.7-166.6	0.75-35.6
h (m)	1.25	1.4	1.4	1.3	1.44	1.3	1.8	1.5
A (m^2)	1.13	2.63	4.67	4.6	1.82	3.71	5.55	1.13
d_{50} (mm)	0.30	0.067	0.108	0.12, 0.17, 0.30	0.108	0.050, 0.080, 0.150	0.62*	0.62*

*Analyses were based on different sediment fractions instead of d_{50}

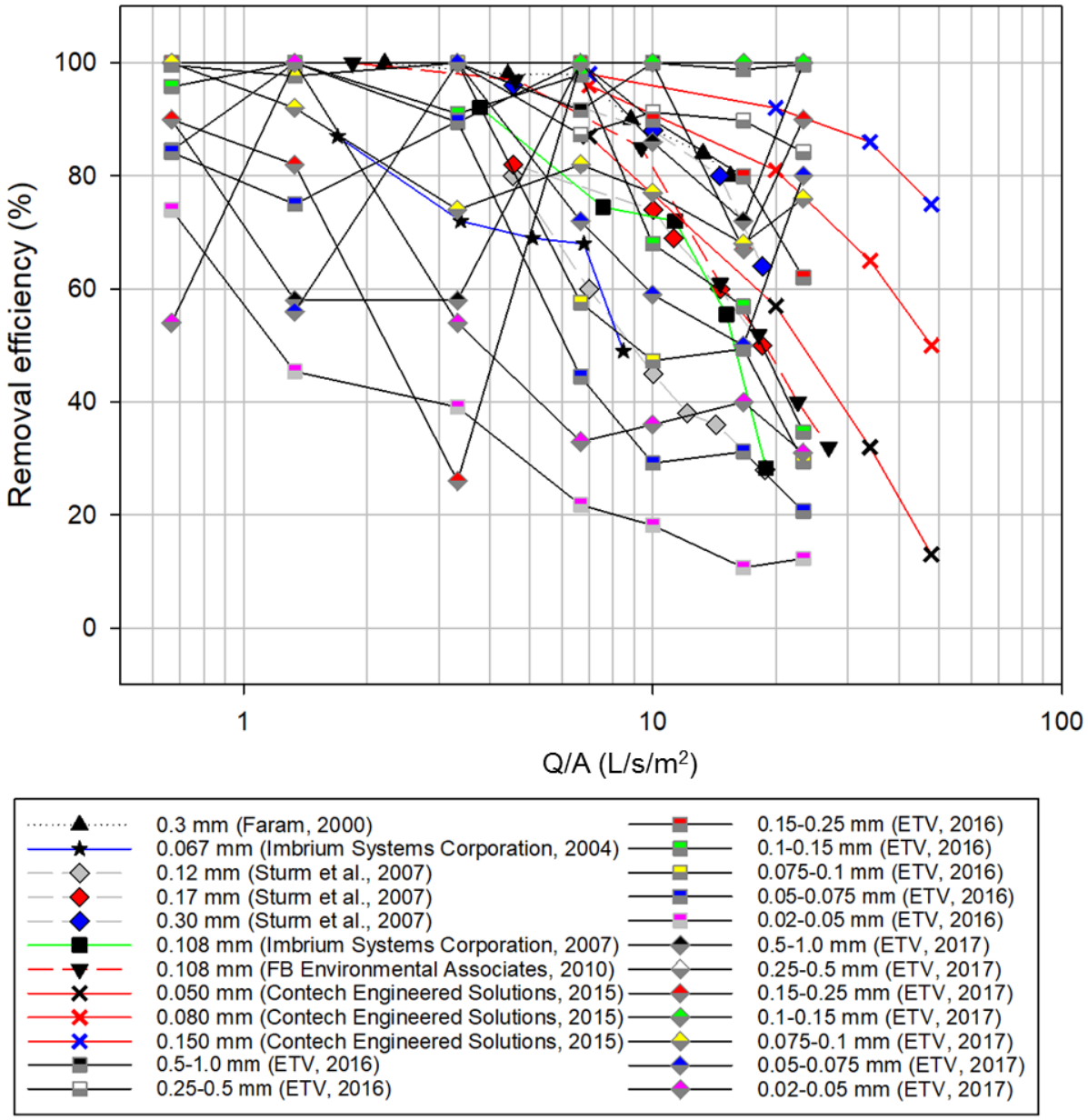

Figure 3-1. Sediment removal efficiency in different OGSs

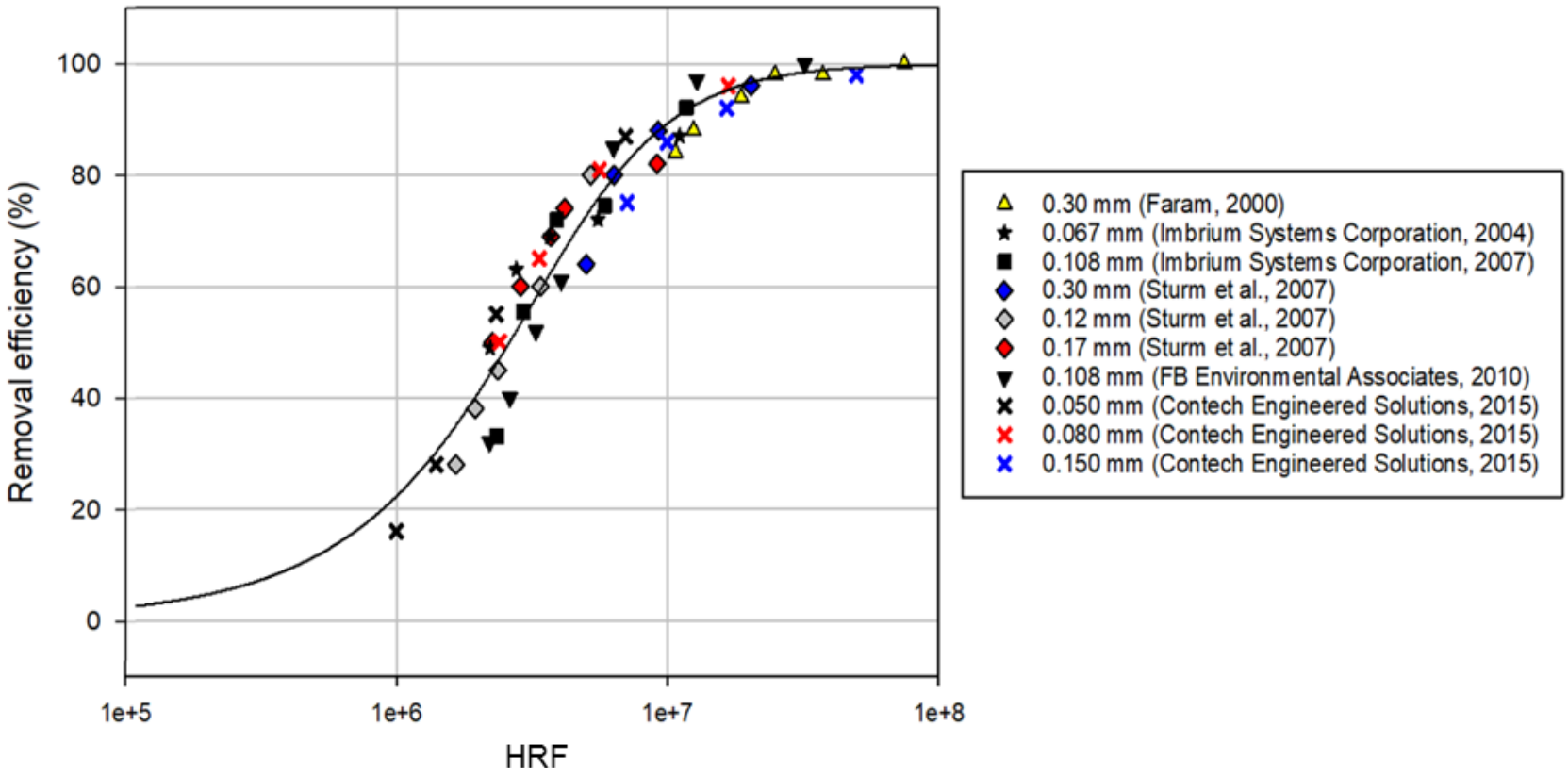

Figure 3-2. Sediment removal efficiency prediction

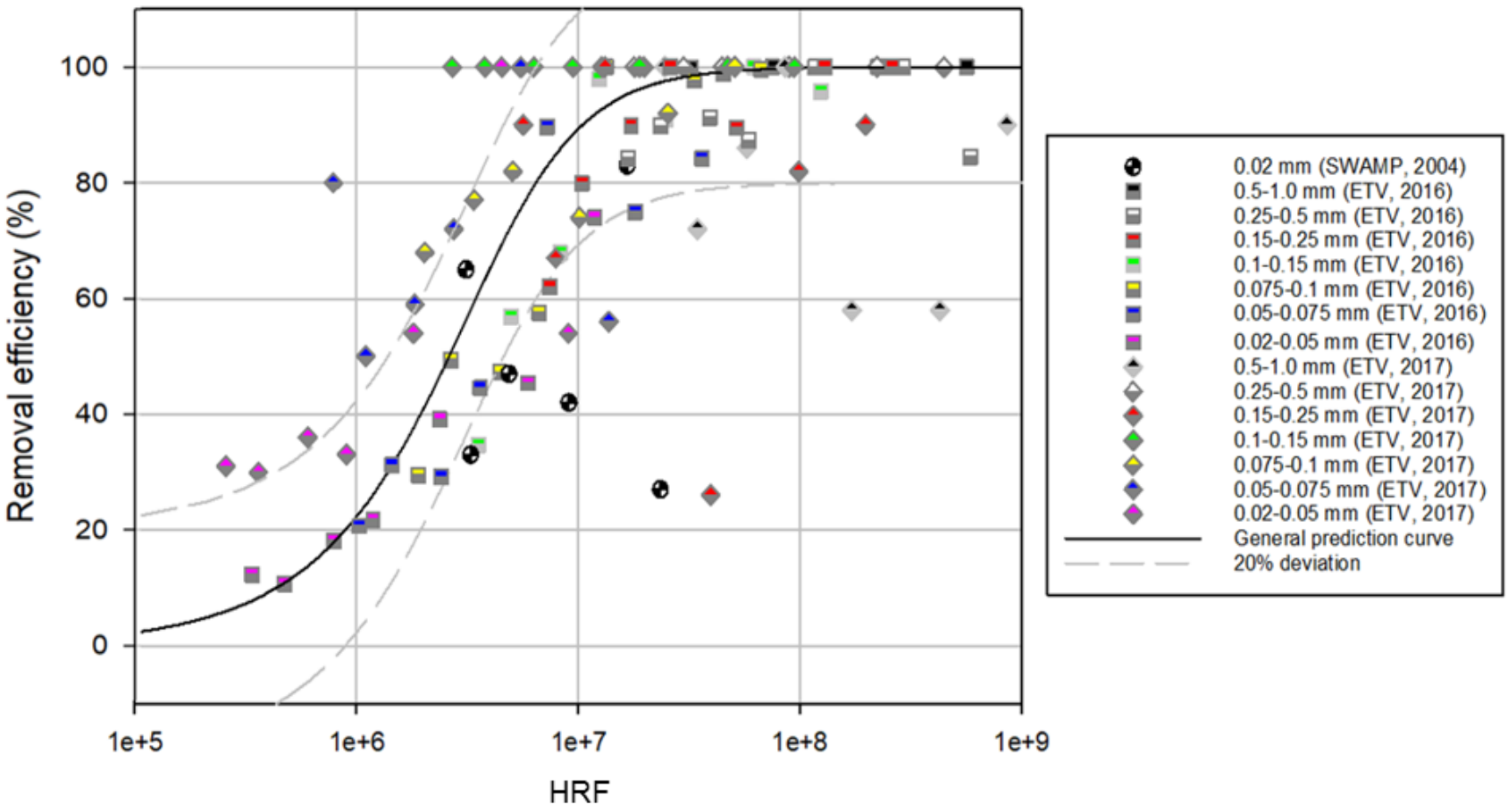

Figure 3-3. Raw data and general prediction curve (SWAMP, 2004; ETV, 2016; ETV, 2017)

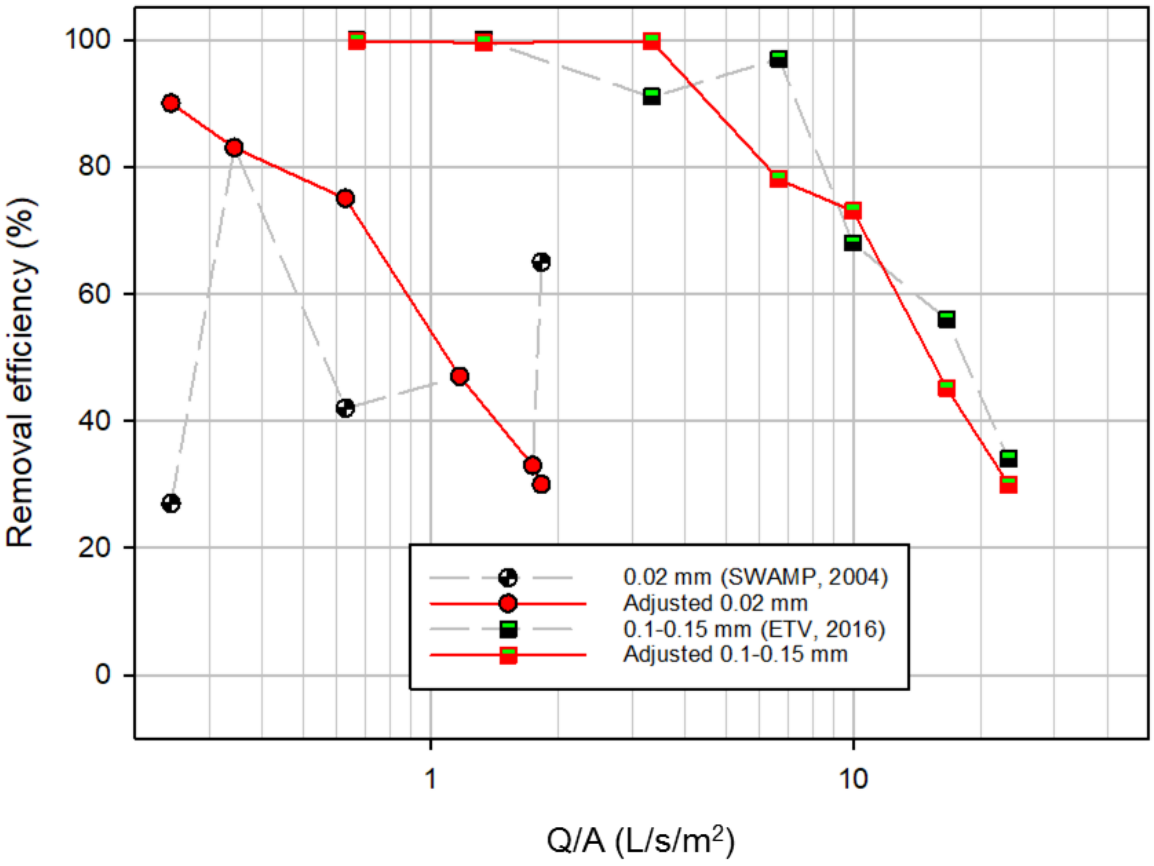

Figure 3-4. Comparison between adjusted data and raw data

Chapter 4. Sediment Depositions in a Submerged Storm Sewer Pipe[2]

Sediment depositions in storm sewer systems have received significant attention due to the implications in urban flooding and environmental impacts. However, only limited attention has been paid to sediment deposition in submerged storm sewers. In this study, a laboratory model was used to study the sediment transport and deposition processes in a submerged storm sewer. The growth of the deposition can be divided into two stages: rapid growth (both deposition height and length increase) and equilibrium growth (only deposition length increases). The sediment loading rate determines the duration of the rapid growth stage, and equilibrium height increases for larger sediment size and higher sediment concentration. The bed shear stress at the equilibrium stage varies from 1.8 to 8.7 N/m^2 corresponding to the variation of bed friction factor from 0.058 to 0.185, which is about 2 – 4 times of that caused by the sediment roughness height alone. This increase in the bed shear stress is mainly due to the significant amount of momentum needed to transport the required sediment loading. A prediction method and its applications are also presented.

4.1. Introduction

Sediment deposition in storm sewers reduces the flow area and can cause pipe blockage, which can lead to surcharge conditions and urban flooding (Butler and Davies, 2011). Pollutants attached to the sediment surface may adversely affect the receiving water quality and aquatic life. These concerns have resulted in various laboratory and field studies on

[2] A paper based on this chapter was submitted to the Journal of Environmental Engineering.

sediment movement and deposition in sewer pipes (Perrusquía, 1991; Ab Ghani, 1993; Lange and Wichern, 2013; Ota and Perrusquía, 2013). In the mid 1970s and early 1980s, several experimental studies were carried out on sewer sediment depositions with a focus on design criteria such as self-cleansing sewers (Ab Ghani, 1993). After the early 1980s, attention was focused on the mechanism of sediment transport in laboratory experiments (e.g., testing the effects of different pipe sizes, slopes, with/without deposition and various flow rates) and conducting field inspection or monitoring in urban combined sewer systems (Perrusquía, 1991). Recently Chin (2020) cautioned the use of full pipe flow conditions in determining the sewer self-cleansing velocity. However, most studies did not pay much attention to submerged storm sewer pipes where their outlets are subjected to a high permanent water level in the receiving water body. In submerged pipes, with the pipe running full and a decreased flow velocity in particular under minor rainfall conditions, these pipes might witness significant amounts of sediment deposition as time goes by. Hence, the sediment movement and deposition in submerged pipes need to be studied prior to any modification of these submerged pipe configurations to avoid the deposition problems.

Sediment movement can generally be divided into erosion, transport and deposition processes (Butler *et al*., 2003). In the erosion part, the critical velocity (or critical shear stress) is typically used to describe the threshold of erosion. Novak and Nalluri (1984) suggested a fundamental equation for the sediment critical velocity in a clean pipe as a function of the pipe size, slope and particle size, which has been commonly used. Perrusquía (1991) stated that the Shields diagram can be used to determine critical shear stress of sediment in partially full pipe flows. Miedema (2012) considered the exposure level effects (i.e., the area subjected

to the flow and not covered by sediment) on the Shields diagram. Miedema (2012) also showed deposited sediment is hard to be eroded with the increase of sediment loading.

As for the study of sediment transport, bed load transport is of interest since it may result in sewer blockage problems that could cause urban flooding. Various bed-load transport studies were conducted for partially full pipes since partially full flow commonly exists in storm sewer systems (May, 1989; Perrusquía and Nalluri, 1995). A bed load equation for pipes, with little or no deposition, was developed by May (1989). Perrusquía and Nalluri (1995) tested various pipe sizes (154 – 450 mm) and sediment sizes (0.9 – 2.5 mm) to generate a bed load equation, whose prediction accuracy was enhanced by applying a coefficient (Arthur *et al.*, 1996). Graf and Acaroglu (1968) used dimensionless bed shear stress and dimensionless transport parameter to quantify the sediment transport capacity, and their method has been widely applied for predicting the sediment transport capacity in pipes (Novak and Nalluri, 1984; Safari, *et al*., 2015). However, the above research focused on sediment transport in partially full pipe without the presence of deposition and full pipe flow condition. The difficulty of studying the bed load transport in full pipe flow is to determine the bed shear stress since it is hard to obtain direct measurements under full pipe flow conditions. In addition to the bed load rate, the movement of bed load particles itself is worth studying. Lee and Hsu (1994) investigated a continuous sediment saltation process on a rigid boundary and found the particle saltation velocity to be related to the bed shear stress and flow velocity.

For the studies on sewer deposition, the majority of the research has so far focused on sanitary and combined sewer systems. A field study conducted by Laplace *et al*. (1992) showed that the sediment volume in a combined sewer system tends to display an asymptotic increase

with time, which means that the solid transport capacity increases as the flow area decreases due to the growth of the deposition. For the deposition build-up rate, Ashley and Crabtree (1992) showed that it is difficult to predict the deposition build-up rate in sewers since many factors (e.g., flow rate, pipe conditions and sediment characteristics) can affect it. Butler *et al*. (2003) summarized the general processes of deposition build-up. Bertrand-Krajewski *et al*. (2006) presented a continuous field experiment over 4 years to monitor the deposition accumulation in an egg-shaped combined sewer in Lyon, France. The deposition depth was found to be an important variable to describe the deposition profile. In recent years, Lange and Wichern (2013) described sedimentation dynamics in combined sewer systems. However, the research about the deposition growth in storm sewer systems is limited.

In this study, the sediment deposition processes in a submerged pipe were studied in the laboratory. The processes of the deposition growth, bed load movement, and flushing on the deposition were observed experimentally. Additionally, the effects of the sediment size, sediment loading rate, flow velocity, and pipe slope on the deposition height were studied. The energy head slope was obtained experimentally and was used to develop a methodology determining the bed shear stress in submerged storm sewer pipes. Moreover, equations regarding the bed load transport, saltation velocity, and equilibrium height prediction were developed.

4.2. Methodology

The experimental setup consisted of a vertical water inlet, a sediment inlet, a 6.0 m long and 184 mm diameter Plexiglas pipe, and a downstream tank, shown in Figure 4-1. The 150 mm diameter vertical inlet pipe had a 350 mm deep sump to provide energy dissipation and create

stable full pipe flow conditions. A mesh was attached to the pipe invert under the deposition to simulate the concrete roughness. The roughness height of the mesh was 1 mm and the mesh grit was 1 mm by 1 mm. Sediment was fed through the sediment inlet which had a 50 mm diameter. A sand feeder (Model SCR-20, Vibra Screw Inc., Totowa, NJ, USA) was used to control the sand feeding rate by adjusting its rotational speed. The slope of the Plexiglas pipe was adjustable through a hydraulic jack located at the upstream end of the frame. The downstream tank was used to collect the sediment and to provide the desired backwater conditions to submerge the full length of the pipe. The tailwater level during the experiment was controlled at a desired level using an outlet control of the downstream tank.

Different flow rates, pipe slopes, sediment concentrations, and sediment sizes were varied in the experiments (Table 4-1). Specifically, the flow rates were 8.0, 13.3, and 19.9 L/s, corresponding to a pipe-full average velocity of 0.30, 0.50, and 0.75 m/s, respectively. All velocities described throughout the paper referred to average velocities. Note that according to the City of Calgary (2011), the maximum velocity corresponding to a 1:100 rainfall event in the submerged pipe is 1.5 m/s to avoid erosion in the downstream pond. The tested pipe slopes were 0.5%, 1%, and 2%, which are also commonly found in submerged pipes. The sediment concentrations were 0.2, 1.1, and 2.0 g/L corresponding to low, medium, and high sediment loadings (Farnworth, 1979). The Sil 7 sand and Sil 8/16 sand (Sil Industrial Minerals, Edmonton, Alberta, Canada) were used to study the deposition growth. The Sil 7 has a size range of 0.04 to 1 mm, a median size d_{50} of 0.4 mm, and the uniformity coefficient of 2.2 ($C_u=d_{60}/d_{10}$, Yalkowsky and Bolton, 1990), while the Sil 8/16 sand has a size range of 0.04 to 2.4 mm, a median size d_{50} of 1.8 mm, and the uniformity coefficient is 2.6. Note that

a value of uniformity coefficient less than 3 is typically considered relatively uniform (Yalkowsky and Bolton, 1990). All particles had a specific gravity of 2.65.

The testing procedure was as follows: the first step was to run water until full pipe flow conditions occurred. After steady-state conditions set in, sediment was added at the pre-determined rate and a video camera started to record the deposition growth. The experimental duration was determined by the time the equilibrium height was reached. Since it was difficult to directly measure the deposition dimensions in the submerged pipe, the deposition longitudinal profiles along the pipe central line were plotted in AutoCAD (with 0.1 mm accuracy). Then, the sediment saltation velocity was recorded on the video once the equilibrium height had been reached. Note that only the Sil 8/16 sand was tested for the saltation velocity since the Sil 7 sand was hard to be observed with the video camera. The pressure drop along the deposition was recorded through manometers. Last, the sand feeder was turned off but pure water continued to flow (the zero sediment concentration case) through the system for several hours until the deposition patterns no longer change, which showed the critical condition regarding the cessation of sediment movement. The final deposition height was recorded and the corresponding critical shear stress was obtained. The repeatability was tested for the whole experiment and the differences were less than 15%.

4.3. Results and discussions

4.3.1. Deposition growth patterns

In general, the growth of deposition can be divided into two stages: rapid growth (both deposition height and length increase) and equilibrium growth (only deposition length increases). Figure 4-2(a) shows the observed deposition growth patterns (for the scenario

consisting of the Sil 8/16 sand, 8.0 L/s flow rate, 0.2 g/L sediment concentration, and 2.0% slope case). At a flow rate of 8.0 L/s, the initial flow velocity before the deposition was 0.30 m/s, which corresponded to a bed shear stress of 0.22 N/m^2 (discussed in later section). This shear stress is smaller than the critical shear stress needed to mobilize the Sil 8/16 sand (1.16 N/m^2 discussed in later section). Thus, at this stage, all added sediment deposited and could not be transported downstream. As can be seen in Figure 4-2(a), the sediment mound rapidly grew in both longitudinal and vertical directions before 22 min. During this period, the bed shear stress at the top of the deposition increased with the increase of the actual flow velocity due to a larger deposition height. At 22 min, an equilibrium height (0.042 m) was reached which gave the bed shear stress of 1.95 N/m^2 (according to the calculation discussed in the later sections). This value is larger than the critical shear stress and is able to transport the sediment loading downstream. Therefore, afterwards the sediment mound only grew in a longitudinal direction. As we can see, the height of the sediment mound stayed at the same level at 22 min, 28 min and 34 min, while the length of the deposition increased at 0.325, 0.370 and 0.428 m, respectively.

Figure 4-2(b) shows the sediment movement pattern once the equilibrium height had been reached. Based on the observations, all sediment subsequently added (see the black dots in Figure 4-2(b)) into the system was picked up by the flow and then transported over the equilibrium height section. Finally, the additional sediment deposited on the downstream side of the deposition mound due to the lower bed shear stress there. During this period, the sand adding rate equaled the sediment transport rate over the equilibrium height section.

The sand feeder stopped adding sediment after 34 min with only clear water running. During the subsequent flushing period, the sediment mound moved in a downstream direction, and

the deposition height decreased with time and finally approached a terminal height of 0.034 m (compared to the earlier equilibrium height of 0.042 m) after a few hours. The sediment deposition also broke into several new sediment mounds (see Figure 4-2(c)), similar to sand dunes in alluvial channels and their heights decreased by 0.020 m with lengths less than 0.090 m. The corresponding bed shear stress at the top of the sediment mound decreased to 1.16 N/m^2 because of a lower mound height (discussed in the later sections). At the end of this last stage, no more sediment movement was observed over the deposition layer since the bed shear stress was slightly smaller than the critical shear stress.

4.3.2. Deposition height

Figure 4-3 shows the growth of the deposition height with time. Two stages (rapid growth and equilibrium growth) can be easily identified since the slope of the curves is steep during the first stage and becomes flat during the equilibrium growth stage. The sediment loading rate is an important factor for how long it will take for the equilibrium height to be established. For example, in Figure 4-3(e) with 8 L/s flow rate, it took 16 minutes for the equilibrium growth stage to set in at a 0.2 g/L sediment concentration, while it took only 8 minutes to establish the equilibrium growth stage at a 2.0 g/L sediment concentration. The equilibrium height varied significantly from 0.018 m to 0.058 m in Figure 4-3(e) in responding to different conditions. Note that the deposition height for Sil 7 and 0.2 g/L sediment concentration scenario was not observed since the bed shear stress is large enough to carry all sediment loading downstream.

Factors affecting the equilibrium height included the flow velocity, sediment concentration, pipe slope, and sediment size (see Figure 4-4). The flow velocity appeared to be the most

important factor influencing the equilibrium height. A larger flow velocity resulted in a smaller equilibrium height due to the larger bed shear stress. In Figure 4-4(a), the equilibrium height was 0.061 m versus a nominal velocity V_0 of 0.30 m/s. Here nominal velocity V_0 is defined as the average flow velocity in the clear pipe without the deposition. The equilibrium height decreased significantly to 0.015 m when the nominal velocity V_0 was increased to 0.75 m/s.

The sediment size also affected the equilibrium height as illustrated by the left and right columns of Figure 4-4. For example, for a sediment concentration of 2.0 g/L and a nominal velocity of 0.30 m/s, the equilibrium height was 0.061 m for the Sil 7 sand (Figure 4-4(c)), while it was 0.075 m for the Sil 8/16 sand (Figure 4-4(d)). The equilibrium height was smaller for finer particles since finer particles can be easily transported downstream. That is, for the same bed shear stress, fine particles display a higher transport rate compared to coarse particles.

In addition, a higher loading rate meant a larger transport capacity, which required a larger bed shear stress thus creating a higher equilibrium height. Therefore, the 2.0 g/L sediment concentration scenario had the highest equilibrium height among all scenarios. For example, in Figure 4-4(b) with a nominal velocity of 0.30 m/s, the equilibrium height was 0.086 m for the high loading scenario while it was 0.072 m for the low loading scenario.

The equilibrium height only slighted decreased with the increase of the pipe slope. For example, with the change of the pipe slope from 0.5% to 2.0% (see Figure 4-4(a) and 4-4(e)), the equilibrium height decreased from 0.061 m to 0.055 m for a sediment concentration of 2.0 g/L and a nominal velocity of 0.30 m/s. In summary, the flow velocity, sediment

concentration, sediment size, and pipe slope were shown to influence the magnitude of the equilibrium height.

4.3.3. Bed shear stress

As discussed above, the two growth stages reflect different bed shear stress conditions while the sand adding rate equaled the sediment transport rate during the equilibrium growth period. In this study, the bed shear stress that limiting the sediment deposition height during the equilibrium growth stage was studied. The deposition surface was flat according to the video tape. The momentum equation was used in the current study with the assumption that the cross section can be divided into two subsections: one related to the deposition bed and the other to the pipe wall (see Figure 4-5). These two subsections share the same flow velocity and the same energy head slope.

Assuming uniform flow where the mean flow velocity does not change over the control volume of length L (over equilibrium height section), the moment equation over the control volume for the water phase can be written as:

$$(P_1A - P_2A) - (\tau_w P_w L + \tau_b P_b L) + \rho g L A S = 0 \qquad \text{(Equation 4-1)}$$

where, ρ is the water density, g is the gravitational acceleration, A is the flow area, P is the wetted perimeter, S is the pipe slope, P_1 and P_2 are pressures at the pipe center, L is the control volume length, τ is the shear stress and subscripts w and b denote wall and bed components. After reorganizing Equation 4-1, the energy head slope can be written as follows:

$$I = \frac{\tau_w P_w + \tau_b P_b}{\rho g A} \qquad \text{(Equation 4-2)}$$

where, I is the energy head slope along the length of the control volume. Figure 4-6 shows the variation of the measured energy head slope (based on the manometer measurements) with the actual flow velocity (in the presence of deposition). The energy head slope increased from 0.21% to over 0.62% with the increase in the actual flow velocity from 0.33 to 0.81 m/s with a seemingly linear relationship.

The wall and bed shear stress can be expressed as (Perrusquía, 1991):

$$\tau_w = \frac{1}{8} f_w \rho V^2 \qquad \text{(Equation 4-3)}$$

$$\tau_b = \frac{1}{8} f_b \rho V^2 \qquad \text{(Equation 4-4)}$$

where, f_w is the friction factor of the pipe wall, f_b is the friction factor of the deposition, and V is the mean flow velocity with deposition. The explicit expression of Colebrook's equation was used to calculate the wall friction factor (Genić *et al*., 2011):

$$f_w = (1.14 - 2\log(e + \frac{21.25}{Re^{0.9}}))^{-2} \qquad \text{(Equation 4-5)}$$

where, e is the relative wall roughness, Re is the Reynolds number ($\frac{4VR_c}{\nu}$), with R_c being the composite hydraulic radius ($\frac{A}{P_b+P_w}$), and ν the kinematic viscosity. Figure 4-7(a) shows the calculated friction factor of the pipe wall. Note that the absolute roughness of the Plexiglas pipe is 0.0015 mm when calculating the friction factor of the pipe wall. As can be seen, f_w is a function of the Reynolds number: it decreases from 0.0205 to 0.0165 when the Reynolds number increases from around 50,000 to 140,000. When considering the roughness height of 0.4 mm and 1.8 mm (corresponding to the Sil 7 and Sil 8/16 sizes), the estimated friction

factor f_s using Eq. (5) is around 0.026 and 0.038 respectively, decreasing slightly with Reynolds number.

Once f_w of Plexiglas pipe is determined, the friction factor of the deposition f_b and the bed shear stress can be obtained from Equations 4-2 and 4-4. Figure 4-7(b) shows the relation between the obtained f_b and the Reynolds number. In addition, the results conducted by Ab Ghani (1993) were also compared to the current study. As can be seen in Figure 4-7(b), generally f_b decreased with the increase of Reynolds number. At a given nominal velocity (e.g., 0.30 m/s or a Reynolds number of about 60,000), the high sediment loading scenario could produce a larger f_b (from 0.153 to 0.185) than that of the low sediment loading scenario (from 0.058 to 0.112). This means that a larger shear stress was needed when the sediment loading increased. For a Reynolds number of about 90,000, f_b varied from 0.065 to 0.120 for high loading scenario, which was around 30% or 20% higher than that of medium and low loading scenarios. In the study by Ab Ghani (1993), f_b varied from 0.060 to 0.105, which was 10% less than that of low loading scenario. For a Reynolds number of about 140,000, f_b (0.080 to 0.120) was slightly smaller in the current study versus in the study by Ab Ghani. In general, the calculation method presented above can be considered valid, after the comparison with the results from the study by Ab Ghani (1993). Note that f_b is about 2 to 4 times larger than that purely due to the roughness height (f_s in Figure 4-7a) in this study. That is, in addition to the friction loss by the deposition roughness, a significantly more energy loss was needed by transporting sediment along the deposition.

Figure 4-8 shows the relationship between the bed shear stress and the actual velocity. Previous studies were compared to the current study (Perrusquía, 1991; Le Bouteiller and Venditti, 2015). In the current study, the bed shear stress increased from around 1.5 N/m^2 to

8.7 N/m^2 when the actual velocity increased from 0.30 to 0.80 m/s. The low loading scenario had smaller bed shear stresses while the high loading scenario could observe much larger bed shear stresses. The particle size has limited impacts on the bed shear stress. In the study by Perrusquía (1991), the bed shear stress range varied from 1.0 N/m^2 to 4.0 N/m^2, which is smaller than what was observed in the current study. This is due to the sediment loading difference (the current study doubled the sediment loading). Le Bouteiller and Venditti (2015) conducted flume experiments to study the bed shear stress near the vegetation layer. Their results on the bed shear stress were from 2.0 to 4.0 N/m^2 at a small flow velocity range of 0.2 to 0.3 m/s. This was mainly due to the larger friction factors created by the vegetation layer, which showed a larger energy loss.

After the equilibrium stage, pure water continued to flow through the system for several hours until the deposition patterns no longer change, which showed the critical condition regarding the cessation of sediment movement. The terminal deposition height was recorded with the energy head slope along the deposition. Followed the bed shear stress calculation method in the above section, the critical shear stress of the Sil 7 sand was 0.22 N/m^2 (terminal height 0.015 m, energy head slope 0.06%, and flow rate 8.0 L/s). The critical shear stress of the Sil 8/16 sand was 1.16 N/m^2 (terminal height 0.034 m, energy head slope 0.11%, and flow rate 8.0 L/s). The critical shear stresses of the Sil 7 and Sil 8/16 sand were 0.22 and 1.22 N/m^2 respectively, which could be obtained through the Shields diagram (Shields, 1936). The calculated results of this study were close to that of the Shields diagram.

Note that the dimensionless shear stress (θ_b) and the dimensionless particle size (D^*) were commonly used to describe the critical condition of sediment movement. They are defined as:

$$\theta_b = \frac{\tau_b}{(s-1)d_{50}\rho g} \quad \text{(Equation 4-6)}$$

$$D^* = d_{50}\sqrt[3]{\frac{(s-1)g}{\nu^2}} \quad \text{(Equation 4-7)}$$

where, s is the specific gravity of sand.

Figure 4-9 presents the relationship between the dimensionless bed shear stress and the dimensionless particle size. The Shields diagram (Shields, 1936) and the initiation of suspension diagram (Bagnold, 1966) are plotted in Figure 4-9 showing the initiation of the bed load and the suspended load, respectively. In the zone above the initiation of suspension diagram, the bed shear stress is large enough to transport sediment as suspended load. Two tests of the Sil 7 sand are in the suspended load zone with larger bed shear stresses. Note that these two tests were not considered in the later bed load equation. In the zone between the Shields diagram and the initiation of suspension diagram, the bed shear stress transports sediment as bed load. The ranges of the dimensionless bed shear stress from previous studies (Graf and Acaroglu, 1968; Novak and Nalluri, 1984; Safari *et al*., 2015) and the current study are plotted in Figure 4-9. All of them located in the zone of bed load transport except for the above two tests with the Sil 7 sand. It appears that the Shields diagram can be applied for pipe flow conditions since the values of the dimensionless critical shear stress (labeled as 0.4, 0.9, 1.8, and 2.5 mm critical) closely resemble the Shields diagram. For example, θ_b is 0.034 and 0.040 for the Sil 7 and Sil 8/16 sand from this study, while θ_b is 0.034 and 0.042 from the Shields diagram.

4.3.4. Bed load transport

As discussed in the previous sections, the sediment transport rate equaled the sand adding rate after the equilibrium height had been reached. The sediment transport rate per unit width of the bottom sediment bed (q_s=$CQ/1000P_b$, kg/m/s, where C is the sediment concentration and Q is the flow rate) is commonly used to describe the bed load transport (Ab Ghani, 1993). Figure 4-10 shows the relationship between q_s and the bed shear stress based on data sitting in the bed load zone. As can be seen, the bed shear stress increased from 1.5 N/m^2 to 8.7 N/m^2 and q_s increased from 0.010 kg/m/s to around 0.470 kg/m/s. Moreover, the high loading scenario needs larger bed shear stresses.

In the literature, Graf and Acaroglu (1968) introduced a method to describe the bed load transport. They developed a bed load model using two dimensionless parameters: the dimensionless bed shear stress (θ_b) and the dimensionless transport parameter (ϕ). The bed load equation was expressed as:

$$\phi = a\,{\theta_b}^b \qquad \text{(Equation 4-8)}$$

where, $\phi = q_s/\rho\sqrt{(s-1)gd_{50}^3}$, a and b are coefficients. The experimental data from the current study and two previous models are plotted in Figure 4-11. As can be seen from Figure 4-11, the fitted curve from the current study (R^2=0.93) displays a similar trend as in the previous studies. The increase in the bed shear stress is expected to result in a higher transport rate. The Sil 7 with high loading scenario (black squares) had the highest bed load transport capacity. The Sil 8/16 sand was more difficult to be transported comparing to the Sil 7 sand since the values of the dimensionless transport parameter were significantly smaller than that of the Sil 7 sand. Different bed load models are summarized in Table 4-2.

4.3.5. Sediment saltation velocity

The sediment saltation velocity during bed load transport was obtained from the experiments as well. For an initial flow velocity of 0.3 m/s, the sediment saltation velocity was from 0.15 m/s to 0.25 m/s. When the initial flow velocity increased to 0.5 m/s, the sediment saltation velocity increased to around 0.35 m/s. As the initial velocity further increased to 0.75 m/s, the sediment saltation velocity reached about 0.55 m/s. According to the literature (Lee and Hsu, 1994), the sediment saltation velocity (V_p) can be expressed as:

$$\frac{V_p}{u^*} = a\, D^{*b}\, T^{*c} \qquad \text{(Equation 4-9)}$$

where, $u^* = \sqrt{\tau_b/\rho}$ is the shear velocity; T^* is the dimensionless bed shear parameter ($\frac{\tau_b - \tau_c}{\tau_c}$) with τ_c being the critical shear stress determined by the Shields diagram and a, b, & c are coefficients.

Figure 4-12 shows the relationship between the dimensionless saltation velocity and the dimensionless bed shear parameter. The study of Lee and Hsu (1994) gave larger saltation velocities compared to the current study. This is mainly due to the deposition roughness, which reduced the saltation velocity in this study. As can be seen from Figure 4-12, with an increase of the dimensionless bed shear stress, the particle velocity increases. An expression was developed based on the experimental data (R^2=0.72), which can be used to predict the sediment saltation velocity in pipes in the presence of deposition:

$$\frac{V_p}{u^*} = 1.87 D^{*0.17}\, T^{*0.36} \qquad \text{(Equation 4-10)}$$

4.3.6. Application: predicting equilibrium height

In order to present the prediction processes on the equilibrium height, a calculation example was applied with some assumed values, which can be commonly found in the field: the sediment concentration varies from 0.2 to 2.0 g/L, the median sediment size is 1.8 mm, the specific density of sand is 2.65, the concrete storm sewer pipe is 1.0 m in diameter, and the flow rate range is from 200 to 500 L/s. Table 4-3 shows the equations for solving the equilibrium height. All listed variables are related to the equilibrium height (H). The bed shear stress can be expressed by substituting nine variables (No. 1 - No. 9) into No. 10, and substituting three variables No. 11, 12, and 13 into No. 14. Equaling No. 10 and No. 14 solves for H. The equilibrium height results are plotted in Figure 4-13. The equilibrium height decreases with the increase of flow rate. Specifically, in the low loading scenario, the equilibrium height decreases from 0.51 to 0.20 m, when the flow rate increases from 200 to 500 L/s. The increase of sediment loading increases the equilibrium height. At 500 L/s, the equilibrium height for the low loading scenario is 0.20 m, while it can reach 0.51 m for the high loading scenario.

Applications to submerged storm sewers were developed: one on the deposition height prediction with different particle sizes and sediment concentration, and the other on the minimum flow velocity for controlling deposition height with different pipe sizes. In the first application, the given parameters included the pipe size (1.0 m), the particle d_{50} sizes (2.0, 1.5, 1.0, and 0.5 mm at 0, 10, 20, and 30 m away from the upstream end of the pipe, respectively), the sediment concentration (0.2, 1.1, and 2.0 g/L), and the flow rate (200 L/s). The predicted deposition heights can be calculated following Table 4-3 and values are plotted in Figure 4-14(a). The higher sediment loading resulted in the higher deposition height. The

deposition height was about 0.75 m for the high sediment loading scenario, while it reached around 0.55 m for the low sediment loading scenario. The deposition height decreased in the flow direction due to the decrease of sediment sizes.

In the second application, the given parameters included the pipe sizes (0.5, 1.0. and 2.0 m), the particle d_{50} (1.0 mm), the sediment concentration (0.2 g/L). The minimum flow velocity for controlling deposition height can be calculated following Table 4-3 for different relative deposition height (*H/D*). Predicted values are plotted in Figure 4-14(b). In a 2.0 m diameter pipe, the minimum flow velocity decreased from 1.78 m/s to 1.30 m/s as *H/D* increased from 2% to 10%. While in a 0.5 m diameter pipe, the minimum flow velocity was almost half of that in a 2.0 m diameter pipe.

4.4. Chapter summary

In this study, deposition growth processes were studied in a submerged storm sewer pipe. The tested particle sizes were 0.4 mm and 1.8 mm. The flow rate range was from 8.0 to 19.9 L/s in a 0.184 diameter Plexiglas pipe with a pre-determined sediment concentration up to 2.0 g/L. The growth of the deposition appears to have two stages: a rapid growth stage followed by an equilibrium growth stage. The sediment loading rate determines the duration of the rapid growth stage. The initial bed shear stress in a clean pipe is 0.22 N/m^2 (the pipe roughness is 0.0015 mm and the nominal velocity is 0.30 m/s). With the continuous sand adding (0.2 g/L of Sil 8/16 sand) and the increase of deposition height, the bed shear stress gradually increased to a larger bed shear stress (1.95 N/m^2 at 0.042 m deposition height). Once the equilibrium height was reached, the sediment transport rate equaled the sediment loading rate.

Several parameters including the sediment size, sediment concentration, pipe slope, as well as flow velocity influence the equilibrium height. The bed friction factor varied from 0.058 to 0.185, which is about 2 – 4 times larger than that caused by the sediment roughness height alone (0.026 and 0.039 for sediment size of 0.4 mm and 1.8 mm, respectively). The increased bed friction factor is due to the significantly increased energy loss to transport the required sediment loading. The bed shear stress obtained from this study varies from 1.8 to 8.7 N/m^2, varying with flow velocity and sediment loading. The Shields diagram and bed load equations were shown to be valid in submerged pipe conditions in the presence of deposition. The sediment saltation velocity is a function of the particle size, shear velocity and dimensionless shear stress. The results of this study have also been applied to estimate the equilibrium height and the minimum flow velocity for controlling deposition height in submerged storm sewers.

Various recommendations are offered for future research. First, the application for different pipe shapes (e.g., rectangular or egg shaped) and pipe sizes should be investigated. Second, cohesive materials should be tested. Moreover, field investigations confirming the sediment growth should be conducted. Finally, the presence of intermittent flow regimes typical for storm sewer systems should be evaluated for the methodology to represent real-life circumstances.

Table 4-1. Experimental parameters and ranges

Parameter	Value
Pipe slope (S)	0.5%, 1.0%, and 2.0%
Sediment medium size (d_{50}: mm)	0.4 and 1.8
Flow rate (Q: L/s)	8.0, 13.3, and 19.9
Sediment concentration (C: g/L)	0, 0.2, 1.1 and 2.0

Table 4-2. Bed load models

Expressions	Conditions	Reference
$\boldsymbol{\phi = 10.39\ \theta_b^{2.52}}$	With deposition, a general curve for different studies	Graf and Acaroglu, 1968
$\boldsymbol{\phi = 11.6\ \theta_b^{2.04}}$	No deposition, D = 0.305 m, 1.3% slope, 0.1 < C < 1.0 g/L	Novak and Nalluri, 1984
$\boldsymbol{\phi = 10.57\ \theta_b^{1.78}}$	With deposition, D = 0.184 m, 0.5 – 2% slope, 0.2 < C < 2.0 g/L	Current study

Table 4-3. Calculation equations for solving the equilibrium height

No.	Variable	Equation	Note
1	α	$cos^{-1}(1\text{-}2H/D)$	*D=1.0 m*
2	P_b	$D \cdot sin\ \alpha$	
3	P_w	$(\pi - \alpha)D$	
4	*A*	$\frac{\pi D^2}{4} - \frac{D^2}{4}(\alpha - \sin\alpha \cdot cos\ \alpha)$	
5	*V*	$\frac{Q}{1000A}$	*Q=200 - 500 L/s*
6	R_c	$\frac{A}{P_w + P_b}$	
7	*Re*	$\frac{4VRc}{\nu}$	ν*=1.00×10*$^{-6}$ *m*^{2}*/s*
8	f_s	$(1.14 - 2log\ (e + \frac{21.25}{Re^{0.9}}))^{-2}$	*e=0.0018 (corresponding to roughness: d_{50}=1.8 mm)*
9	f_b	$3\ f_s$	*A coefficient is within the range (2 - 4)**
10	$\boldsymbol{\tau_b}$	$\boldsymbol{\frac{1}{8} f_b \rho V^2}$	ρ*=1000 kg/m*^{3}
11	q_s	$\frac{CQ}{1000P_b}$	*C=0.2 - 2.0 g/L*
12	ϕ	$\frac{q_s}{\rho\sqrt{(s-1)g d_{50}^3}}$	*g=9.81 m/s*^{2}*, s=2.65*
13	θ_b	$0.27\ \phi^{0.56}$	
14	$\boldsymbol{\tau_b}$	$\boldsymbol{\theta_b (s-1) d_{50} \rho g}$	

* Based on the experimental results, f_b is 2 to 4 times that of f_s in this study.

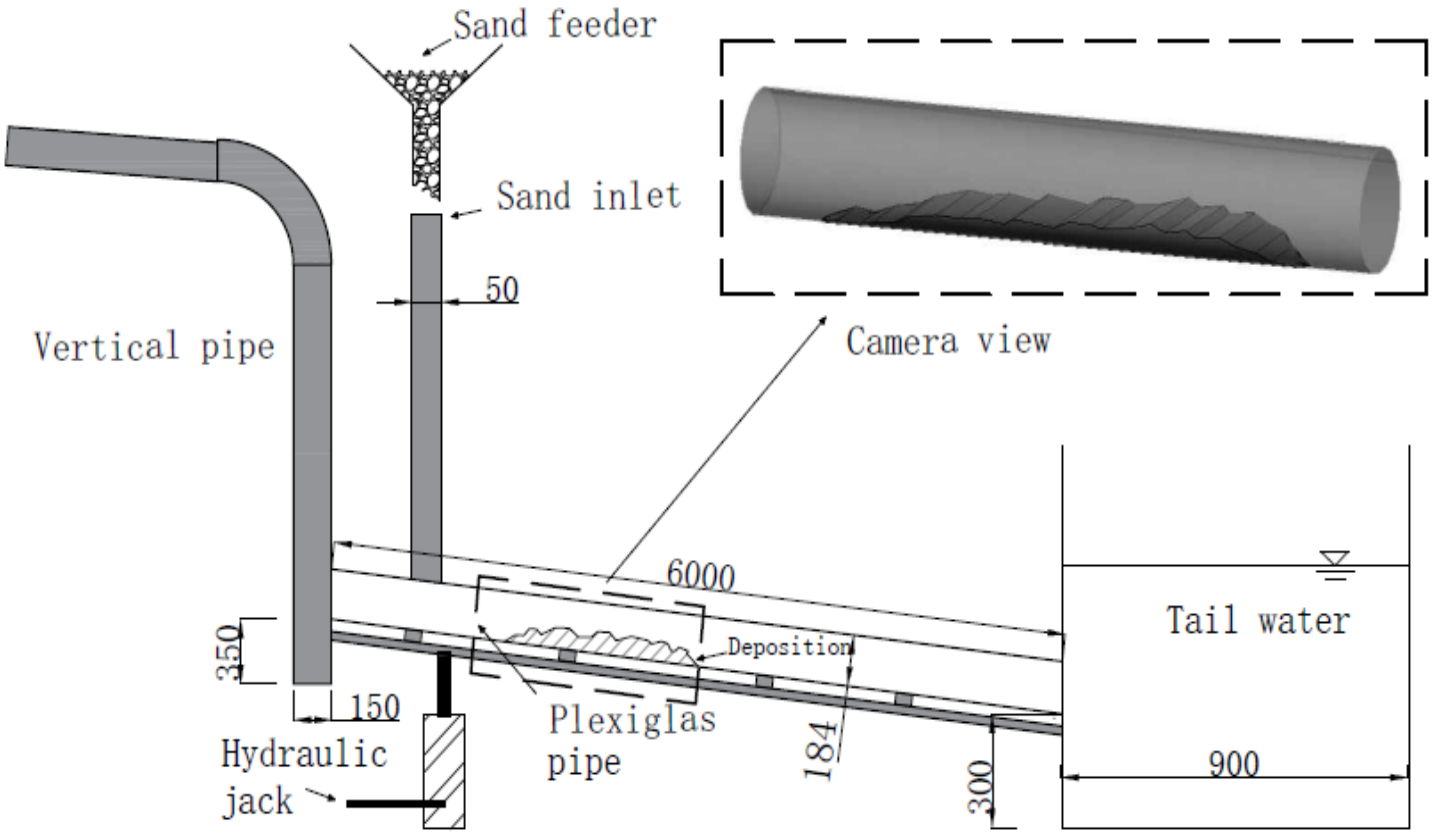

Figure 4-1. Experimental setup and sketch of sediment deposition (unit: mm)

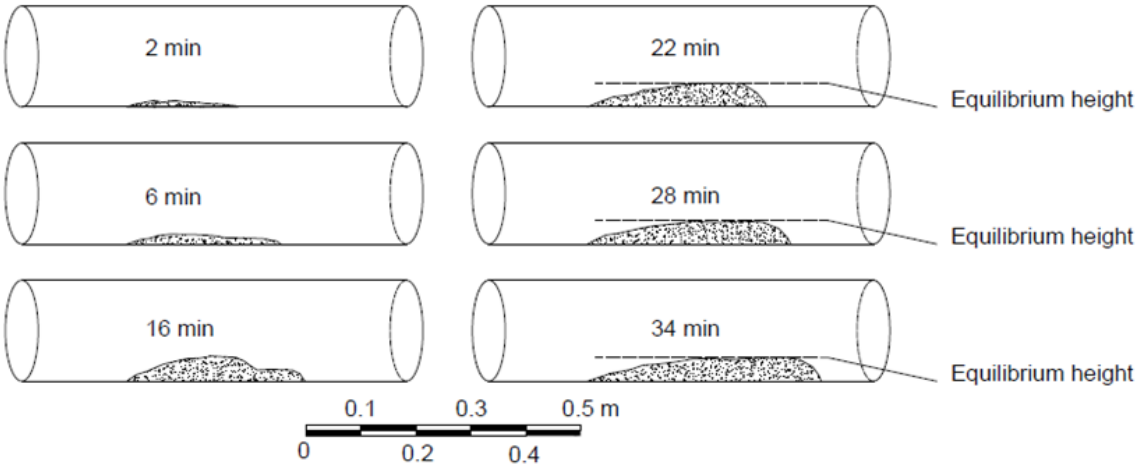

(a) Sediment deposition growth

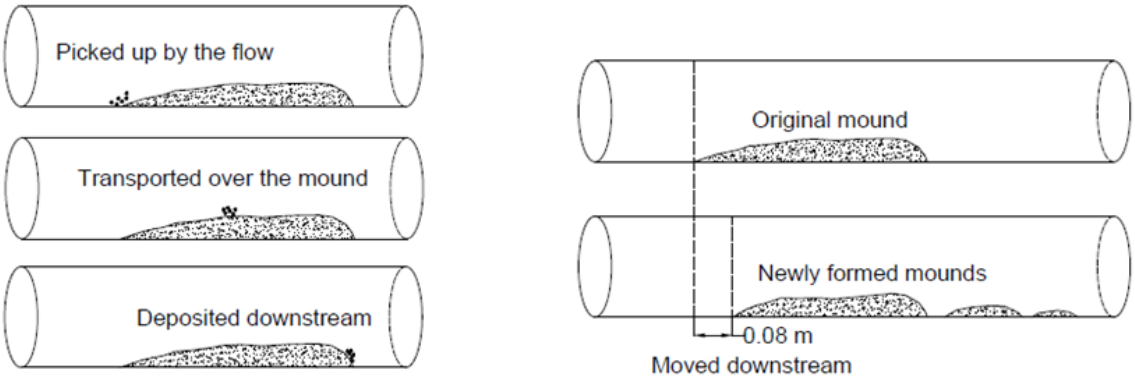

(b) Sediment movement pattern (c) Deposition mound change with water flushing

Figure 4-2. Sediment deposition patterns (8.0 L/s flow rate, 0.2 g/L sediment concentration, 1.0% pipe slope, and Sil 8/16 sand)

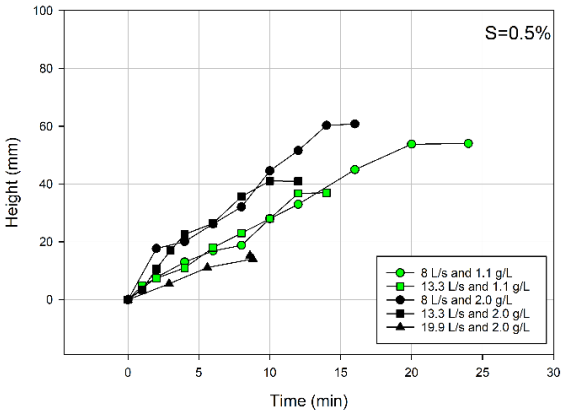

(a) Sil 7 sand 0.5% slope

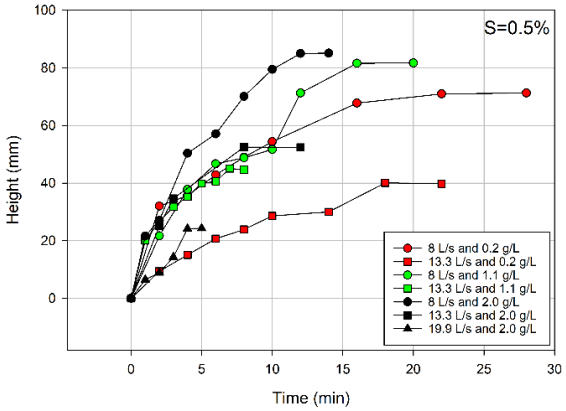

(d) Sil 8/16 sand 0.5% slope

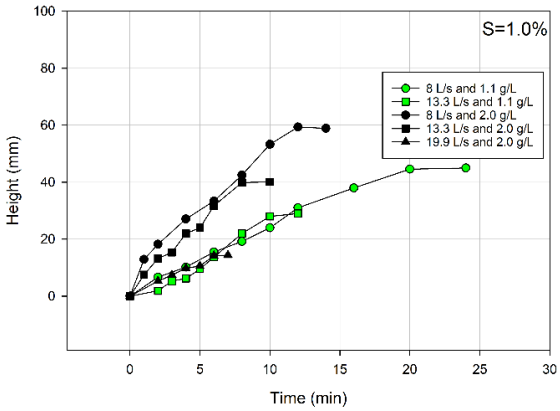

(b) Sil 7 sand 1.0% slope

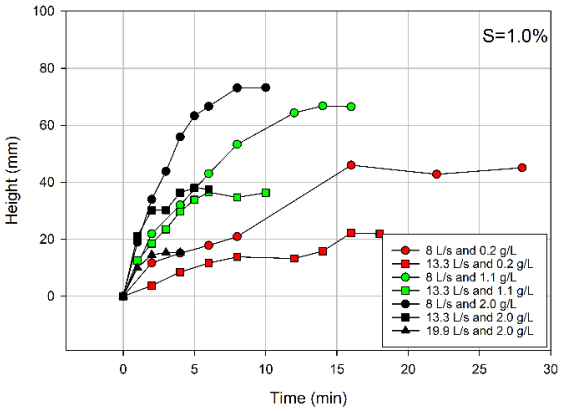

(e) Sil 8/16 sand 1.0% slope

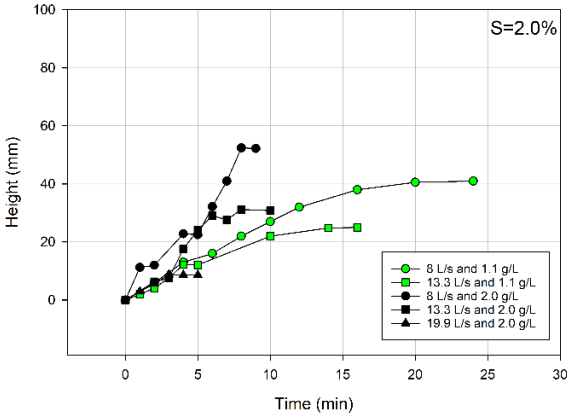

(c) Sil 7 sand 2.0% slope

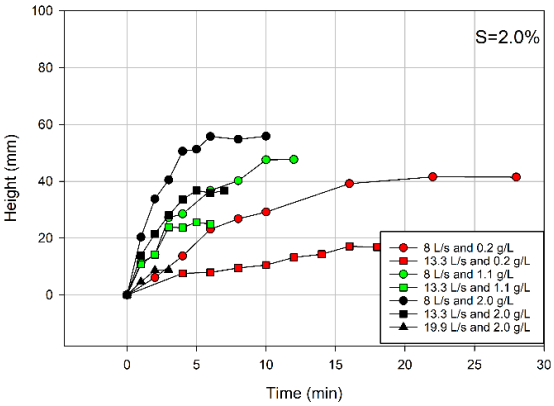

(f) Sil 8/16 sand 2.0% slope

Figure 4-3. Deposition height growth under different conditions

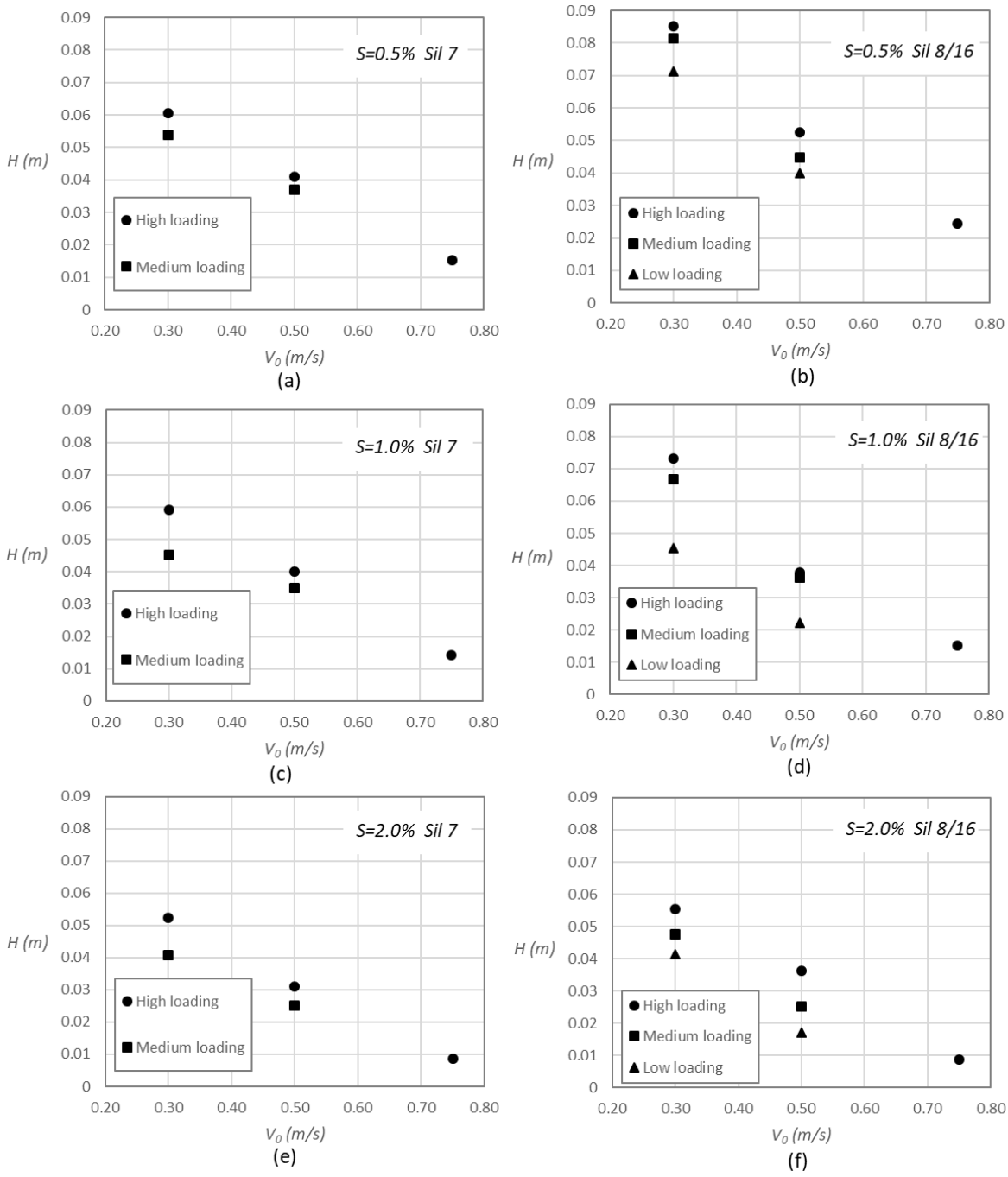

Figure 4-4. Equilibrium height (H) compared to nominal velocity (V_0) under different conditions

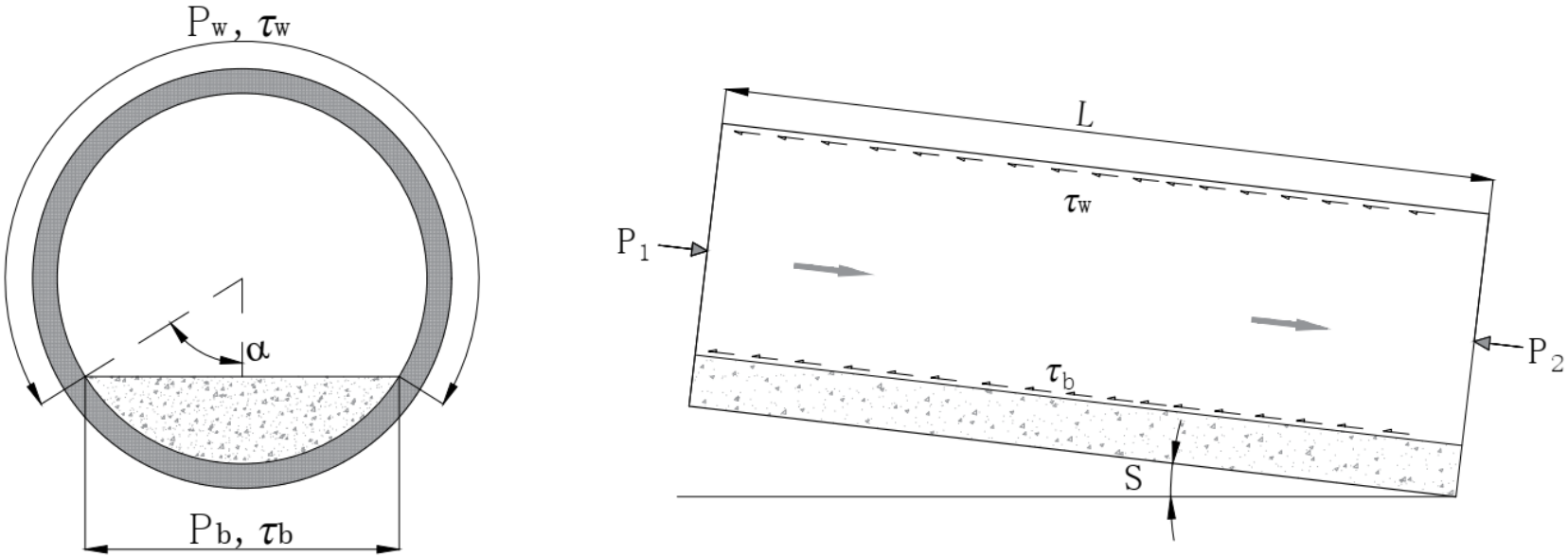

Figure 4-5. Sketch for control volume

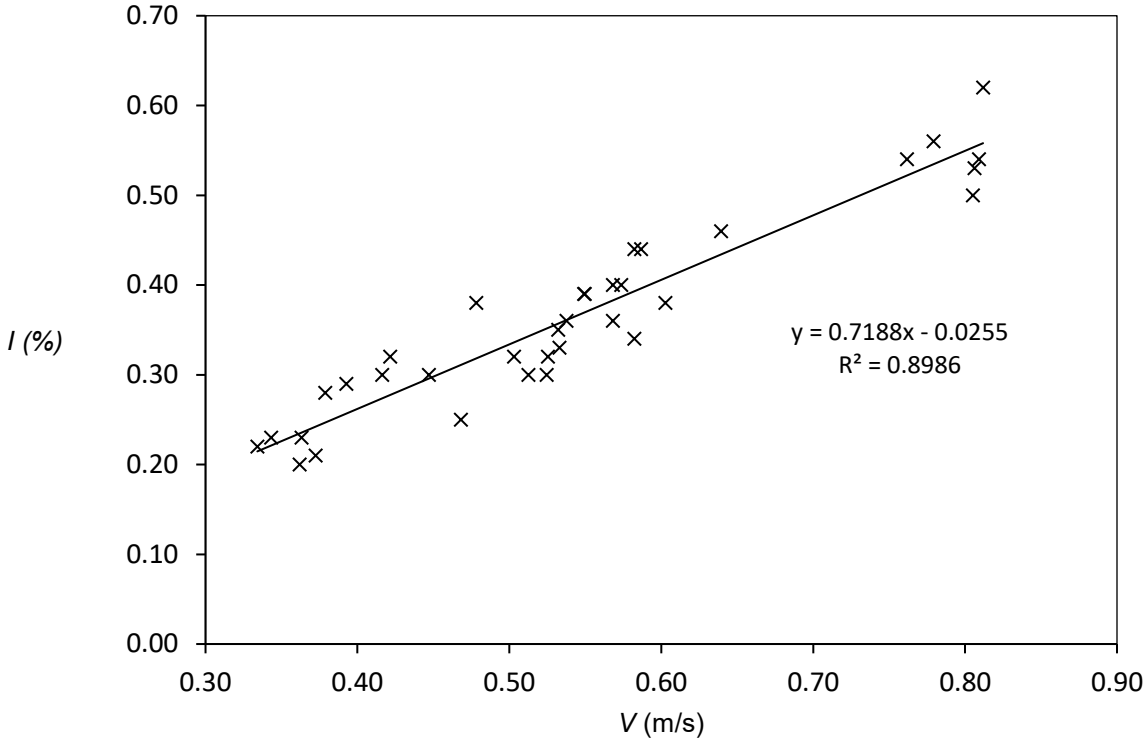

Figure 4-6. Relationship between measured energy head slope (I) and actual average flow velocity (V)

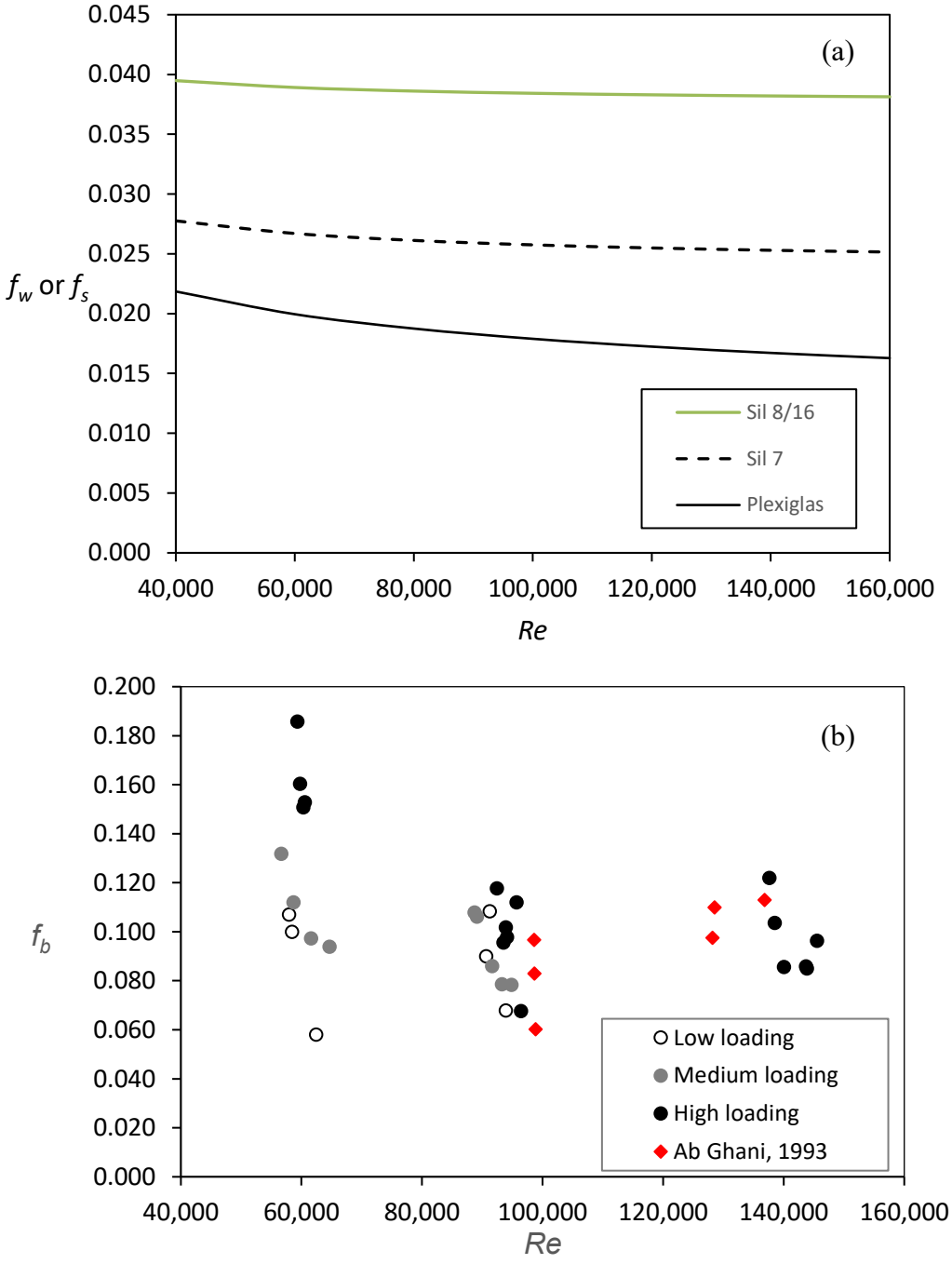

Figure 4-7. Relationship between wall friction factor or bed friction factor (f_w or f_b) and Reynolds number (Re)

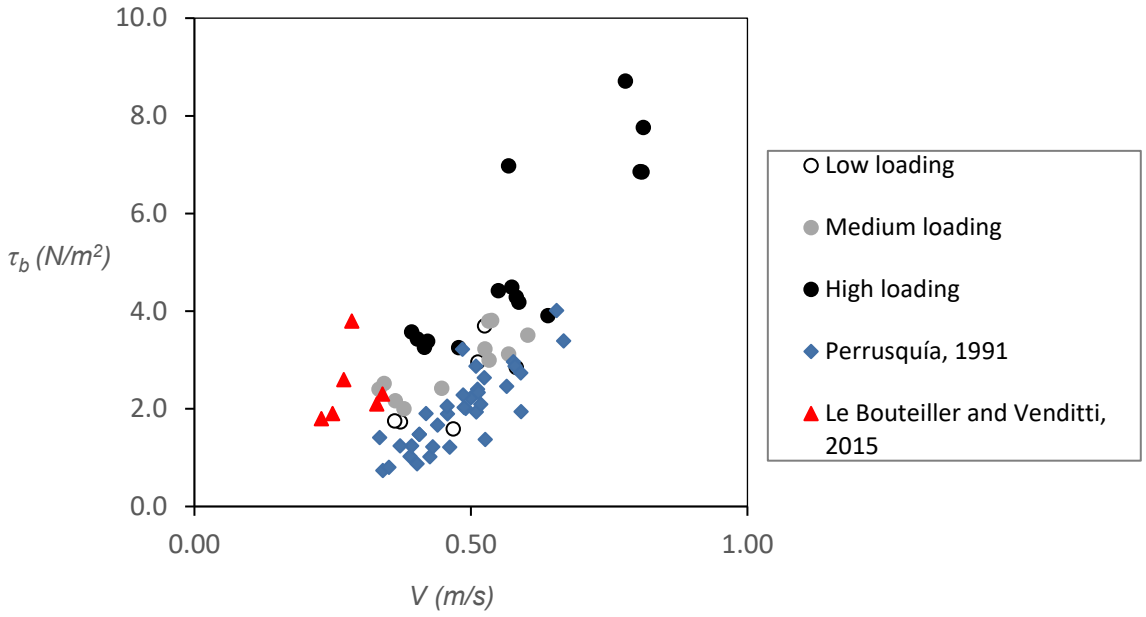

Figure 4-8. Relationship between bed shear stress (τ_b) and actual average flow velocity (V)

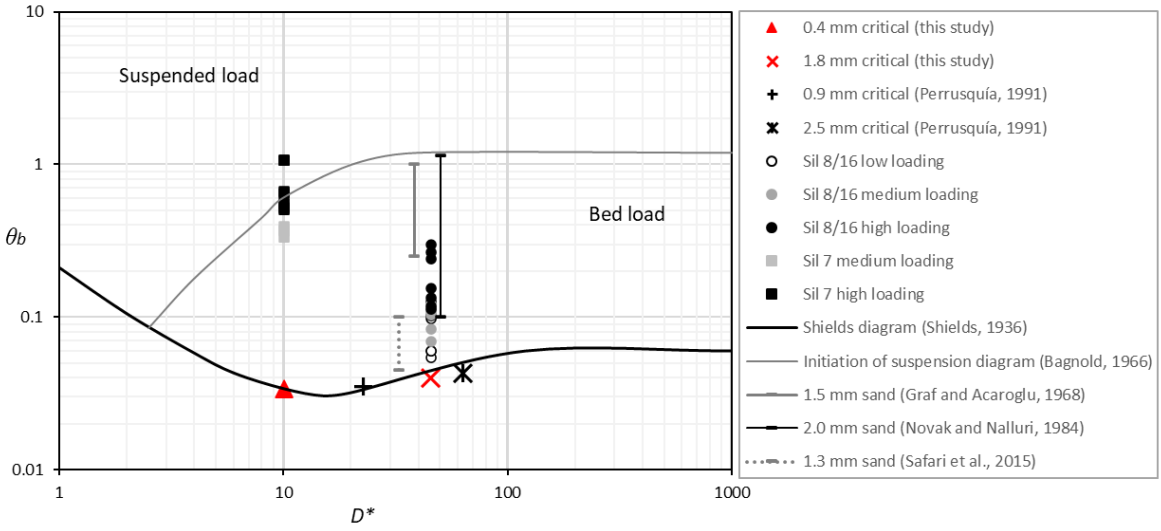

Figure 4-9. Relationship between dimensionless bed shear stress (θ_b) and dimensionless particle size (D^*) in different studies

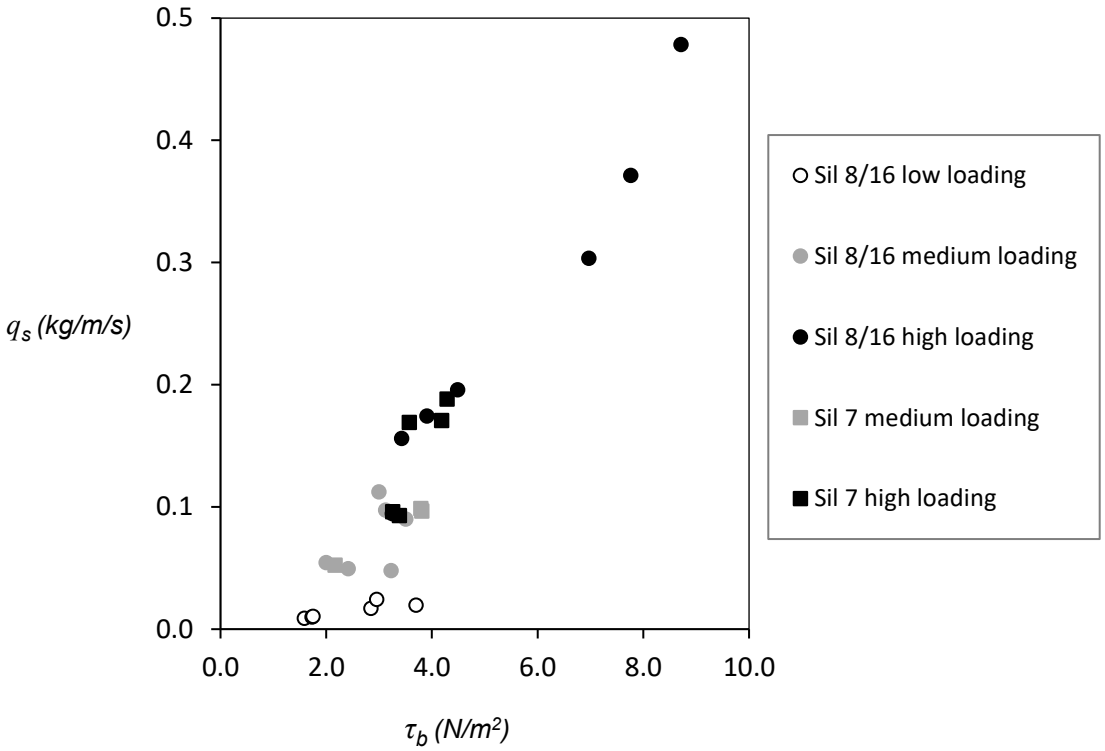

Figure 4-10. Relationship between transport rate per unit width (q_s) and bed shear stress (τ_b)

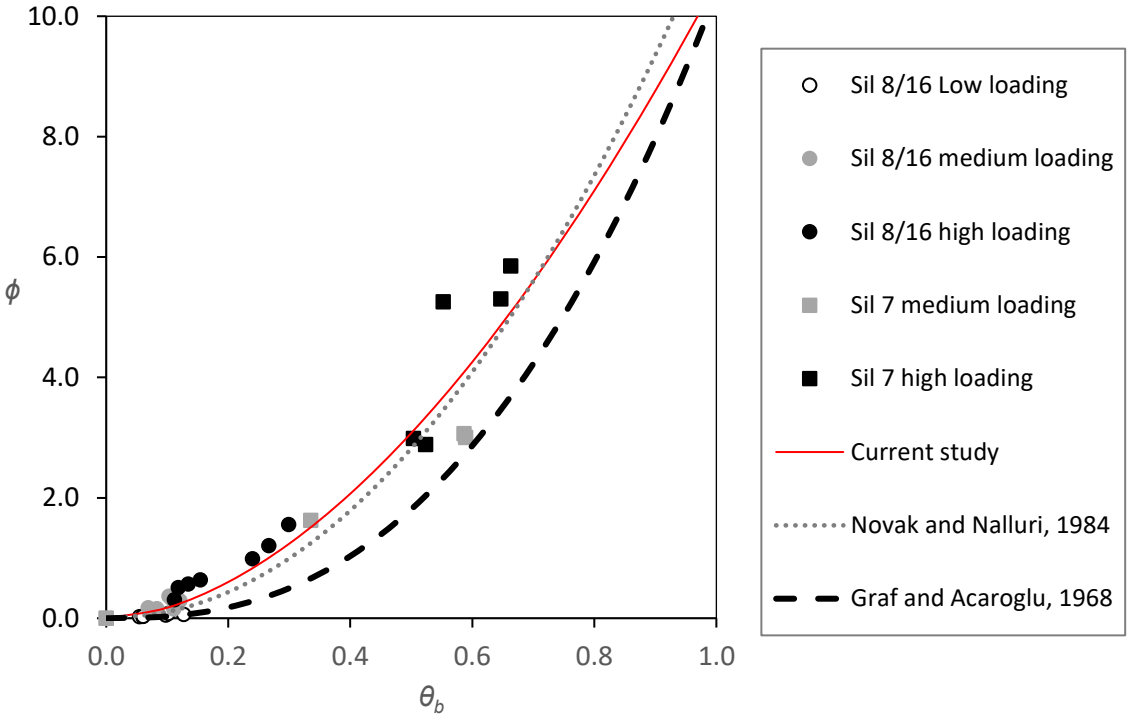

Figure 4-11. Bed load models and experimental data

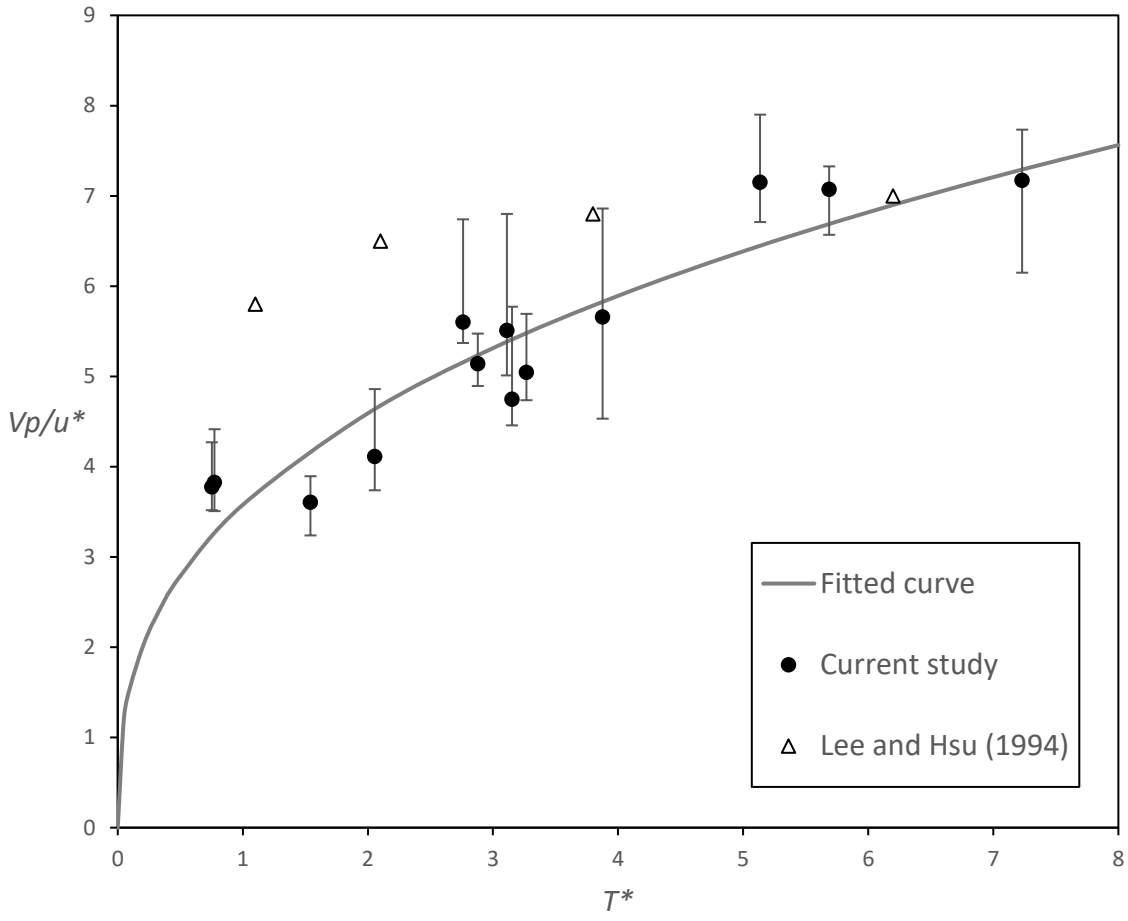

Figure 4-12. Dimensionless saltation velocity (V_p/u^*) compared to dimensionless bed shear parameter (T^*)

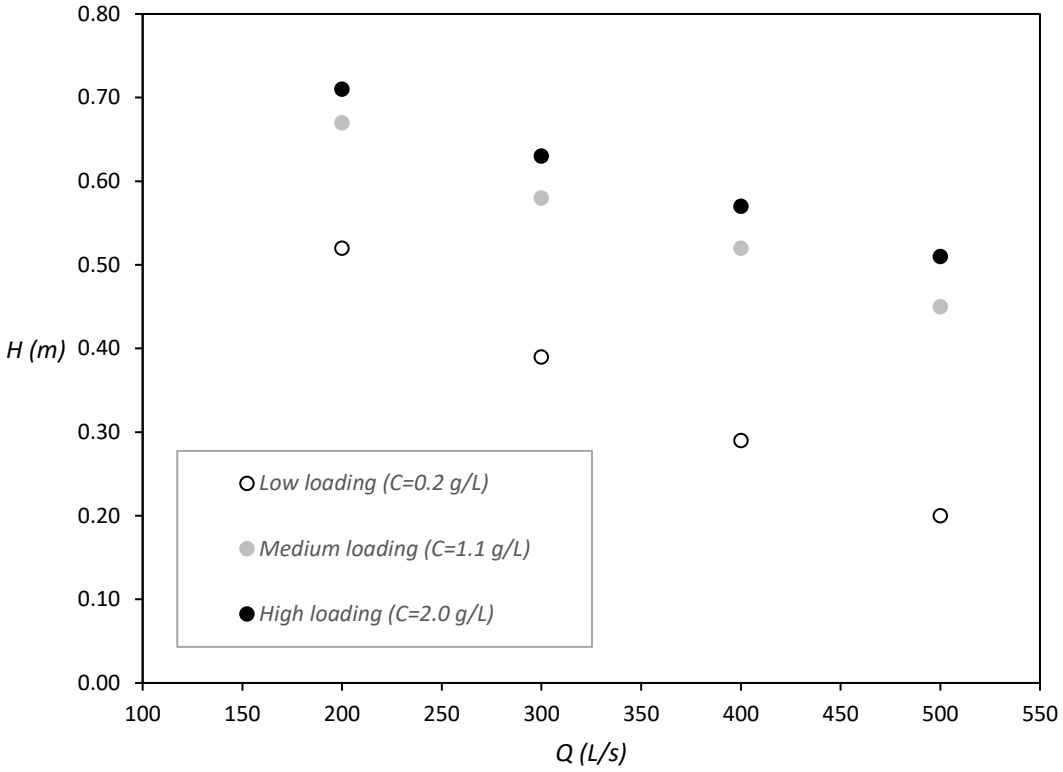

Figure 4-13. Equilibrium height (H) prediction with different flow rates (Q) and sediment concentration (C)

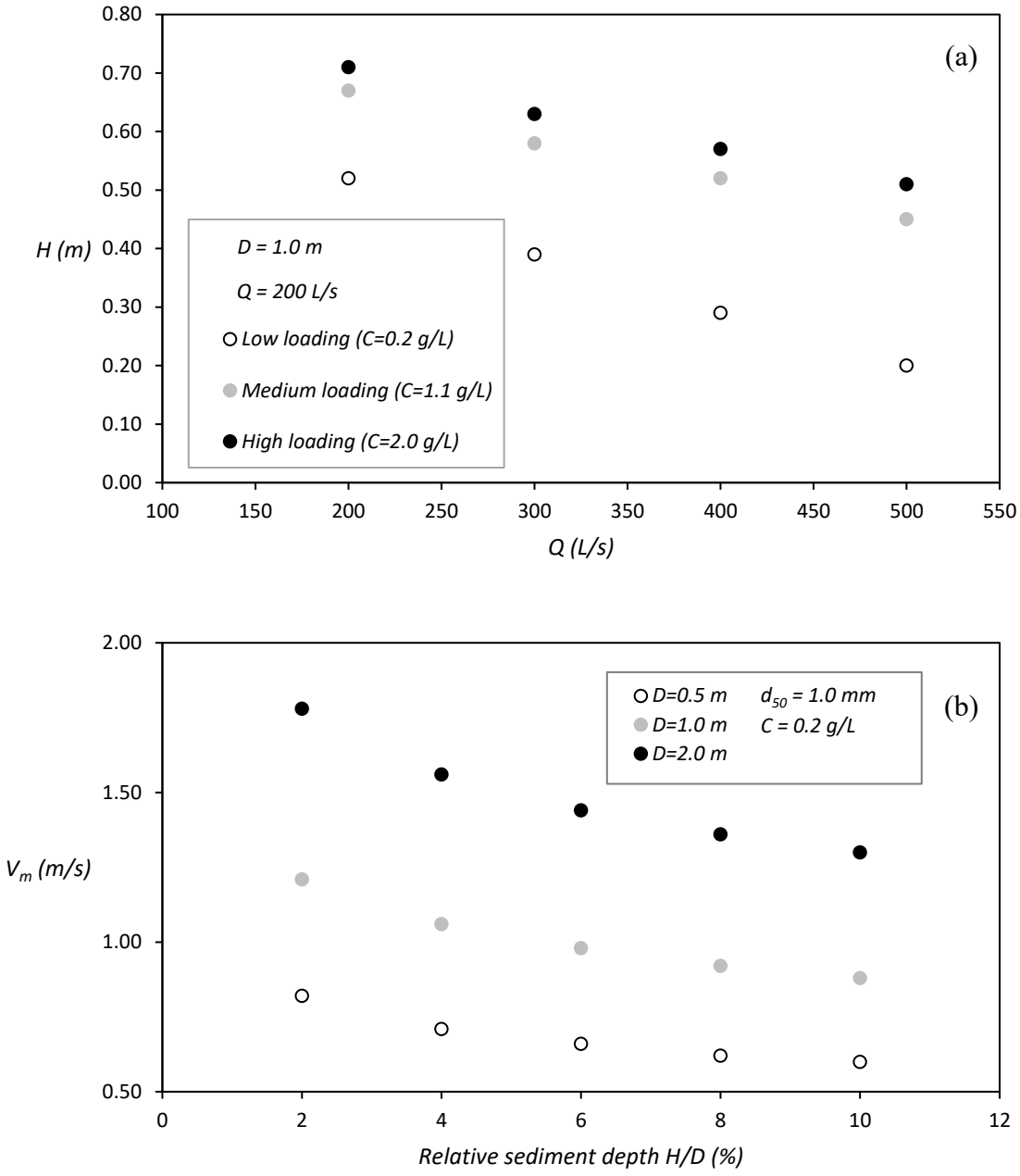

Figure 4-14. (a) Variations on equilibrium height (H) with distance in a submerged pipe (particle sizes: 2.0, 1.5, 1.0, and 0.5 mm at 0, 10, 20, and 30 m away from the upstream end of the pipe); (b) Minimum flow velocity for controlling deposition height (V_m) as a function of relative sediment depth (H/D)

Chapter 5. Erosion on Cohesive Deposition in Storm Sewers

Erosion of sediment deposition in storm sewers is dominated by the bed shear stress and the deposition characteristics. A laboratory study investigated the critical shear stress and the erosion processes for different types of deposition in storm sewers. The critical shear stress increased from 0.19 N/m^2 to 0.41 N/m^2 for the 0.4 mm sand when the weight content of silt-clay changed from 0% to 20%, while the critical shear stress increased from 0.98 N/m^2 to 1.98 N/m^2 for the 1.8 mm sand deposition. A prediction method for the critical shear stress was developed based on the particle size and silt-clay content. The erosion patterns can be classified as ripple surface, dune surface, flat surface, and rugged surface, mainly determined by the cohesive effect, particle size, and bed shear stress. The erosion rate is a function of the sediment transport rate per unit width and particle transport distance. A field sampling program was conducted to obtain sediment deposition characteristics in a storm trunk sewer. Based on the sediment characteristics and the estimated flow rate, the predicted deposition profile using the method developed in this study compared well with the field measurements.

5.1. Introduction

Sediment deposition in storm sewers can cause pipe blockage and increase the possibility of urban flooding during major storm events. The deposition occurs during the more frequent, less severe storm events, and consolidates during dry weather conditions. For non-cohesive deposition, the initiation of erosion is determined by the critical shear stress, which is mainly a function of the sediment size. Due to the different sources of storm sewer sediment, the deposited particles range from clay and silts (micrometer size) to gravels (millimeter size) (Selbig and Bannerman, 2011). Construction sites are notorious for generating very fine silt-

clay sediment during even minor rainfall events (Boogaard *et al*., 2014). When the clay content is over 5%, the mixture of sand and clay becomes cohesive, and the cohesive material provides additional resistance to erosion which may lead to permanent deposition (Jain and Kothyari, 2009). The magnitude of the silt-clay content is an important factor in determining the critical shear stress and the consolidation of the deposited materials (Alvarez-Hernandez, 1990). This consolidation can form large chunks during the dry weather conditions between storm events (Huygens and Tito, 1994). Li *et al.* (2013) reported that it takes about 10 days for the consolidation to be fully developed. In a storm sewer field study by Xu *et al.* (2017), massive chunks were observed in the deposition and they prevented the deposition being further eroded.

Sewer flushing is often applied in storm sewers to erode bottom depositions (Pisano *et al.*, 2003; Campisano *et al*., 2004; Fan, 2004). The flushing process consists of the erosion of the deposited materials and the transport of the eroded sediment. Previous flume experiments were conducted to study the erosion rate or the pick-up rate of non-cohesive sediment under flushing conditions. Various equations were presented to describe the erosion capacity (Fernandez-Luque, 1974; Nagakawa and Tsujimoto, 1980; Van Rijn, 1984). The erosion rate is a function of the bed shear stress and sediment size, and can be calculated as a function of the transport rate per unit width and sediment saltation distance (Van Rijn, 1984). However, studies pertaining to the erosion of sediment in sewer pipes are limited. Campisano *et al*. (2004) studied the erosion of non-cohesive deposition in flumes, and reported that sufficiently high flow velocities and shear stresses can scour and transport the sewer deposits. Campisano *et al.* (2008) and Todeschini *et al*. (2010) studied the erosion of cohesive soft

materials without consolidation effects. Both studies demonstrated that with an increase in clay content, the magnitude of the critical shear stress increased.

As for deposition patterns, Simons and Senturk (1977) summarized potential bed form depositions as flat beds, ripples, or dunes. When the bed shear stress is small, the bed form has a flat bed pattern. With an increase of the shear stress or the sediment transport capacity, the bed form changes into ripples or dunes. Sand less than 0.7 mm in diameter can form ripples with a height less than 5 cm. Sand larger than 0.7 mm in diameter can form sand dunes with relatively large dimensions. With respect to field studies about deposition patterns, the majority of the research has focused on sanitary and combined systems (Ashley *et al.*, 2005). Verbanck (1992) investigated the deposition characteristics in a combined sewer in Brussel, Belgium. The total volume of the deposition in the network appeared to be influenced by the magnitude of the rainfall events and human sewer-cleaning practices. A field study on a combined sewer system by Laplace et al. (1992) showed that the sediment volume increased asymptotically with time, meaning that the sediment accumulation was slowed down due to increased erosion capacity at certain flow rates. Few studies have been conducted pertaining to the deposition characteristics in storm sewer systems. The absence of regular flushing flows and the potential for the formation of massive chunks that resist erosion add significance to this work (Xu et al., 2017).

In this current study, laboratory experiments were conducted to study the initiation of erosion and associated critical shear stress as a function of various parameters (i.e., flow rate, sediment size, and presence of non-cohesive sand and cohesive materials). A method for predicting the magnitude of the critical shear stress was subsequently developed. The deposition patterns and erosion processes were examined and the erosion rate was studied

for different flow rates and deposition characteristics. A prediction method was developed for the erosion rate. In addition, a field sampling program was conducted to obtain the sediment deposition characteristics in an actual storm trunk sewer, and to verify the method developed in this study.

5.2. Methodology

This study was composed of two parts: a laboratory experiment to study the erosion processes for different deposition types and a field sampling program to collect information about the deposition in an actual storm trunk sewer. Figure 5-1 shows the experimental set-up. The 8.0 m long 0.20 m diameter Plexiglas pipe was set at a 0.25% slope and had an opening on top and a bed load trap at the downstream end. The deposition was set at 0.04 m thick (corresponding to a 20% deposition height in the 0.20 m pipe) and 2.0 m long, and was laid through the pipe opening. Pitot tubes were used to measure the velocity profile through the pipe opening. A video camera recorded the erosion processes.

Different flow rates, sediment sizes, and silt-clay contents were applied in this study (Table 5-1). The flow rate (Q) was varied from 2.5 to 26.0 L/s corresponding to a velocity range of 0.40 to 1.30 m/s. Sil 7 and Sil 8/16 sands from *Sil Industrial Minerals, Edmonton, Alberta, Canada* were used in the experiments. The Sil 7 sand has a size range of 0.04 to 1.0 mm, a median size d_{50} of 0.4 mm, and a uniformity coefficient of 2.2 ($C_u=d_{60}/d_{10}$). The Sil 8/16 sand has a size range of 0.04 to 2.4 mm, a median size d_{50} of 1.8 mm, and a uniformity coefficient of 2.6. Note that a value of uniformity coefficient less than 3 classifies the sand as uniform (Yalkowsky and Bolton, 1990). The above particles have a specific gravity of 2.65. The silt-clay sediment mixture was obtained from the *Black Dirt Company, Edmonton,*

Alberta, Canada, and has a specific gravity of 2.50. In the silt-clay mixture, 51.5% of the particles are less than 2 μm. *Exp. A* used Sil 7 sand and different amounts of the silt-clay mixture to form the deposition, while *Exp. B* used Sil 8/16 sand, also with different amounts of the silt-clay mixture. The amount of the silt-clay mixture in the deposition varied from 0, 10% to 20% by weight in both sets of the experiments, thus generating a total of six sets of experiments (*Exp. A-0, 10, 20* and *Exp. B-0, 10, 20)*.

The preparation of sediment deposition before the experiments is discussed here. In order to represent non-cohesive depositions, the non-cohesive sediment (Sil 7 and Sil 8/16) was laid on the pipe invert without compaction. The deposition was set at 2 m long and 0.04 m high. The weight of the initial deposition was recorded. As for cohesive deposition, the silt-clay mixture was fully mixed with the non-cohesive sediment to obtain the desired silt-clay content (i.e., 10% or 20% by weight) before laying the mixed particles on the pipe invert without compaction. Again, the deposition was 2 m long and 0.04 m high. The weight of the initial deposition was recorded. Subsequently, water was gently introduced into the deposition by a bucket and the deposition was over saturated after about 5 minutes. Finally, the deposition was air-dried for 10 days, in order to make sure the silt-clay material and non-cohesive particles fully consolidated (Li *et al*., 2013).

At the beginning of the experiments, a pump supplied water at a small flow rate in order to obtain a stable flow condition. The flow rate was slowly increased to obtain the critical condition when particles started to be eroded. The water depth was recorded with 1 mm accuracy and the velocity profile was measured by Pitot tubes. Note that the velocity profile was used to determine the critical bed shear stress. Measurements during the critical

condition took less than three minutes, therefore only limited sediment was eroded and there was no change in the deposition profile.

After the critical condition, the flow rate was increased to the pre-determined value. The evolution of the deposition profile and water depth with time were recorded by the video camera. The continuous flow eroded the deposition not only by shoveling the deposition height but also by transporting the sediment from the upstream end to the downstream end of the deposition. Eventually, the deposition reached the equilibrium state, which means the deposition height did not change and the deposition propagated downstream as a result of erosion. At the equilibrium state, the deposition was eroded at the front and all eroded sediment was transported over the mound top. Eroded sediment deposited at the tail which means all eroded sediment was transported downstream. Then, the velocity profile was measured by Pitot tubes. The test was shut down after the velocity profile had been recorded, and the test duration for the erosion stage was recorded. The test duration for the erosion stage did not include the time duration under the critical condition. The equilibrium deposition was then collected, dried and weighted.

Some supplementary information regarding the velocity profile and erosion rate determination is shown below. The vertical range of the velocity profile should be larger than 3 times the value of d_{50} and less than 1/5 of the total water depth within the log law region (Wilcock, 1996). Therefore, three locations were chosen within this range. In *Exp. A*, the three locations were 3, 5, and 7 mm above the deposition, while in *Exp. B* they were 5, 10, and 16 mm above the deposition. The flow velocities were obtained from Pitot tube measurements. The erosion rate was determined by the transport rate per unit width and sediment saltation distance (for detailed equations see later section). The transport rate per

unit width was calculated using the average transport rate and the average width. The average transport rate was estimated from the difference between the initial and equilibrium deposition weight over the test duration for the erosion stage. The average width was calculated as the mean value of the initial deposition width and the equilibrium deposition width.

A field sampling program was conducted on August 22, 2019 to collect information on the actual deposition observed in a storm trunk sewer in the Walden community in southeast Calgary. The storm trunk sewer in question connects to a storm water pond located north of Walgrove Heights S.E. This section of the storm trunk sewer is usually fully submerged reflecting common design practice of inlets into storm ponds in Calgary (City of Calgary, 2011). According to field inspections by the City of Calgary, the deposition in storm trunk sewers tends to be significant in the submerged pipes leading into stormwater ponds. The section of the trunk sewer examined is a 30.0 m long, 1.05 m diameter concrete pipe at a 0.18% slope. The stormwater pond had been dewatered to allow safe access to the trunk sewer. The Walden community has been recently developed and is still under construction. As of August 2019, the size of the catchment area discharging into the stormwater pond was about 43,000 m^2. In spite of the presence of sumps in the catchbasins and erosion & sediment control measures in place, sediments with a relatively high silt-clay content had entered the upstream storm sewer system and deposited in the storm trunk. The deposition profile was recorded through detailed in-situ measurements along the trunk sewer. Field samples were collected and the compositions were analyzed through sieve and hydrometer analyses by a commercial lab of *ALS, Edmonton, Alberta, Canada*.

5.3. Results and discussions

5.3.1. Critical shear stress for initial deposition

At the beginning of the tests, the flow rate was slowly increased to obtain the critical condition when the initialization of particle motions began to be observed (Ab Ghani, 1993). The critical shear stress represents the minimum bed shear stress when particles start to be eroded. The measurements of the vertical velocity profiles can be used to indirectly determine the bed shear stress. The bed shear stress τ_b is related to the shear velocity u^* as:

$$\tau_b = \rho u^{*2} \quad \text{(Equation 5-1)}$$

where, ρ is the water density. The shear velocity can be determined from the following equation (Wilcock, 1996):

$$v = \frac{u^*}{\kappa} ln \frac{z}{z_0} \quad \text{(Equation 5-2)}$$

where, v is the measured flow velocity, κ = 0.40, which is the von Karman constant, z is the height above the deposition, and z_0 is the roughness height. Figure 5-2 shows the relationship between velocity values and *ln z* values under the critical conditions. In *Exp. A*, the measured velocity was relatively small, varying from 0.15 to 0.29 m/s, while the measured velocity in *Exp. B* varied from 0.27 to 0.42 m/s. In all sub-plots, R^2 values are over 0.76, which show a good fit. The slope in Figure 5-2 gave the value of $\frac{u^*}{\kappa}$, allowing for the calculation of the bed shear stress from Equation 5-1.

The momentum equation can also be applied to calculate the bed shear stress, which allows for comparison with the obtained values from the velocity profile. Assuming uniform flow where the mean flow velocity does not change over the control volume of length L (i.e., over the deposition height), the moment equation for the water phase can be written as:

$$\rho g L A S - (\tau_w P_w L + \tau_b P_b L) = 0 \qquad \text{(Equation 5-3)}$$

where, g is the gravitational acceleration, A is the flow area, P is the wetted perimeter, S is the slope of the hydraulic grade line, L is the control volume length, τ is the shear stress, and subscripts w and b denote wall and bed components, respectively. After reorganizing Equation 5-3, the hydraulic grade line slope can be written as follows:

$$S = \frac{\tau_w P_w + \tau_b P_b}{\rho g A} \qquad \text{(Equation 5-4)}$$

$$\tau_w = \frac{1}{8} f_w \rho V^2 \qquad \text{(Equation 5-5)}$$

where, f_w is the wall friction factor and V is the mean velocity. The wall friction factor can be calculated by the explicit expression of Colebrook's equation (Genić *et al*., 2011):

$$f_w = (1.14 - 2\log(e + \frac{21.25}{Re^{0.9}}))^{-2} \qquad \text{(Equation 5-6)}$$

where, e is the relative wall roughness, Re is the Reynolds number (based on average flow velocity and hydraulic diameter). The absolute roughness of Plexiglas pipe is 0.0015 mm in this study.

The critical shear stresses based on the above two methods are calculated and plotted in Figure 5-3(a). The differences between the two sets of data were less than 20%, which

indicates the measurement uncertainty was small. As can be seen from Figure 5-3(a), the critical shear stress (τ_c) in *Exp. A-0* is around 0.19 N/m^2. For the cohesive sediment experiments, the critical shear stress is defined as τ_c^c, where the superscript indicates the percentage of the silt-clay content (by weight). For example, in *Exp. A*, τ_c^{10} and τ_c^{20} are 0.25 and 0.41 N/m^2 respectively, reflecting the 10% and 20% percent of the silt-clay mixture in the bottom deposit. These two values are 31% and 116% larger than that of the Sil 7 sand itself. The more silt-clay mixture was added, the greater the increase of the critical shear stress. The critical shear stress in *Exp. B-0* is 0.98 N/m^2, which is about 5 times larger than that in *Exp. A-0* due to the significant difference in particle size (1.8 mm vs. 0.4 mm). In the presence of the 10% and 20% silt-clay mixture, the critical shear stress approached 1.42 and 1.98 N/m^2, respectively, which is 45% and 102% larger than that of the Sil 8/16 sand.

The effect of the silt-clay content on the sediment critical shear stress is further examined by introducing the results from some previous studies in Figure 5-3(b) (Campisano et al., 2008; Todeschini et al., 2010). The X-axis represents the silt-clay content while the Y-axis shows the ratio of τ_c^c and τ_c. As can be seen from Figure 5-3(b), the increase of silt-clay content can increase the ratio of τ_c^c and τ_c. A fitted curved was developed as:

$$\frac{\tau_c^c}{\tau_c} = 0.068C + 1 \qquad \text{when } C < 36.8 \qquad \text{(Equation 5-7a)}$$

$$\frac{\tau_c^c}{\tau_c} = 3.5 \qquad \text{when } 36.8 \leq C \leq 60 \qquad \text{(Equation 5-7b)}$$

where, C is the silt-clay content. Note the data are limited when the silt-clay content is over 36%, therefore the ratio of τ_c^c and τ_c was assumed as a constant 3.5. The above expressions can be used to estimate the critical shear stress for sediment in the presence of silt-clay. As

for the prediction processes, first, the critical shear stress can be obtained through the shear stress can be obtained through the Shield diagram for non-cohesive particles based on the d_{50} sizes (see the later section). Then the cohesive effect was considered by the value of τ_c^c/τ_c obtained through Equations 5-7a and 5-7b when the proportion of silt-clay mixture is known. Consequently, τ_c^c can be estimated.

The Shields diagram (Shields, 1936) is commonly used to describe the initiation of motion of non-cohesive sediment. The dimensionless bed shear stress (θ_b) and the dimensionless particle size (D^*) are used in the Shields diagram:

$$\theta_b = \frac{\tau_b}{(s-1)d_{50}\rho g} \quad \text{(Equation 5-8)}$$

$$D^* = d_{50}\left(\frac{(s-1)g}{\nu^2}\right)^{1/3} \quad \text{(Equation 5-9)}$$

where s is the specific density of sand, and ν is the water kinematic viscosity. Experimental data about non-cohesive sediment from this study and two previous studies (Perrusquía, 1991; Campisano *et al.*, 2008) are plotted with the Shields diagram in Figure 5-4. The symbols representing non-cohesive particles closely resemble the Shields diagram, which confirms the Shield diagram can be used to predict the critical shear stress for non-cohesive particles. For sediment with 10% or 20% of silt-clay, the dimensionless bed shear stresses are over 50% or 100% larger than that of non-cohesive sediment.

5.3.2. Development of deposition patterns

After obtaining the critical shear stress, the flow rate was increased to a pre-determined value and the resulting deposition patterns were recorded. Generally, four deposition patterns were observed: ripple surface, dune surface, flat surface and rugged surface. The flow depth, deposition height and bed shear stress for different tests are presented in Table 5-1. Note that 6 test results are plotted in Figure 5-5 as examples.

All cases in *Exp. A-0* displayed a ripple surface deposition pattern. *Exp. A-0* at 2.5 L/s case is plotted in Figure 5-5(a) as an example. During the first 10 minutes, the deposition was generally eroded across its entire surface, and its surface remained relatively flat. At this stage, the flow over the deposition had a large sediment transport capacity, which continuously transported the eroded sediment downstream. With the decreasing flow velocity, the bed shear stress at the deposition surface decreased, and so did the sediment transport capacity. During the period from 10 to 20 minutes, the eroded sediment could only be transported downstream for a certain distance and settled at the surface of the deposition. Ripples started to form at the surface of the deposition. Generally, these ripples were 5 to 10 cm in length. They slightly fluctuated in height and length, and some ripples could turn into a flat surface. Starting from 20 minutes, more ripples formed, which slowly moved in the flow direction. Finally, all ripples kept approximately the same height around 40 minutes and the corresponding deposition height was interpreted as the equilibrium height. After the equilibrium height had been reached, all ripples were travelling in the direction of the flow at nearly the same traveling velocity, which means erosion was still happening but the erosion rate did not change anymore. According to the observation, the deposition height and the water depth did not change anymore once the equilibrium height had been reached, which

meant the bed shear stress was unchanged after 40 minutes (at 0.71 N/m^2 based on the momentum equation).

All cases in *Exp. B-0* displayed a dune surface deposition pattern. *Exp. B-0* at 26.0 L/s case is plotted in Figure 5-5(b) as an example. In the first 2 minutes, the eroded sediment was transported downstream continuously and the deposition surface was flat. At 4 minutes, sand dunes formed gradually. The sand dunes were over 30 cm in length, which is over three times longer than the ripples in Figure 5-5(a). In the period between 6 and 8 minutes, the particles at the front of the sand dune were picked up by the flow and migrated downstream. Once they passed over the crest of the sand dune, they deposited at the descending surface of the sand dune. With the continuous sediment movement, the deposition propagated downstream. Note that, once the deposition started to propagate, the equilibrium height and the flow depth kept unchanged. The erosion rate did not change since the bed shear stress was unchanged. The bed shear stress was 3.94 N/m^2, which is over three times the value of the critical shear stress resulting in a higher sediment erosion (Tang *et al.*, 2020).

As can be seen in Figure 5-5(a) and 5-5(b), the non-cohesive sediment could form sand ripples or dunes, and the formation of the sand ripples or dunes were significantly impacted by particle sizes. In a study by Simons and Senturk (1977), they summarized that sand less than 0.7 mm in diameter can form ripples (*Exp. A-0*), while sand larger than 0.7 mm in diameter can form sand dunes (*Exp. B-0*) with relatively large dimensions. Moreover, the particle Reynolds number was used to determine whether the deposition could form sand dunes (Fredsøe, 1986). The particle Reynolds number was defined as (Fredsøe, 1986):

$$Re_p = \frac{d_{50} u^*}{\nu} \qquad \text{(Equation 5-10)}$$

Florez and de Moraes Franklin (2016) reported that for Re_p larger than 70, the deposition could form dunes in the hydraulic rough regime. In *Exp. B-0*, Re_p varied from 82 to 106, which was in the hydraulic rough regime thus forming the sand dunes.

The majority of the cases displayed a flat surface deposition pattern, see *Exp. A-10* and *Exp. A-20* (for all flow rates), *Exp. B-10* at 9.0 L/s and *Exp. B-20* at 9.5 L/s. Note that all these cases concerned cohesive sediments and had a flow rate less than 9.5 L/s. Figure 5-5(c) and 5(e) are for *Exp. A-10* at 8.0 L/s and *Exp. A-20* at 8.0 L/s, respectively. The deposition surface remained flat during the erosion stage, which means the cohesive feature played an important role. Once the equilibrium height had been reached, the deposition moved towards the downstream slowly and the erosion rate was unchanged. The bed shear stresses were 2.28 and 2.31 N/m^2, respectively. Some large sediment chunks could be observed after the nearby loose sands were flushed away.

Exp. B-10 (at 17.0 L/s and 26.0 L/s), *Exp. B-20* (at 17.0 L/s and 26.0 L/s) displayed the same rugged surface deposition pattern. Note that the above four cases had a flow velocity exceeding 0.8 m/s, which means relatively large shear stresses. Figure 5-5(d) and 5-5(f) show the development of the rugged surface deposition. In Figure 5-5(f), only within the first minute, the deposition was relatively flat. After that, the surface of the deposition appeared as rugged. The observations showed that, in addition to the loose sand, massive chunks were eroded from the deposition and flushed downstream. The equilibrium height was relatively small due to the high velocity and the large bed shear stress (4.22 N/m^2). The deposition slowly moved downstream.

The ripple and dune surface patterns for non-cohesive material are commonly described in the literature (Simons and Senturk, 1977). The flat surface occurs when bed shear stress is small for both non-cohesive and cohesive materials. However, the rugged surface is unique for cohesive materials with relatively large bed shear stress. Therefore, in the presence of the silt-clay materials, the deposition surface is flat or rugged. This phenomenon can be used to visually estimate the magnitude of the equilibrium bed shear stress without measurements (i.e., a small shear stress for flat surface scenarios and a large one for rugged surface scenarios).

5.3.3. Erosion rate

The erosion rate can be calculated from the bed load transport rate and the particle transport distance (Van Rijn, 1984):

$$E = q_s/\lambda \qquad \text{(Equation 5-11)}$$

where, E is the erosion rate (kg/m^2/s), q_s is the transport rate per unit width (kg/m/s), and λ is the particle saltation distance (m). The particle saltation distance can be calculated by (Lee and Hsu, 2000):

$$\frac{\lambda}{d_{50}} = 2.428D^{*0.27}\left(\frac{\tau_b-\tau_c}{\tau_c}\right)^{1.01} \qquad \text{(Equation 5-12)}$$

In the pipe flow, with the change in deposition height, the deposition width changed continuously. Therefore, the transport rate per unit width in this study was defined as:

$$q_s = \frac{Q_s}{W} \qquad \text{(Equation 5-13)}$$

where, Q_s is the average transport rate, which was measured through the difference between the initial and equilibrium deposition weight over the test duration for the erosion stage, W is the average of the initial deposition width and the equilibrium deposition width. Then, the erosion rate can be calculated. The weight, time duration and width measurements were relatively accurate with relatively small uncertainty. Note that the uncertainty of the erosion rate in this study reflects that it is a time averaged value while the real erosion rate is an instantaneous value. However, the time averaged value is more realistic and representative compared to the instantaneous value since the deposition also changes continuously in real sewers. The relationship between erosion rate and bed shear stress from the experimental data (Table 5-1) and results by Van Rijn (1984) is plotted in Figure 5-6. As can be seen in Figure 5-6, for a certain particle size, with increasing bed shear stress, the erosion rate increases and the relationship appears to be linear. Particle size also affected the erosion rate. Larger particles are harder to be eroded. A larger resistance can be found for cohesive deposition. Specifically, at the same bed shear stress, the erosion rate decreases as the silt-clay content increases.

The dimensionless erosion parameter, ϕ, was used to describe the erosion capacity among different deposition types (Van Rijn, 1984):

$$\phi = \frac{E}{\rho_s((s-1)gd_{50})^{0.5}} \quad \text{(Equation 5-14)}$$

where, ρ_s is the sediment density. Fernandez-Luque (1974) proposed an equation to describe the relationship between the dimensionless erosion parameter and the dimensionless bed shear stress for a particular particle size:

$$\phi = 0.02(\theta_b - \theta_c)^{1.5} \quad \text{(Equation 5-15)}$$

where, θ_c is the dimensionless bed shear stress corresponding to the critical shear stress for a particular particle size, which can be obtained from the Shields diagram. In addition, Nagakawa and Tsujimoto (1980) presented an equation to describe the erosion capacity for different particle sizes (less than 0.3 mm):

$$\phi = 0.02(1 - \frac{0.035}{\theta_b})^3\theta_b \quad \text{(Equation 5-16)}$$

The experimental data from the current study and Van Rijn (1984) and the above equations are plotted in Figure 5-7. As can be seen in Figure 5-7, the equation from Fernandez-Luque (1974) works well for non-cohesive particles, but it is related to the particle size (since each θ_c is corresponding to a particular particle size) and cannot be used as a general prediction method for a wide size range or cohesive material. The equation from Nagakawa and Tsujimoto (1980) was derived as a general function for a size range of non-cohesive particles that are less than 0.3 mm; it could not be applied for this study given the larger particle sizes and cohesive material used in the current study. Therefore, a new general function for a wide particle size range and considering cohesive material was developed which expresses the erosion capacity as:

$$\phi = 0.057(\theta_b - (0.030 + 0.06C))^{0.97+0.2C} \quad \text{(Equation 5-17)}$$

R^2 is over 0.93 which shows a good fit. This developed equation can be used to predict the erosion capacity for both cohesive and non-cohesive deposition.

5.3.4. Deposition in real storm sewers: measurements and predictions

As described above, a field sampling program was conducted to collect information on the actual deposition in a storm trunk sewer in the Walden community in southeast Calgary. This particular trunk sewer was selected as the City of Calgary is interested in the degree of residual deposition in trunk sewers in a community where the catchbasins have sumps which is different from most other communities in Calgary where the catchbasins do not have sumps. To intercept the bed load supply to storm pipes with standing water before Calgary's stormwater management ponds, the City of Calgary has asked for the implementation of large oil-grit separators since 2014. Because these structures come at a significant cost, catchbasins with sumps are being considered as an alternate design option. The section of trunk sewer examined is a 30 m long, 1.05 m diameter concrete pipe at a 0.18% slope. At the time of the August 22, 2019 field visit, the size of the catchment area draining into the storm trunk sewer was about 43,000 m^2. The Walden community started to develop in 2014 and is still under construction.

The deposition profile along the pipe was recorded (Figure 5-8(a)). The first measurement point was 0.5 m away from the upstream manhole where the deposition reached its highest level at 0.46 m or close to 50% of the diameter of the pipe. The deposition height was measured in a downstream direction with a 1.5 m spacing along the central axis of the storm trunk sewer with a total of 19 data points. The deposition height gradually decreased to zero (Figure 5-8(a)). Sediment samples were collected along the deposition centerline at five locations named S1 to S5 at a distance of 0.5 m, 6.5 m, 12.5 m, 18.5 m, and 24.5 m away from the upstream manhole, respectively.

Figure 5-8(a) shows the deposition profile along the storm trunk sewer, and Figure 5-8(b) shows the sediment composition at the sampling locations S1 to S5. In Figure 5-8(b), the clay size is less than 2 μm, the silt size is from 2 μm to 50 μm, the sand size is from 50 μm to 2 mm, and the gravel size is over 2 mm. At the upstream end of the pipe (S1), gravels made up over 50% of the total weight. At the downstream end of the deposition, the majority of the sediment consisted of silt and clay material (S4 and S5). The silt-clay content increased significantly in a downstream direction from 22% to around 74%. The value of d_{50} (representing the gravel and sand mixture excluding the silt-clay content) became smaller along the flow direction (i.e., from 2.1 mm to 0.8 mm). The critical shear stress can be predicted following the methods presented in the previous section. The non-cohesive critical shear stress can be obtained from the Shield diagram as a function of the known values for d_{50} (τ_c in Table 5-2). The value for $\tau_c{}^c$ be obtained from Equations 5-7a and 5-7b and the predicted values are shown in Table 5-2. The critical shear stress decreased from 3.37 to 1.50 N/m^2 in a downstream direction along the pipe.

Based on the City of Calgary's storm sewer design guidelines (City of Calgary, 2011), the design flow (corresponding to a 5-year storm event) for this storm trunk sewer is estimated at 300 L/s for a catchment area of 43,000 m^2. Since the Walden community started to develop in 2014, the design flow could be treated as the maximum flow most likely. The maximum flow rate would erode the deposition to its lowest level, with the lowest deposition height corresponding to a bed shear stress equaling the critical shear stress (Tang *et al.*, 2020). The bed shear stress can be calculated as:

$$\tau_b = \frac{1}{8} f_b \rho V^2 \qquad \text{(Equation 5-18)}$$

where, f_b is the bed friction factor. In the study by Tang *et al.* (2020), the actual bed friction factor is two to four times the friction factor (when solely considering the deposition roughness) since more energy loss was incurred by the transport of the sediment along the deposition. The friction factor (due to the deposition roughness) can be calculated from Equation 5-6. On the right-hand side of Equation 5-18, the bed friction factor is three times the deposition roughness friction factor and the average flow velocity (V) is a function of the deposition height and the flow rate (300 L/s). On the left-hand side of Equation 5-18, τ_b equals $\tau_c{}^c$ from Table 5-2. Consequently, the deposition height can be estimated and its values are superimposed in Figure 5-8(a). Then, two smaller flow rates (100 L/s and 200 L/s) were assumed as the maximum flow. For these flow rates the deposition profiles were also predicted and shown in Figure 5-8(a).

The predicted profile for the 300 L/s scenario appears to be close to the actual field measurements. The predicted heights at S4 and S5 are higher than the actual heights. This is likely due to the limitation of the prediction method for the critical shear stress when the silt-clay content is over 60%. In addition, the layer effect of the actual deposition was not considered, that is, the finer sediment on the actual deposition surface was easier to be eroded and it resulted in the smaller actual deposition height. However, the two smaller flow rates result in much higher deposition heights. This suggests that the observed deposition profile reflects the occurrence of a flow rate that had been close to the design flow rate. However, there is a degree of uncertainty in that the method presented in this study is based on a short period of steady flow rather than the actual hydrographs observed in storm sewer systems. Therefore, additional investigations are planned to examine the various infrequent and

unsteady flow regimes present in storm sewer systems as a function of upstream flow and sediment control provisions.

5.4. Chapter summary

In this study, the erosion processes were investigated experimentally for non-cohesive deposition and cohesive deposition. The critical shear stress was obtained through velocity measurements and the momentum equation. In *Exp. A-0*, the critical shear stress is around 0.19 N/m^2. In *Exp. A*, when the deposition had silt-clay mixture materials, τ_c^{10} and τ_c^{20} increased to 0.25 and 0.41 N/m^2 respectively. In the *Exp. B-0*, the critical shear stress is 5 times the value of that in the *Exp. A-0* (0.98 N/m^2) due to the significant difference in particle sizes. In the presence of 10% and 20% silt-clay content, the critical shear stress approached 1.42 and 1.98 N/m^2, respectively. The Shield diagram was used to predict the critical shear stress for non-cohesive deposition. A method was developed to predict the critical shear stress for both non-cohesive and cohesive materials.

As for the erosion processes, the deposition was eroded continuously and it approached a equilibrium height. Once the equilibrium height had been reached, the deposition continued to propagate downstream; however, the erosion rate was unchanged. In specific, four general patterns, including (1) ripple surface, (2) dune surface, (3) flat surface, and (4) rugged surface, were classified. For the non-cohesive deposition, the formation of the sand ripples or dunes were significantly impacted by the particle Reynolds number. For the cohesive deposition, it would form a flat or rugged surface depending on the magnitude of the bed shear stress. As for the erosion rate, with the increase in the bed shear stress, the erosion rate increases and the relationship between these two parameters seems to be linear. The erosion

capacity can be expressed through the dimensionless bed shear stress (θ_b) and the dimensionless erosion parameter (ϕ). A new equation was proposed to predict the erosion capacity in the presence of the silt-clay materials.

A field sampling program was conducted to study the actual deposition in a storm trunk sewer. An actual deposition profile was recorded which showed a decrease in the deposition height in a downstream direction. The particle sizes decreased from the upstream to the downstream end of the pipe. The critical shear stresses were estimated to range from 3.37 to 1.50 N/m^2 at five locations along the pipe. Moreover, the deposition heights at five sections were predicted based on different flow rates and compared to the actual heights, which suggests that the observed deposition profile reflects the occurrence of a flow rate that had been close to the design flow rate.

Table 5-1. Experimental parameters and measurement results

Test #	Sand type	Sil-clay content (%)	Flow rate (L/s)	Equilibrium deposition height (m)*	Flow depth (m)**	Bed shear stress (N/m^2)***	Erosion rate ($kg/m^2/s$)	Deposition pattern
Exp. A-0	Sil 7	0	2.5	0.045	0.074	0.71	1.36	Ripple
			4.0	0.038	0.080	1.12	2.49	Ripple
			8.0	0.026	0.097	2.21	4.11	Ripple
Exp. A-10	Sil 7	10	2.5	0.043	0.074	0.73	1.11	Flat
			4.0	0.039	0.081	1.23	2.37	Flat
			8.0	0.026	0.096	2.28	4.01	Flat
Exp. A-20	Sil 7	20	2.5	0.042	0.075	0.83	1.10	Flat
			4.0	0.039	0.082	1.32	2.21	Flat
			8.0	0.032	0.100	2.31	3.79	Flat
Exp. B-0	Sil 8/16	0	9.0	0.035	0.108	2.32	1.05	Dune
			17.0	0.031	0.143	3.21	2.32	Dune
			26.0	0.030	0.160	3.94	3.19	Dune
Exp. B-10	Sil 8/16	10	9.0	0.034	0.110	2.65	1.28	Flat
			17.0	0.028	0.145	3.91	2.77	Rugged
			26.0	0.018	0.163	4.73	3.91	Rugged
Exp. B-20	Sil 8/16	20	9.5	0.032	0.105	2.89	1.27	Flat
			17.0	0.018	0.130	4.22	2.85	Rugged
			26.0	0.016	0.165	5.61	4.30	Rugged

* The equilibrium deposition height was obtained when the erosion rate stayed unchanged
** The flow depth was measured above the equilibrium deposition height
*** The bed shear stress was calculated through the velocity profile above the equilibrium deposition height

Table 5-2. Field results in the storm trunk sewer

Location	S1 (0.5 m)	S2 (6.5 m)	S3 (12.5 m)	S4 (18.5 m)	S5 (24.5 m)
d_{50} (mm)	2.1	1.1	0.9	0.8	0.8
Silt-Clay (%)	22	31	37	70	74
τ_c (N/m^2)	1.35	0.64	0.47	0.39	0.39
${\tau_c}^c$ (N/m^2)	3.37	1.92	1.60	1.50	1.50
Deposition height (m)	0.46	0.28	0.25	0.14	0.09

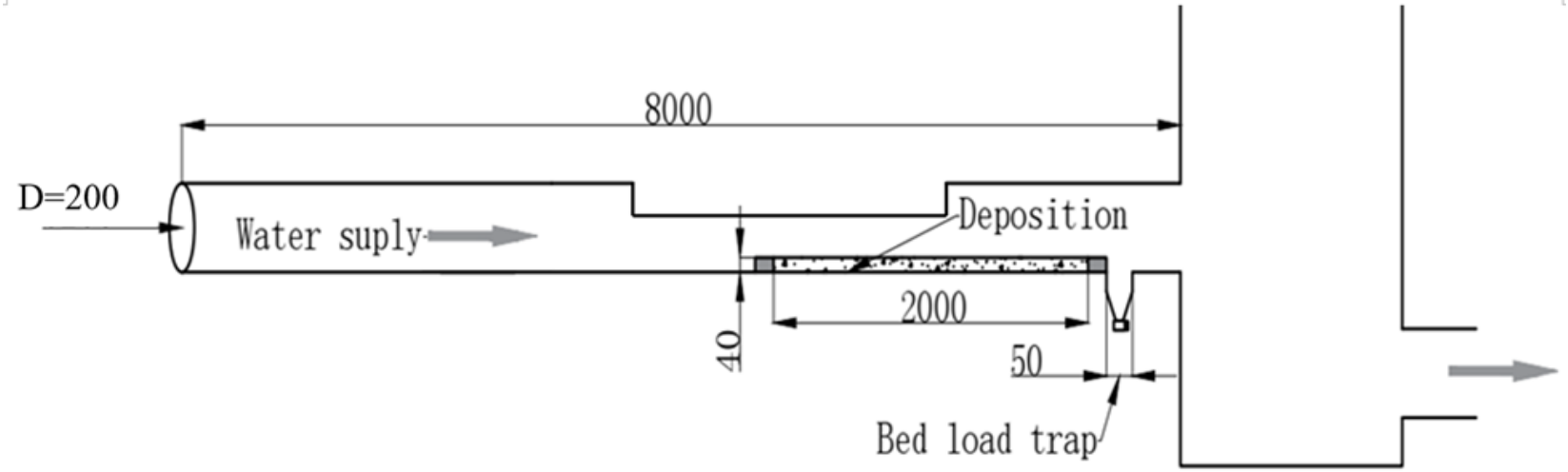

Figure 5-1. Experimental setup for deposition erosion (unit: mm)

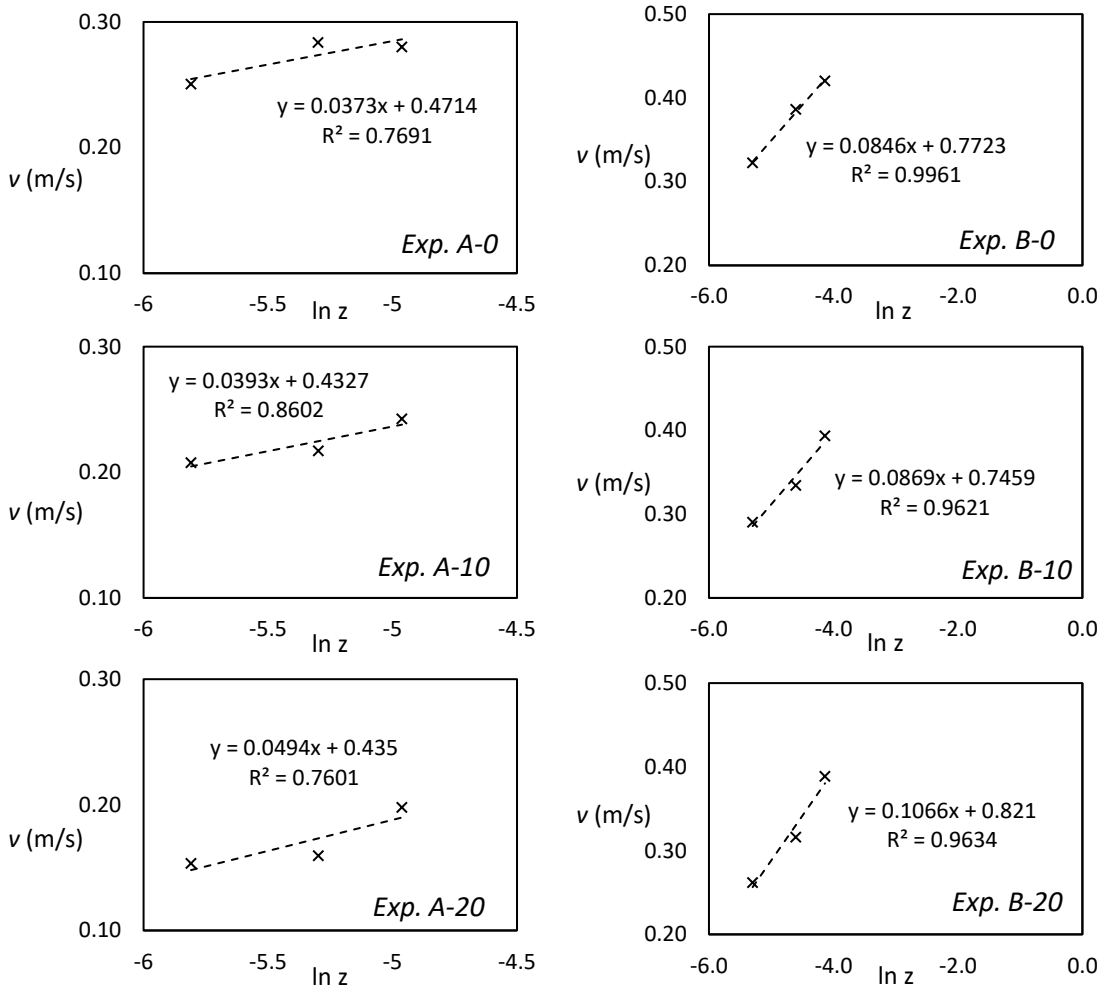

Figure 5-2. Measured water velocity (*v*) versus *ln z*

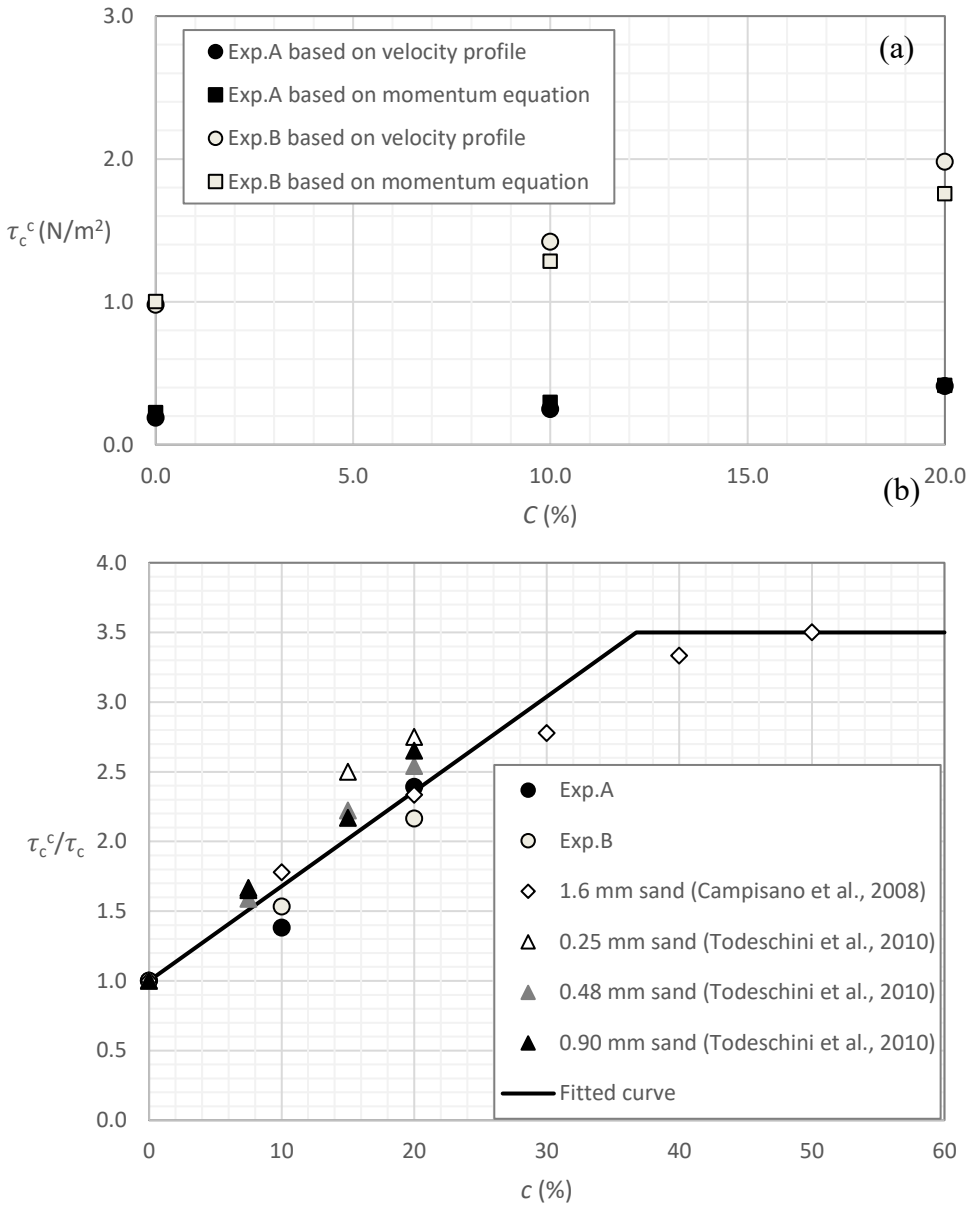

Figure 5-3. (a) Relationship between critical shear stress (τ_c^c) and silt-clay content (C); (b) Relationship between relative critical shear stress (τ_c^c/τ_c) and silt-clay content (C)

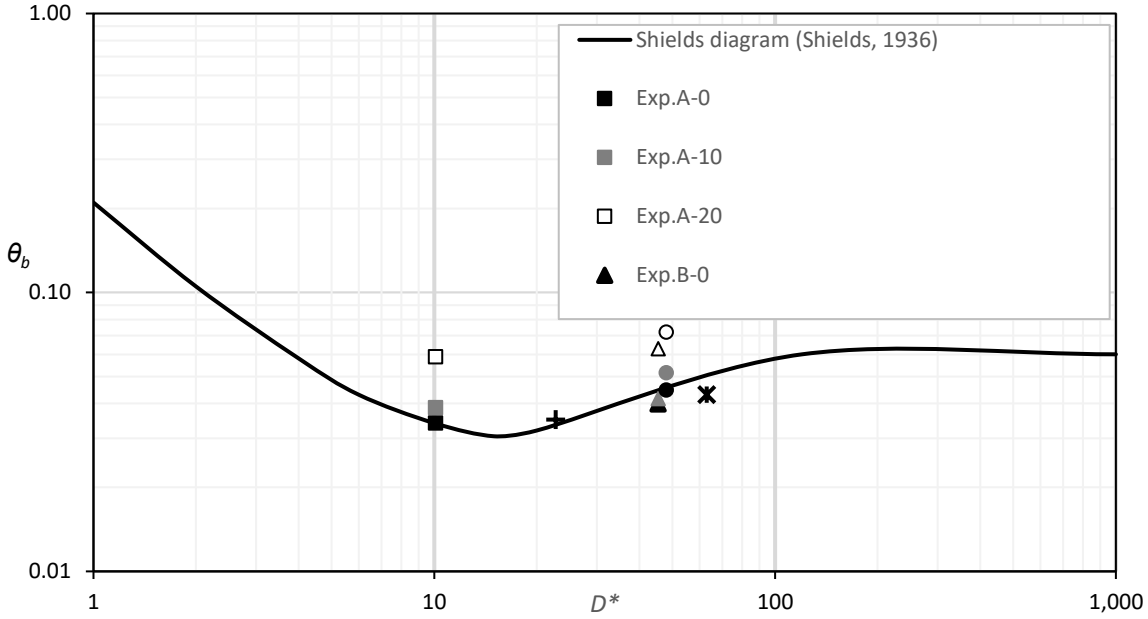

Figure 5-4. Initiation of movement among different studies

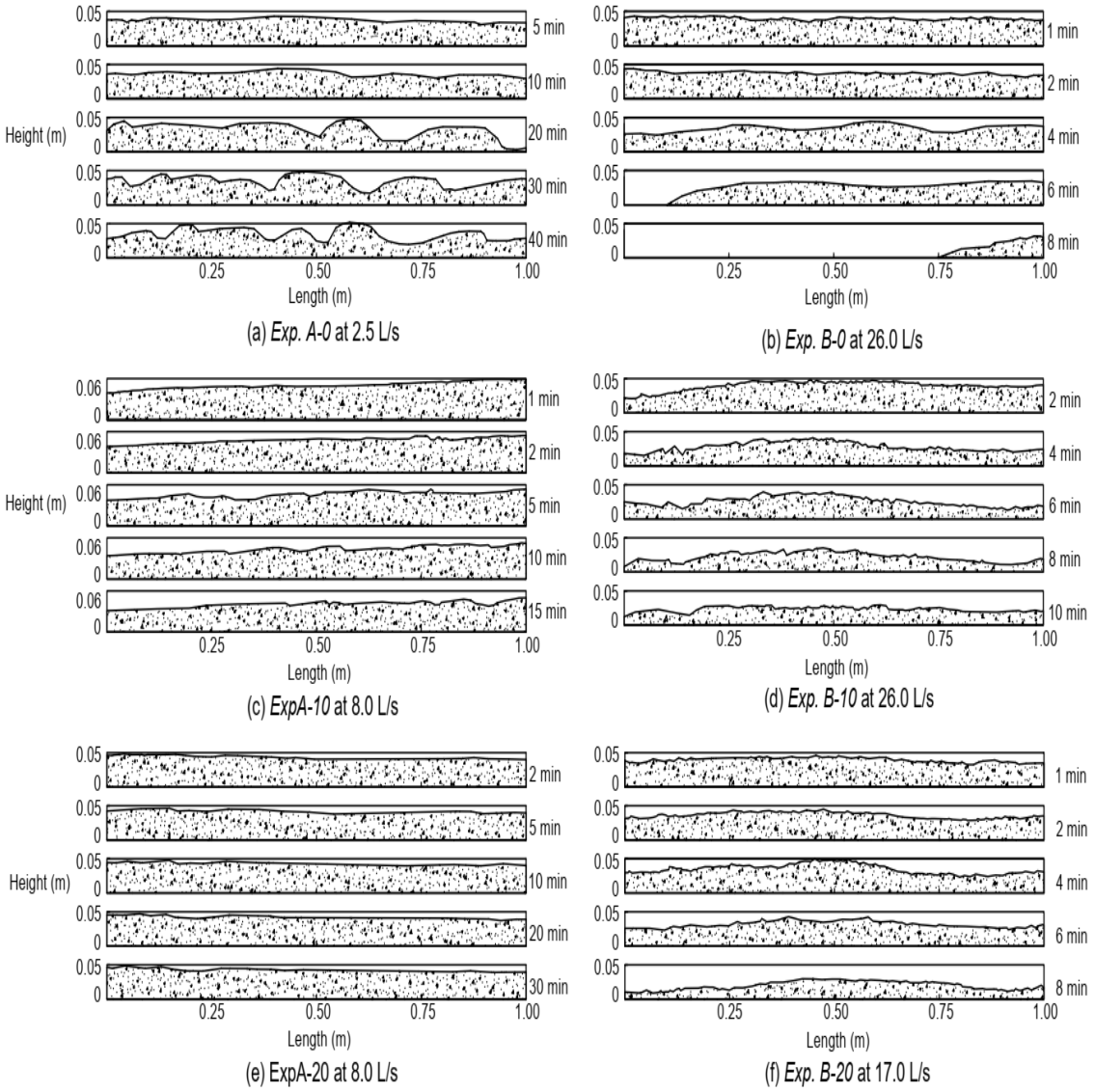

Figure 5-5. Deposition patterns: (a) Ripple surface; (b) Dune surface; (c) and (e) Flat surface; (d) and (f) Rugged surface

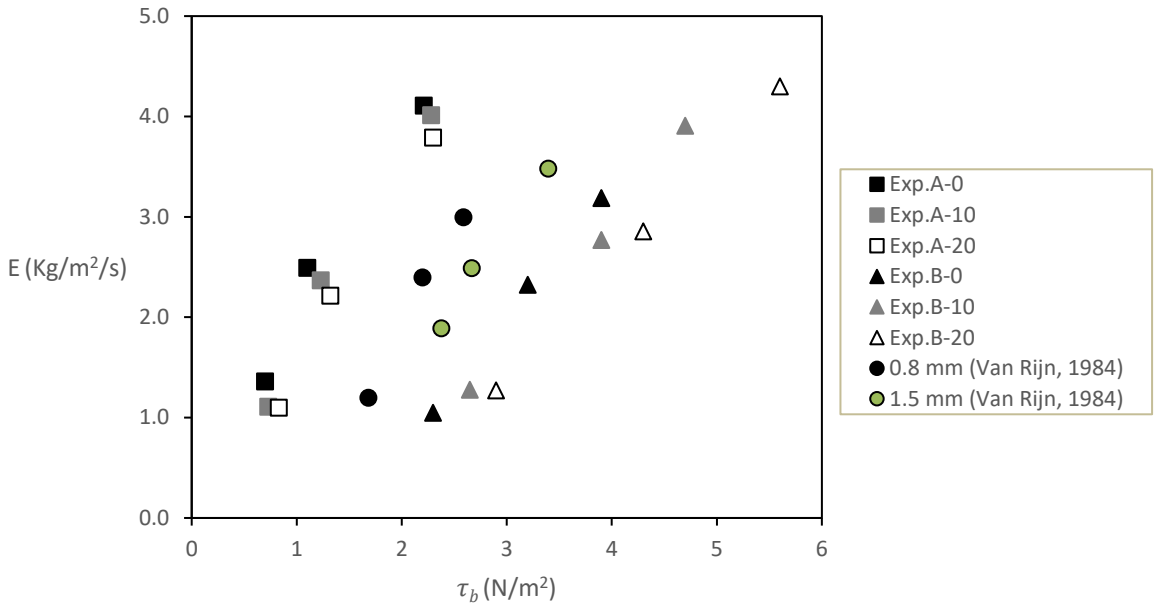

Figure 5-6. Relationship between erosion rate (E) and bed shear stress (τ_b)

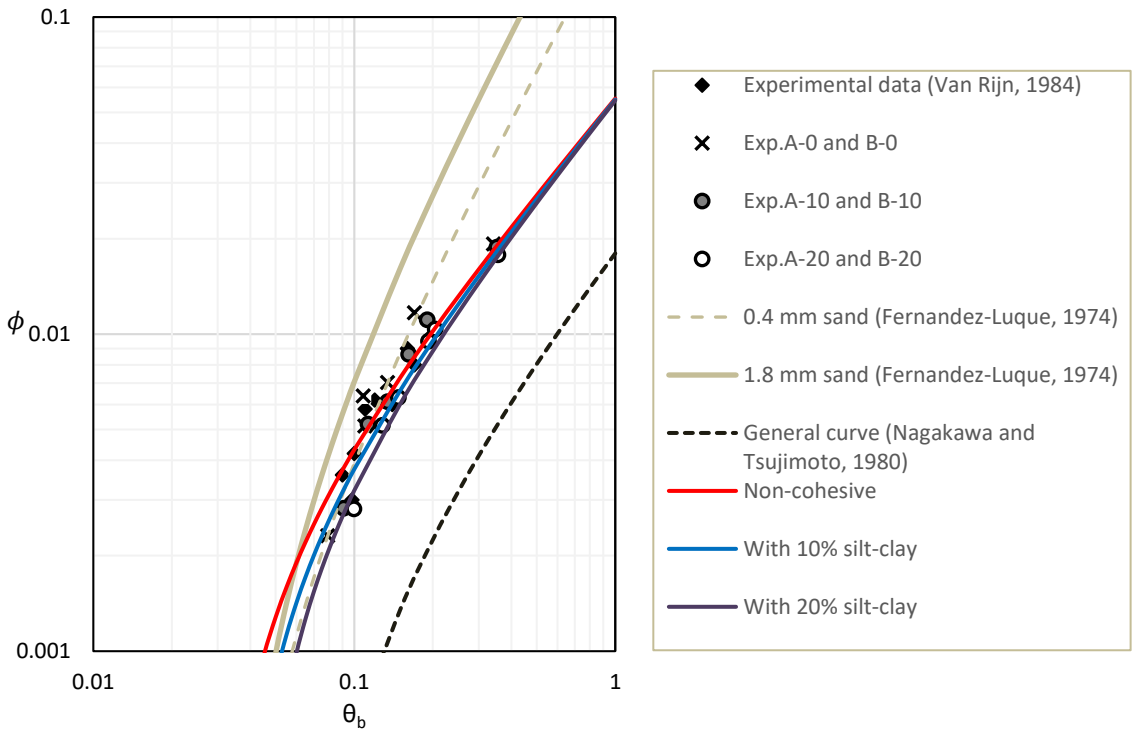

Figure 5-7. Relationship between dimensionless erosion capacity (ϕ) and dimensionless bed shear stress (θ_b)

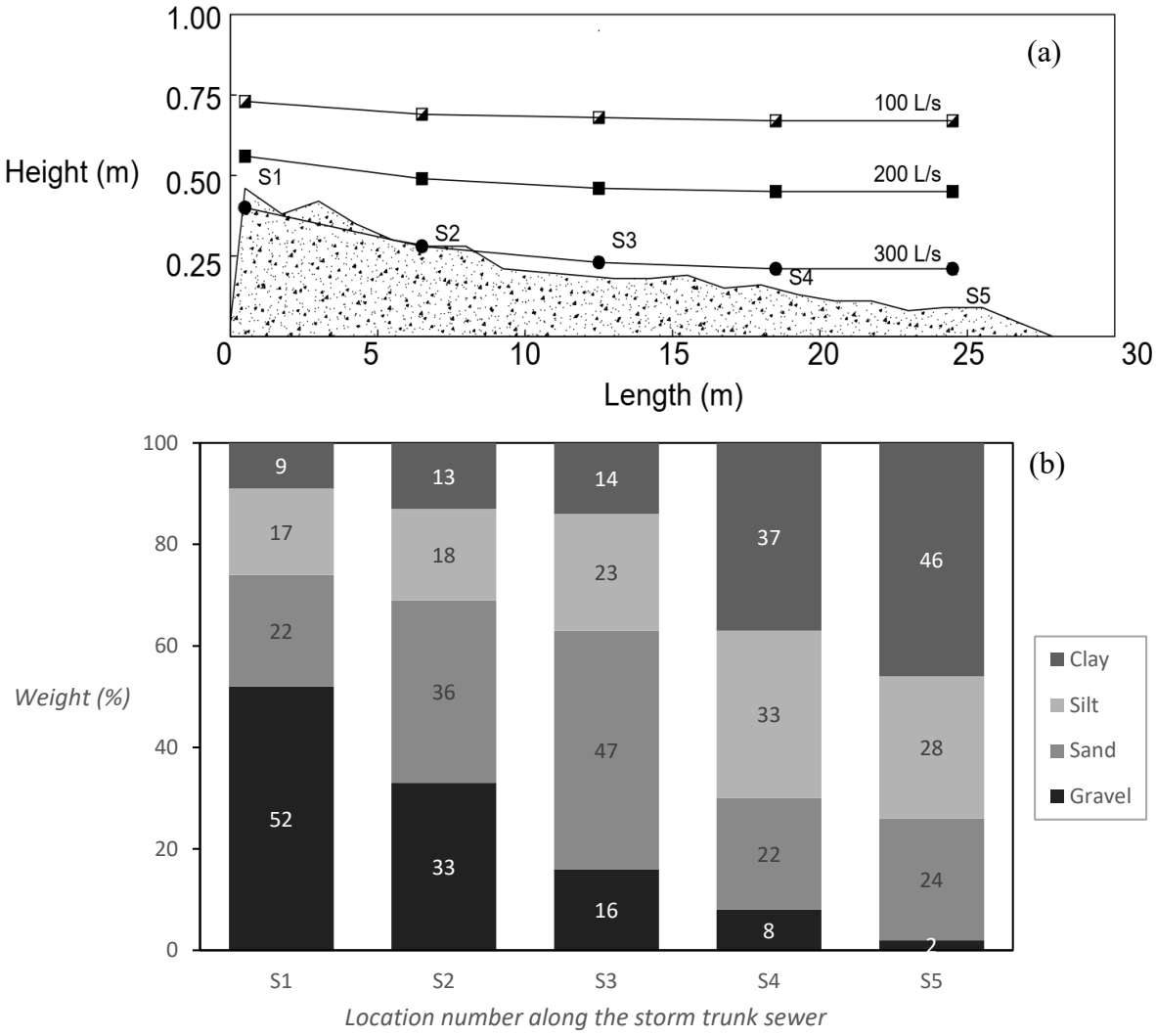

Figure 5-8. Field sampling results: (a) Deposition profile in a storm trunk sewer; (b) Sediment components among five sections

Chapter 6. Conclusions and Recommendations

In this thesis, a literature review on sediment in storm sewer systems was presented. One analytical technique about sediment removal efficiency in OGSs was conducted. Two sets of experiments were conducted in the T. Blench Hydraulic laboratory at the University of Alberta. The first experiment focused on the deposition growth in a submerged pipe, and the second experiment focused on erosion on storm sewer deposition. A field sampling was conducted to collect real storm sewer sediment and record real deposition profile in a storm trunk sewer. Some conclusions and recommendations are listed below.

6.1. Conclusions

- Storm sewer sediment characteristics

Sources of storm sewer sediment include the atmosphere, wash-off within catchment surfaces, sewer pipes themselves and construction sites. Storm sewer solids vary in size from gravel to clay. The variation in particle size is due to catchment conditions, vehicular activities, surface runoff characteristics and the application of winter de-icing sand materials. Fine sediment (clay or silt) can be easily introduced into the storm sewer systems from construction sites by small rainfall or runoff, and coagulates during dry weather, which becomes permanent deposition thus decreasing sewer capacity.

- Sediment removal in OGSs

There are three different types of OGSs in the current market based on different removal methods: (1) gravity action type, (2) swirl action type, and (3) screening action type. Hazen

number, Reynolds number and Froude number were chosen as scaling parameters based on different flow and sediment movement characteristics. A combination of these three parameters expressed as *HRF* was chosen to describe the removal efficiency in OGSs. *HRF* is a function of sediment settling velocity, hydraulic residence time, and water depth. The generalized prediction method can be used as a preliminary performance indicator for OGS units that have not yet been subjected to rigorous laboratory testing. Moreover, based on the general tendency of the removal efficiency, an adjustment method was developed that can be applied for both laboratory and field data calibrations.

- Deposition growth in a submerged pipe

Growth of deposition appeared to have two stages: rapid growth stage and equilibrium growth stage. Bed friction factors varied from 0.058 to 0.185, which were in the same range of previous study. Bed shear stress obtained from this study was from 1.5 to 8.7 N/m^2 corresponding to a transport rate per unit width range 0.010 to 0.470 kg/m/s under different conditions. Shields diagram and bed load equation were proved valid in submerged pipe conditions in the presence of deposition. The sediment saltation velocity was a function of the particle size, shear velocity and dimensionless shear stress. A general prediction method to calculate the equilibrium height was developed by a calculation table, which provided valuable information regarding to sewer design, cleansing and maintenance.

- Field investigation on sediment characteristics and deposition profile

Appendix provided valuable information regarding real sediment in real storm sewers and catch basins. Clay contents in six catch basins varied from 4% to 29%, which meant, except for one location, all other locations had cohesive feature. Deposition profile was measured

through in-sewer measurements. At 0.50 m away from the upstream manhole, the deposition reached the highest, which was 0.46 m. The deposition height gradually decreased to zero along flow direction. Five samples were collected along the deposition and samples. The sediment size became smaller along the flow direction. At the end of the pipe, majority of the deposition was silt and clay material. The silt and clay content increased significantly from 22% to around 74% from upstream to downstream.

- Erosion on storm sewer depositions

Erosion processes were investigated experimentally in this study. Four general patterns were summarized, including (1) ripple surface deposition, (2) dune surface deposition, (3) flat surface deposition, and (4) rugged surface deposition. Cohesive material can provide additional resistance to the bed shear stress. The critical shear stress was able to be predicted in the presence of cohesive materials. The erosion rate was predicted through dimensionless bed shear stress (θ_b) and dimensionless erosion parameter (ϕ) in the presence of cohesive materials.

6.2. Recommendations

- Improvement of sediment capture efficiency in OGSs

Laboratory tests and field monitoring should be conducted for aimed OGSs. This will help to understand current performance of OGS designs. Then some possible design optimizations should be tested in experimental study. Flow monitoring in the field should be conducted in order to obtain presentative flow scenarios. Large and intermittent flows simulating real

flows should be applied in these studies. In addition, through lab work, efficient cleansing methods can be developed for reducing time or resources of cleansing OGSs.

- Effects of different pipe characteristics

Firstly, application of different pipe shapes (e.g., rectangular or egg shaped) should be investigated to examine the feasibility of applying predictions of particle saltation velocity, sediment deposition equilibrium height, bed shear stress, and bed load equations. Secondly, different pipe materials might need to be tested when considering cohesive material. Finally, the presence of unsteady flow regimes should be evaluated in order to understand real-life circumstances with changes of pipe sizes, slopes and flow directions.

- Numerical study on sediment transport and deposition

Numerical model will be a good idea to develop. Aimed model could simulate sediment movement and deposition growth in storm sewers. The model can provide information on mound dimension prediction. Deposition growth rate could reflect necessary sediment cleansing frequency and sediment deposition locations, which helps the city operation team on sediment cleansing, sewer inspection, emergency maintenance, etc.

- Real storm sewer condition

Real deposition should be studies considering organic matters and temperatures. Not only physical characteristics but also chemical & biological characteristics are worth studying. The intermittent flow regimes should be further studied. Prediction methods on transport rate, erosion rate, and transport velocity should all be examined once real storm sewer sediment is applied.

- City operation and maintenance

A process code should be developed for a better regulation of storm sewer systems. The code should include field investigation method, structure optimization guidance, the prediction on deposition locations, and cleansing frequency determination.

Bibliography

Ab Ghani, A. (1993). Sediment transport in sewers. PhD thesis. Newcastle University, England.

Ackers, J., Butler, D., Leggett, D., and May, R. W. P. (2001). Designing Sewers to Control Sediment Problems. Urban Drainage Modeling, 818–823. [online] http://ascelibrary.org/doi/abs/10.1061/40583(275)77.

Ackers, P. (1984). Sediment transport in sewers and the design implications. In Prof. of Int. Conf. On the Planning, Construction, Maintenance and Operation of Sewerage Systems, Cranfield BHRA The Fluid Engineering Centre.

Alberta Environment (1995). Alberta user guide for waste managers, Edmonton.

Alvarez-Hernandez, E. M. (1990). The influence of cohesion on sediment movement in channels of circular cross-section. PhD thesis. Newcastle University, England.

Aronson, G., Watson, D., and Pisano, W. (1983). Evaluation of catch basin performance for urban stormwater pollution control, Cincinnati.

Arthur, S., Ashley, R. M., and Nalluri, C. (1996). Near bed solids transport in sewers. Water Science and Technology, 33(9), 69-76.

Aryal, R. K. and Lee, B. K. (2009). Characteristics of suspended solids and micropollutants in first-flush highway runoff. Water, Air, and Soil Pollution: Focus, 9(5-6), 339–346.

Ashley, R. M. and Crabtree, R. W. (1992). Sediment origins, deposition and build-up in combined sewer systems. Water Science and Technology, 25(8), 1–12.

Ashley, R. M., and Crabtree, R. W. (1992). Sediment origins, deposition and build-up in combined sewer systems. Water Science and Technology, 25(8), 1.

Ashley, R. M., and Hvitved-Jacobsen, T. (2002). Management of sewer sediments. R. Field, & D. Sullivan (Eds.). CRC Press/Lewis Publishers, Boca Raton, FL.

Ashley, R. M., Arthur, S. S., Coghlan, B. P., and McGregor, I. I. (1994). Fluid sediment in combined sewers. Water Science and Technology, 29(1-2), 113-123.

Ashley, R., and Verbanck, M. (1996). Mechanics of sewer sediment erosion and transport. Journal of Hydraulic Research, 34(6), 753-769.

Ashley, R., Bertrand-Krajewski, J. L., & Hvitved-Jacobsen, T. (2005). Sewer solids—20 years of investigation. Water Science and Technology, 52(3), 73-84.

ASTM International (2012). C1746/C1746M-12 Standard test method for measurement of suspended sediment removal efficiency of hydrodynamic stormwater separators and underground settling devices, West Conshohocken, PA, 2012, http://dx.doi.org/10.1520/C1746_C1746M-12.

Bagnold, R. A. (1966). An approach to the sediment transport problem for general physics. Geological Survey Professional Paper, 422-1, Washington, D.C.

Belfiore, L. A. (2003). Transport phenomena for chemical reactor design, John Wiley and Sons.

Bertrand-Krajewski, J. L. (2003). Sewer sediment management: some historical aspects of egg-shaped sewers and flushing tanks. Water Science and Technology, 47(4), 109-122. ISSN 0273-1223.

Bertrand-Krajewski, J. L., Bardin, J. P., and Gibello, C. C. (2006). Long term monitoring of sewer sediment accumulation and flushing experiments in a man-entry sewer. Water Science and Technology, 54(6/7), 109-117.

Bertrand-Krajewski, J. L., Bardin, J. P., Gibello, C., and Laplace, D. (2003). Hydraulics of a sewer flushing gate. Water Science and Technology, 47(4), 129–136.

Boogaard, F., van de Ven, F., Langeveld, J., and van de Giesen, N. (2014). Stormwater Quality Characteristics in (Dutch) Urban Areas and Performance of Settlement Basins. Challenges, 5(1), 112–122.

Buckingham, E. (1914). On physically similar systems - Illustrations of the use of dimensional equations. Physical Review, 4: 345–376.

Butler, D. and Karunaratne, S. H. P. G. (1995). The suspended solids trap efficiency of the roadside gully pot. Water Research, 29(2), 719–729.

Butler, D. D. and Davies, J. W. (2011). Urban Drainage, London, New York: Spoon Press.

Butler, D. D., Davies, J. W., Jefferies, C. C., and Schütze, M. M. (2003). Gross solid transport in sewers. Proceedings of ICE: Water and Maritime Engineering, 156(2), 175-183.

Butler, D., and Davis, J. W. (2011). Urban drainage. London; New York: Spoon Press.

Butler, D., and Karunaratne, S. H. P. G. (1995). The suspended solids trap efficiency of the roadside gully pot. Water research, 29(2), 719-729.

Camp, T. R. (1945). Sedimentation and the design of settling tanks, Paper No 2285 in Transactions of the American Society of Civil Engineers., 1–5.

Campisano A., Creaco E. and Modica C. (2004). Experimental and numerical analysis of the scouring effects of flushing waves on sediment deposits. Journal of Hydrology, 299(3-4), 324-334.

Campisano, A., Creaco, E., & Modica, C. (2008). Laboratory investigation on the effects of flushes on cohesive sediment beds. Urban Water Journal, 5(1), 3-14.

Chien, N. and Wan, Z. (1999). Mechanics of sediment transport, American Society of Civil Engineers.

Chin, D. A. (2020). Issues in Hydraulic Design of Sanitary Sewers. Journal of Environmental Engineering, 146(4), 04020016.

Contech Engineered Solutions (2015). Vortechs guide, [online] http://www.conteches.com/DesktopModules/Bring2mind/DMX/Download.aspx?Command=Core_Download&EntryId=12891&language=en-US&PortalId=0&TabId=144.

Cornu, P. Le, Faram, M. G., and Andoh, R. Y. G. (2000). “A novel device for the removal of grits and oils from stormwater run-off” in CIWEM/AETT Millennium Conference:

"Wastewater Treatment: Standards and Technologies to meet the Challenges of the 21stCentury." Leeds.

Crabtree, R. W. (1989). Sediment in sewers. Water and Environment Journal, 3(6), 569-578.

Dettmar, J. and Staufer, P. (2005a). Behavior of the activated storage-volume of flushing waves on cleaning performance. In Proceedings of 10th International Conference on Urban Drainage, Copenhagen, Denmark, 21-26 August 2005.

Dettmar, J., and Staufer, P. (2005b). Modelling of flushing waves for optimizing cleaning operations. Water science and technology, 52(5), 233-240.

Dettmar, J., Rietsch, B. and Lorenz, U. (2002). Performance and operation of flushing devices - results of a field and laboratory study. Proc of the 9th International Conference on Urban Drainage, Portland, Oregon, USA. 8-13 September 2002.

Dufresne, M., Vazquez, J., Terfous, A., Ghenaim, A., and Poulet, J. B. (2009). Experimental investigation and CFD modelling of flow, sedimentation, and solids separation in a combined sewer detention tank. Computers and Fluids, 38(5), 1042-1049.

Ebtehaj, I., & Bonakdari, H. (2013). Evaluation of sediment transport in sewer using artificial neural network. Engineering Applications of Computational Fluid Mechanics, 7(3), 382-392.

Einstein, H. A. (1942). Formulas for the transportation of bed load. Trans. ASCE Paper, 2140, 561-597.

El-Zaemey, A. K. S. (1991) Sediment transport over deposited bed sewers, Ph.D. thesis, University of Newcastle upon Tyne.

ETV (2014). Procedure for laboratory testing of oil - grit separators, [online] https://sustainabletechnologies.ca/app/uploads/2013/06/ETV-OGS-Procedure_final_revised-June_2014.pdf.

ETV (2016). Technology verified: Downstream Defender, Toronto. [online] http://etvcanada.ca/wp-content/uploads/2017/02/Canadian-ETV-VS-TFS-Hydro-International_September-2016.pdf.

ETV (2017). Verification statement of Stormceptor EF4 and EFO4 Oil-Grit Separators, Whitby. [online] http://etvcanada.ca/wp-content/uploads/2017/11/ISO-14034-Verification-Statement-_Stormceptor_2017-11-10.pdf.

Fan, C. Y. (2004). Sewer sediment and control: a management practices reference guide. United States Environmental Protection Agency, Office of Research and Development, National Risk Management Research Laboratory, Water Supply and Water Resources Division, Urban Watershed Management Branch.

Faram, M. G. (2000). “Removal of Sediments and Oils from Urban Run-off Using the Downstream DefenderTM” in Stormwater Management: Issues and Solutions. Bradford.

Farnworth, E. G. (1979). Impacts of sediment and nutrients on biota in surface waters of the United States. Environmental Research Laboratory, Office of Research and Development, US Environmental Protection Agency.

FB Environmental Associates (2010). Independent review of CDS 2015 product evaluation, Portland. [online] http://www.rainwatermanagement.ca/wp-content/uploads/2014/04/CDS-OK-110-Removal-Efficiency-and-Re-suspension-Report.pdf.

Fenner, R. A. and Tyack, J. N. (1997). Scaling laws for hydrodynamic separators. Journal of Environmental Engineering, 123(10), 1019–1026.

Ferguson, R. I. and Church, M. (2004). A Simple Universal Equation for Grain Settling Velocity. Journal of Sedimentary Research, 74(6), 933–937. [online] http://jsedres.sepmonline.org/cgi/doi/10.1306/051204740933.

Fernandez Luque, R. (1974). Erosion and transport of bed-load sediment. Dissertation, KRIPS Repro BV, Meppel, The Netherlands.

Florez, J. E. C., & de Moraes Franklin, E. (2016). The formation and migration of sand ripples in closed conduits: experiments with turbulent water flows. Experimental Thermal and Fluid Science, 71, 95-102.

Fredsoe, J. (1982). Shape and dimensions of stationary dunes in rivers. Journal of the Hydraulics Division, 108(8), 932-947.

Fredsøe, J. (1986). Formation of Ripples, Dunes, and Antidunes in River Beds. In Physics of desertification (pp. 327-343). Springer, Dordrecht.

Genić, S., Aranđelović, I., Kolendić, P., Jarić, M., Budimir, N., and Genić, V. (2011). A review of explicit approximations of Colebrook's equation. FME transactions, 39(2), 67-71.

Goncalves, C. and van Seters, T. (2012). Characterization of particle size distributions of runoff from high impervious urban catchments in the Greater Toronto Area, Toronto, Onatario. [online] http://www.sustainabletechnologies.ca/wp/wpcontent/uploads/2013/03/ PSD-2012-final.pdf.

Graf, W. H., and Acaroglu ER. (1968) Sediment transport in conveyance systems (Part 1): a physical model for sediment transport in conveyance systems. Hydrol Sci J 13(2):20–39.

Guo, Q., Fan, C.-Y., Raghaven, R., and Field, R. (2004). Gate and Vacuum Flushing of Sewer Sediment: Laboratory Testing. Journal of Hydraulic Engineering, 130(5), 463–466.

Higgins, P. R. (2000). The characterisation of the hydrodynamic vortex separator using residence time distribution analysis. PhD Thesis. Liverpool John Moores University, UK.

Howard, A. K., Mohseni, O., Gulliver, J. S., and Stefan, H. G. (2012). Hydraulic analysis of suspended sediment removal from storm water in a standard sump. Journal of Hydraulic Engineering, 138(JUNE), 491–502.

Howie, P. E. (2011). Technology assessment protocol - ecology (TAPE) process overview, Washington. [online] https://fortress.wa.gov/ecy/publications/documents/1110010.pdf.

Huygens, M., & Tito, L. (1970). Sediment transport of mixtures of cohesive and non-cohesive materials in sewer conduits. WIT Transactions on Ecology and the Environment, 7.

Imbrium Systems Corporation (2004). NJCAT technology verification Stormceptor, [online] http://www.imbriumsystems.com/Portals/0/documents/sc/testing/NJCAT Verification Stormceptor STC Scour Addendum 2010.pdf.

Imbrium Systems Corporation (2007). NJCAT technology verification Stormceptor OSR, [online] http://www.imbriumsystems.com/Portals/0/documents/sc/testing/NJCAT Verification Stormceptor OSR 2007.pdf.

International Organization for Standardization (2002) Geotechnical investigation and testing – identification and classification of soil. ISO 14688-1.

Jain, A. K. (1976). Accurate explicit equation for friction factor. Journal of the Hydraulics Division, 102(5), 674-677.

Jain, R. K., & Kothyari, U. C. (2009). Cohesion influences on erosion and bed load transport. Water Resources Research, 45, W06410.

Kamphuis, J. W., and Hall, K. R. (1983). Cohesive material erosion by unidirectional current. Journal of Hydraulic Engineering, 109(1), 49-61.

Kirchheim N., Schaffner J., Oberlack M. (2005). Parameter study of a flush wave using numerical modelling. 10th International Conference on Urban Drainage, 10 ICUD, 21-26 August 2005, Copenhagen, Denmark.

Lager, J., Smith, W., and Tchobanoglous, G. (1977). Catch basin technology overview and assessment, California.

Lange, R. L., and Wichern, M. M. (2013). Sedimentation dynamics in combined sewer systems. Water Science and Technology, 68(4), 756-762.

Laplace, D., Bachoc, A., Sanchez, Y., & Dartus, D. (1992). Trunk sewer clogging development–description and solutions. Water Science and Technology, 25(8), 91-100.

Le Bouteiller, C., and Venditti, J. G. (2015). Sediment transport and shear stress partitioning in a vegetated flow. Water Resources Research, 51(4), 2901-2922.

Lee, H. Y., and Hsu, I. S. (1994). Investigation of saltating particle motions. Journal of Hydraulic Engineering, 120(7), 831-845.

Lee, H. Y., Chen, Y. H., You, J. Y., & Lin, Y. T. (2000). Investigations of continuous bed load saltating process. Journal of Hydraulic Engineering, 126(9), 691-700.

Li, L., Alvarez, I. C., & Aubertin, J. D. (2013). Self-weight consolidation of slurried deposition: tests and interpretation. International Journal of Geotechnical Engineering, 7(2), 205-213.

Luyckx, G., Vaes, G., and Berlamont, J. (2005). Solids separation efficiency of combined sewer overflows. Water Science and Technology, 51(2), 71–78.

Macke, E. (1982) About Sedimentation at Low Concentrations in Partly Filled Pipes, Mitteilungen, Leichtweiss-Institut fu¨r Wasserbau der Technischen Univ. Braunschweig, Heft 76.

Malesevic, L., Tang, J., and Van Doesburg, J. (2014). "Performance assessment of oil/grit separators for stormwater management in road applications" in CSCE Annual Conference. Halifax.

May, R. W. P., Ackers, J. C., Butler, D., and John, S. (1996). Development of design methodology for self-cleansing sewers. Water Science and Technology, 33(9), 195–205.

May, R. W. P., Brown, P. M., Hare, G. R., and Jones, K. D. (1989). Self-cleansing conditions for sewers carrying sediment. Hydraulic Research Station Report SR 221.

Mayerle, R. (1988). Sediment transport in rigid boundary channels. PhD thesis. University of Newcastle upon Tyne, England.

Miedema, S. A. (2012). Constructing the Shields Curve: Part B Sensitivity Analysis, Exposure and Protrusion Levels, Settling Velocity, Shear Stress and Friction Velocity, Erosion Flux and Laminar Main Flow. Journal of Dredging Engineering, 12(1), 50-92.

Nakagawa, H., & Tsujimoto, T. (1980). Sand bed instability due to bed load motion. Journal of the Hydraulics Division, 106(12), 2029-2051.

Nalluri, C. C., El-Zaemey, A. K., & Chan, H. L. (1997). Sediment transport over fixed deposited beds in sewers: an appraisal of existing models. Water Science and Technology, 36(8-9), 123-128.

NJDEP (2013). Laboratory protocol to assess total suspended solids removal by a filtration manufactured treatment device, New Jersey. [online] http://www.nj.gov/dep/stormwater/pdf/filter-protocol-1-25-13.pdf.

Novak, P. and Nalluri, C. (1975). Sediment transport in smooth fixed bed channels. J. Hydraul. Div.-Proc. A.S.C.E., 101, HY9, 1975.

Novak, P. and Nalluri, C. (1984). Incipient motion of sediment particles over fixed beds. Journal of Hydraulic Research 22(3), 181 - 197.

Ota, J. J. and Nalluri, C. (2003). Urban Storm Sewer Design: Approach in Consideration of Sediments. Journal of Hydraulic Engineering, 129(4), 291–297.

Ota, J. J., and Perrusquia, G. S. (2013). Particle velocity and sediment transport at the limit of deposition in sewers. Water Science and Technology, 67(5), 959-967.

Perrusquía, G. (1991). Bedload Transport in Storm Sewers. Stream Traction in Pipe Channels.

Perrusquía, G. and Nalluri, C. (1995). Modelling of bed-load transport in pipe channels. Proc. Int. Conf. On the transport and sedimentation of solid particles. Prague.

Pisano, W. C., O'Riordan, O. C., Ayotte, F. J., Barsanti, J. R., & Carr, D. L. (2003). Automated sewer and drainage flushing systems in Cambridge, Massachusetts. Journal of Hydraulic Engineering, 129(4), 260-266.

Pisano, W.C., Barsanti, J.R. and Ayotte, F.J. (2001). Sewer sediment flushing evaluation and design: a case study. Draft interim report under EPA Contract No. 68-C98-157. Urban Watershed Management Branch, Water Supply and Water Resources Division, National Risk Management Research Laboratory, U.S. Environmental Protection Agency, Edison, NJ., U.S., 2001.

Roesner, L. A., & Kidner, E. M. (2007). Improved protocol for classification and analysis of storm-borne solids. Proceedings of the Water Environment Federation, 2007(13), 5539-5566.

Safari, M. J. S., Aksoy, H., and Mohammadi, M. (2015). Incipient deposition of sediment in rigid boundary open channels. Environmental Fluid Mechanics, 1-16.

Schlutter, F., & Schaarup-Jensen, K. (1998). Sediment transport under dry weather conditions in a small sewer system. Water Science and Technology, 37(1), 155-162.

Selbig, W. R. and Bannerman, R. T. (2011). Characterizing the size distribution of particles in urban stormwater by use of fixed-point sample-collection methods, Madison.

Shields, A. (1936). Application of similarity principles and turbulence research to bed-load movement. Mitt. der Preuss. Versuchsamst. für Wasserbau und Schiffbau, Heft 26, Berlin, Deutschland.

Simons, D. B., & Senturk, F. (1977). Sediment Transport Technology, 807 pp. Water Resour. Publ., Highlands Ranch, Colo.

Sturm, T. W., Costanza, J., and Pennell, K. (2007). Hydraulic model study of oil/grit separator, Atlanta. [online] https://smartech.gatech.edu/bitstream/handle/1853/42345/98699_SkimproFinalReport.pdf.

SWAMP (2004). Performance assessment of two types of oil and grit separator, Toronto, Onatario. [online] http://www.sustainabletechnologies.ca/wp/wp-content/uploads/2013/03/OGS_entire-report.pdf.

Tang, Y., Zhu, D. Z., Rajaratnam, N., and Van Duin, B. (2016). Experimental study of hydraulics and sediment capture efficiency in catch basins. Water Science and Technology, 74(11), 2717–2726.

The City of Calgary (2011). Storm management and design manual, Calgary. [online] http://www.calgary.ca/PDA/pd/Documents/urban_development/bulletins/2011-stormwater-management-and-Design.pdf.

The City of Edmonton. (2007). Winter street sand recycling. Edmonton. (https://www.fcm.ca/Documents/presentations/2007/mission/Winter_Street_Sand_Recycling_EN.pdf).

Todeschini, S., Ciaponi, C., and Papiri, S. (2010). Laboratory Experiments and Numerical Modelling of the Scouring Effects of Flushing Waves on Sediment Beds. Engineering Applications of Computational Fluid Mechanics, 4(3), 365–373.

Tränckner, J., Bönisch, G., Gebhard, V. R., Dirckx, G., and Krebs, P. (2008). Model-based assessment of sediment sources in sewers. Urban Water Journal, 5(4), 277–286.

Van Rijn, L. C. (1984). Sediment pick-up functions. Journal of Hydraulic Engineering, 110(10), 1494-1502.

Vanoni, V. A., and Brooks, N. H. (1957). Laboratory studies of the roughness and suspended load of alluvial streams.

Verbanck, M. (1992). Field investigations on sediment occurrence and behavior in Brussels combined sewers. Water Science and Technology, 25(8), 71-82.

Verbanck, M. A. (2000). Computing near-bed solids transport in sewers and similar sediment-carrying open-channel flows. Urban Water -Amsterdam-, 2(4), 277-284.

Verstraeten, G. and Poesen, J. (2000). Estimating trap efficiency of small reservoirs and ponds: methods and implications for the assessment of sediment yield. Progress in Physical Geography, 24(2), 19–51.

Wilcock, P. R. (1996). Estimating local bed shear stress from velocity observations. Water Resources Research, 32(11), 3361-3366.

Wilson, M. A., Mohseni, O., Gulliver, J. S., Hozalski, R. M., and Stefan, H. G. (2009). Assessment of Hydrodynamic Separators for Storm-Water Treatment. Journal of Hydraulic Engineering, 135(5), 383–392.

Wu, P., Hirshfield, F., & Sui, J. (2015). Armour layer analysis of local scour around bridge abutments under ice cover. River research and applications, 31(6), 736-746.

Xu, Z., Wu, J., Li, H., Liu, Z., Chen, K., Chen, H., & Xiong, L. (2017). Different erosion characteristics of sediment deposits in combined and storm sewers. Water Science and Technology, 75(8), 1922-1931.

Yalkowsky, S. H., and Bolton, S. (1990). Particle size and content uniformity. Pharmaceutical research, 7(9), 962-966.

Yang, C. T. (1996). Sediment transport: theory and practice. McGraw-Hill, Singapore.

Yang, H., Zhu, D. Z., and Li, L. (2018). Numerical modeling on sediment capture in catch basins. Water Science and Technology, wst2018009.

Appendix A: Field Investigation on Sediment Depositions in Catch Basins and a Storm Trunk Sewer in Walden, Calgary

A1. Introduction

In recently years, sediment deposition in sewer systems has received significant attention due to two major issues including pipe blockage and environmental problems. Sediment deposition in sewers reduces flow area and can cause pipe blockage, consequently leading to surcharge flows and urban floods. Under certain hydraulic conditions, sediment in sewers can form deposition layer, for which 10% of sediment bed can cause up to 30% flow capacity losses. The research about deposition in real storm sewers is limited. This fieldwork provided valuable information regarding real sediment characteristics and the deposition patterns.

Staff of City of Calgary Water Services, Mr. Mohd Gazi, Mr. Dwayne Giesbrecht, and U of A team participated in this fieldwork on August 22, 2019. The fieldwork could be divided into two parts: sediment sampling in catch basins and deposition profiling in a submerged trunk sewer in Walden community. The Walden community is a newly developed area in southern Calgary and the storm trunk sewer is connecting to a storm water pond in the Walden area. Drawings and related information were collected for catch basins, the storm trunk sewer, and the storm water pond. Six sediment samples were collected in six catch basins, which could cover the whole community. The detailed profile of the real deposition in the storm trunk sewer was obtained. Subsequently, six samples were collected from the real deposition. Pictures and videos were recorded during the whole field sampling.

A2. Sediment deposition in catch basins

A2.1. Sampling locations

The Walden community is newly developed with continuously ongoing construction activities. The clay material can be easily found on construction sites. Clay can coagulate between the non-cohesive and cohesive materials during dry weather conditions (with certain level of base flow). When the clay content is over 5%, the deposition layer can be cohesive, which is hard to be flushed away by the next mild storm and probably becomes permanent deposition thus decreasing sewer capacity. Therefore, it is important to investigate the clay content in the catch basins since it could reflect the feature of the catchment surface. Figure A1 shows the locations of catch basins and six catch basins (marked in orange color) are chosen to conduct the sediment sampling program.

A2.2. Sampling method and procedures

Note that the sediment depth data were collected in six catch basins. The SST bottom dredge sampler (*No. 445.10, AMS*) was used to collect the sediment samples in catch basins. The sediment sample was collected at different depths. A vacuum truck was used to remove the deposition layer which had already been sampled. Each sample contained equal volume of sediment at different locations, which could represent the characteristics of sediment at different depth.

A2.3. Observations

Five catch basins contained significant amount of deposition depth (varied from 42 to 102 cm). The deposition depth in No. 2 catch basin was relatively small (13 cm). Sediment

contained different sizes from clay to gravels, but the majority of it was clay material due to the construction activities. There was limited level of standing water above the sediment bed (less than 2 cm). Figures A2 and A3 show the observations for No. 2 and No. 5 catch basins.

A2.4. Sediment components for six catch basins

Figure 1-3 shows the components of sediment samples in six catch basins. The clay content in #1 catch basin was the highest (29%) one since it was close to the activated construction site. The clay content in #4 and #6 was around 5%, which was close to lawn areas. The sand content was relatively high in all locations, which meant the main component of deposition was sand which was relate to the winter street sand.

A3. Sediment deposition in a storm trunk sewer

A3.1. Storm trunk sewer information

The storm trunk sewer is a submerged pipe connecting to a storm water pond. It is 30 meter in length and 1.05 meter in diameter. The pipe slope is mild (0.18%). It is a concrete pipe and the upstream manhole is without sump.

A3.2. Profiling and sampling method

The storm trunk sewer was dry (only 10 cm standing water above the deposition). Therefore, the profile of deposition was obtained by manually measurement along the flow direction. Deposition depths were recorded every 1.5 m in length. After the profile measurement, five sediment samples were collected from the deposition layer (from S1 to S5).

A3.3. Deposition profile and observations

Figure 5-10 shows the deposition profile along the longitudinal direction. The sediment characteristics were different along the pipe. At the first 10 meters, big gravels occupied around 50%. The sediment size became smaller along the flow direction. At the downstream end of the deposition, the majority of the deposition was sand or clay material. The deposition height decreased from 46 cm to zero along the flow direction.

A3.4. Particle size distributions

Figure 5-11 shows the particle sizes from S1 (the upstream end of the pipe) to S5 (the downstream end of the deposition). The clay (<0.002 mm) content increased significantly from S1 to S5 (10% to around 48%). The particle size decreased along the flow direction (from S1 to S5). Over 52% of sediment was gravel in S1, meanwhile sediment was mainly silt and clay mixture in S5.

A4. Summary

In this field trip, we collected six samples from six catch basins which covered the entire Walden community area. From those samples, the general information about the sediment components were obtained. Moreover, the detailed deposition profile along the 30-meter-long pipe was obtained, which provided the real picture of the deposition in the trunk sewer. In addition, six samples along the flow direction in the trunk were collected. The trunk sampling was challenging but extremely valuable data were obtained. The laboratory analyses about sediment components were conducted.

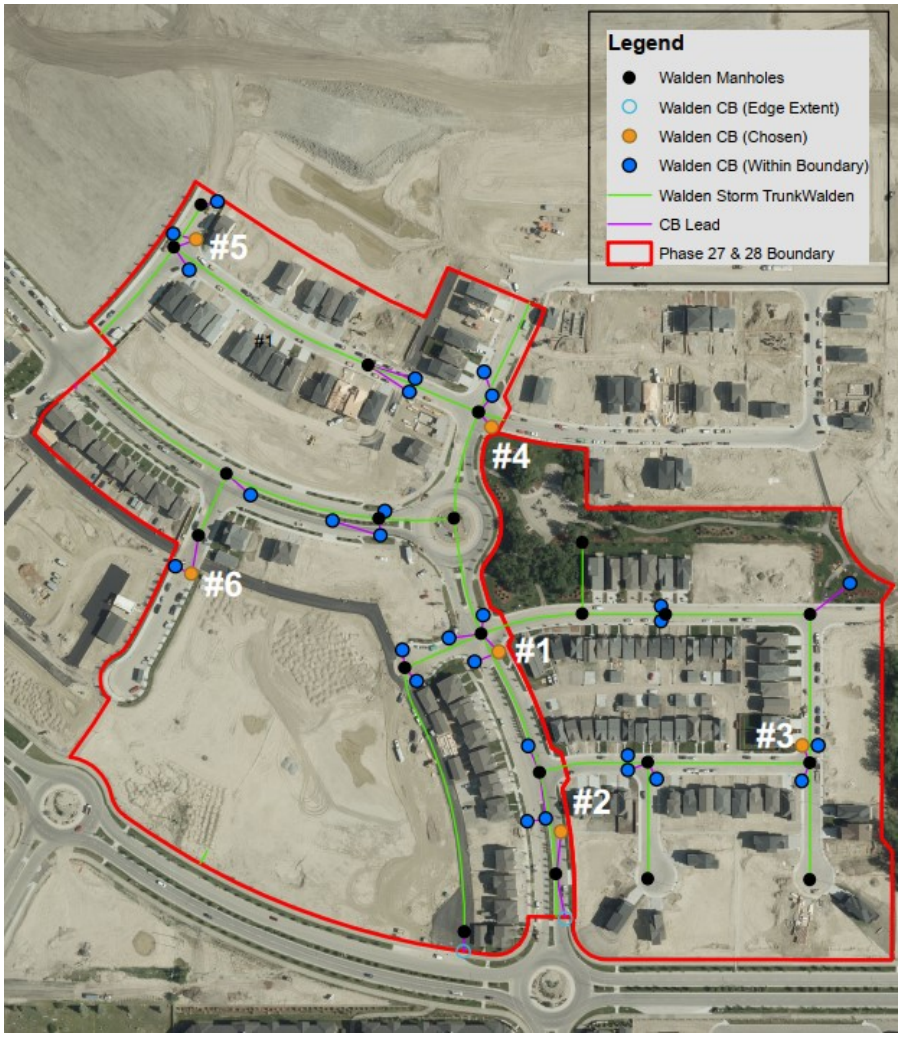

Figure A1. Catchment area and six sampled catch basins (#1 - #6)

Figure A2. No. 2 catch basin observation

Figure A3. No. 5 catch basin observation

Appendix B: Erosion patterns

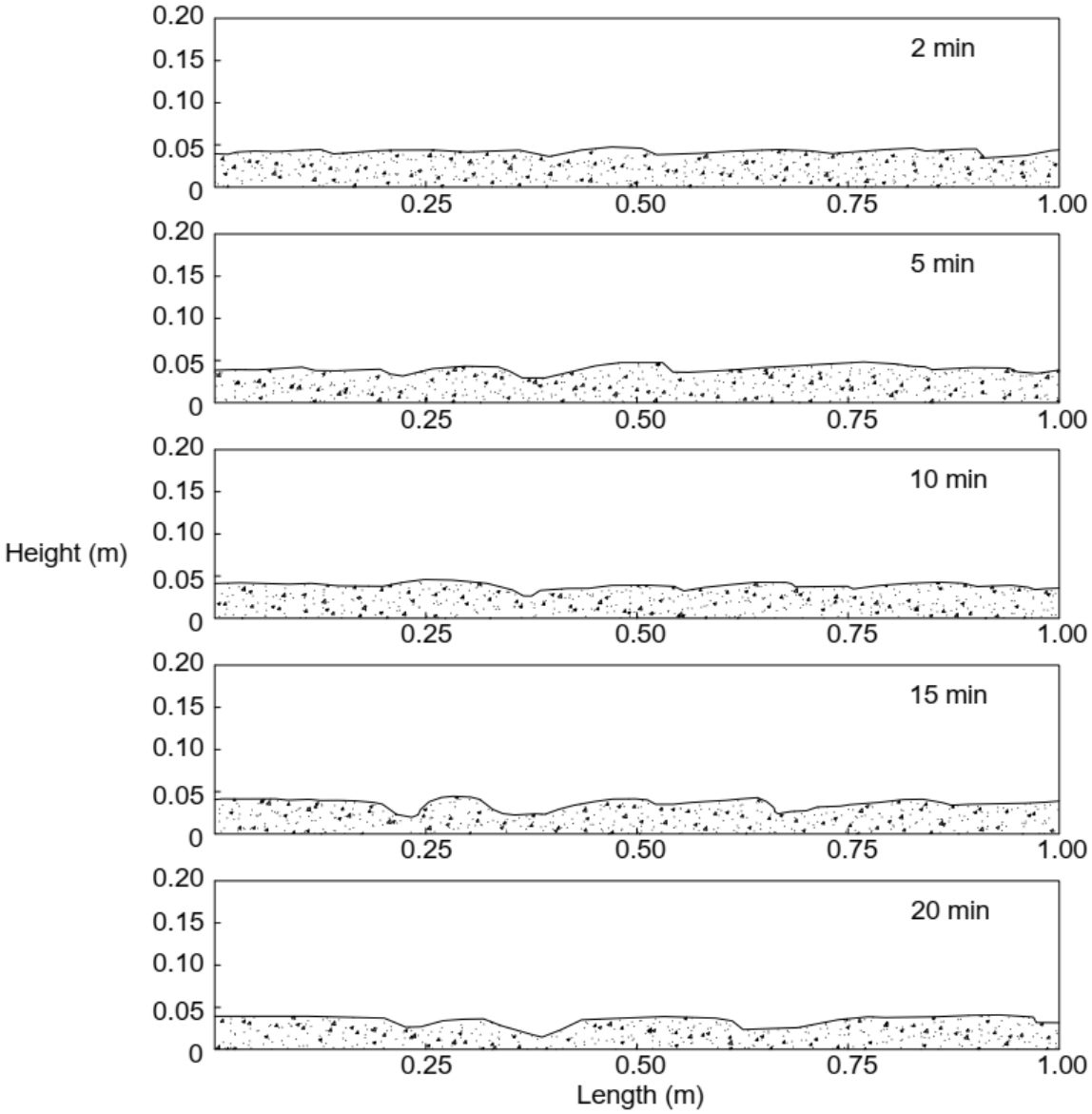

Figure B1. Exp. A-0 at 4.0 L/s

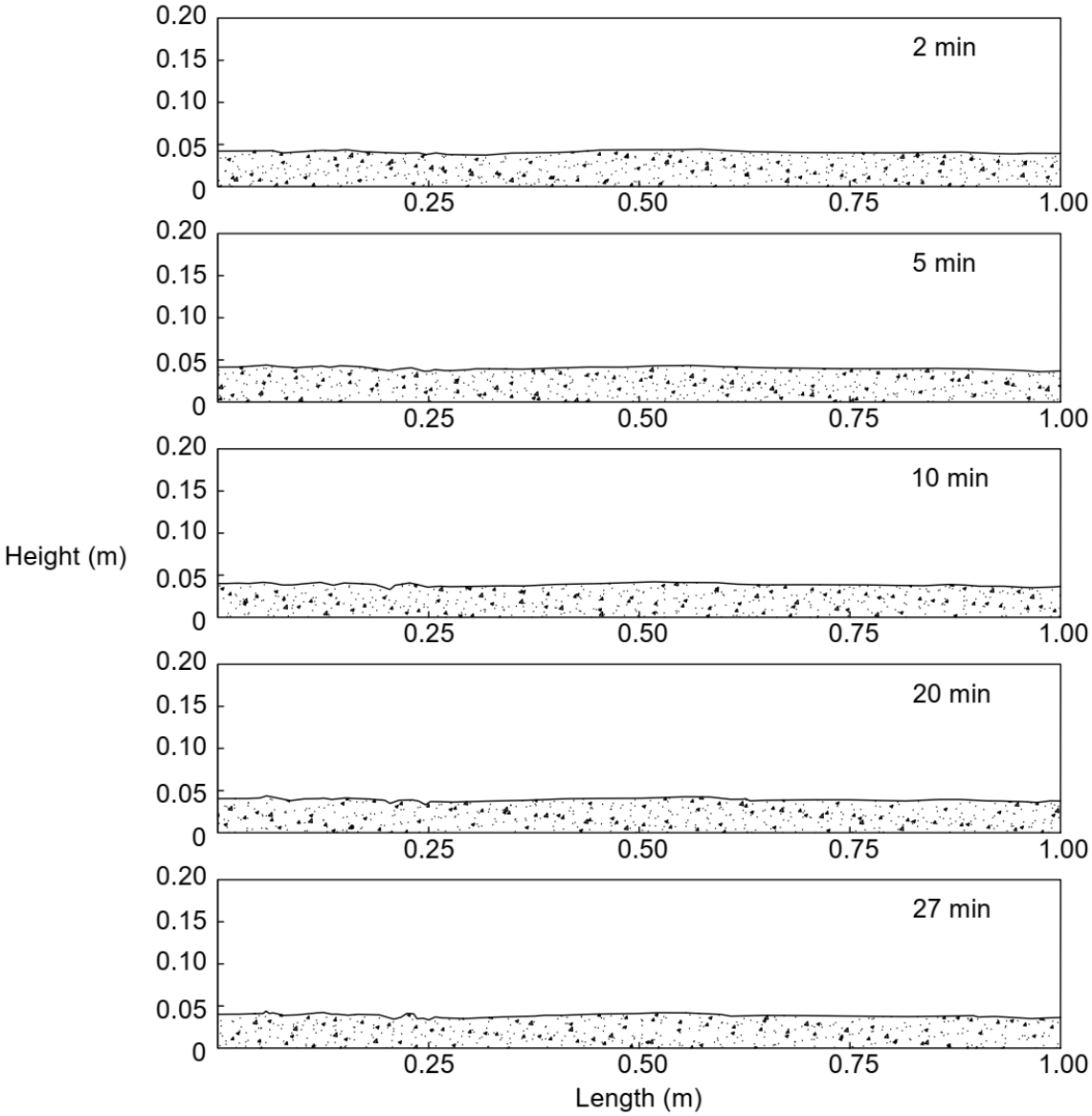

Figure B2. Exp. A-10 at 2.5 L/s

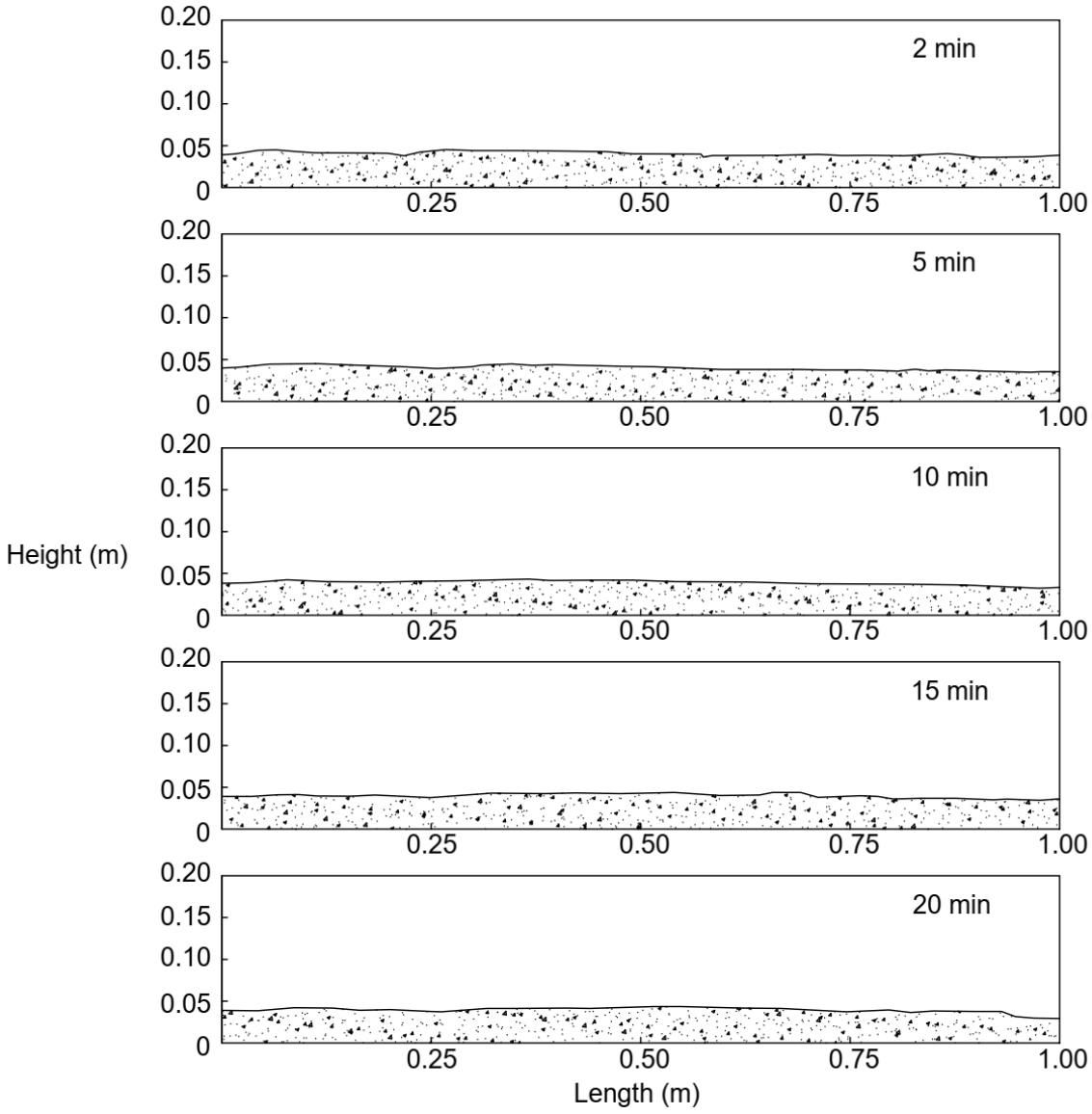

Figure B3. Exp. A-10 at 4 L/s

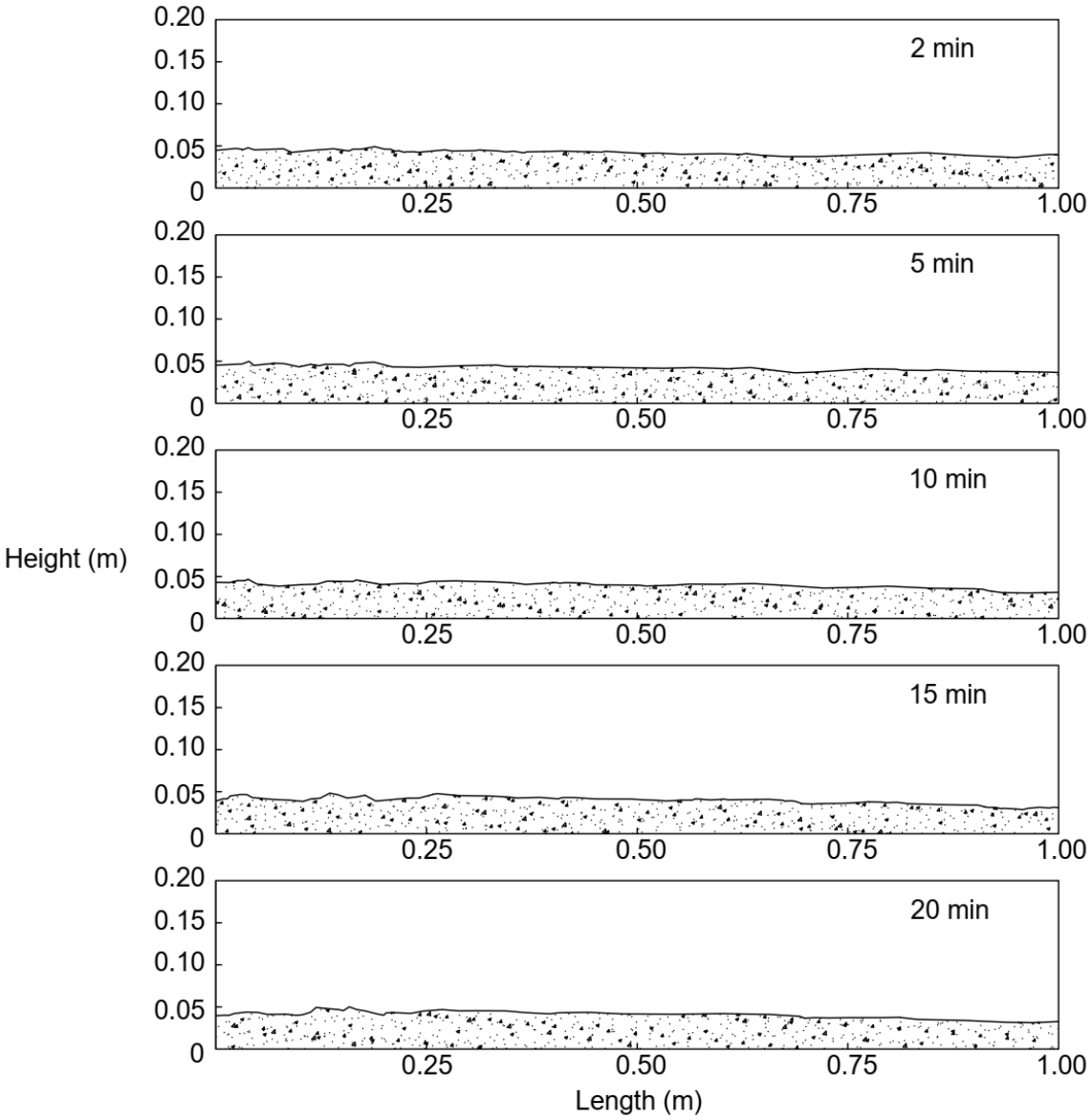

Figure B4. Exp. A-20 at 2.5 L/s

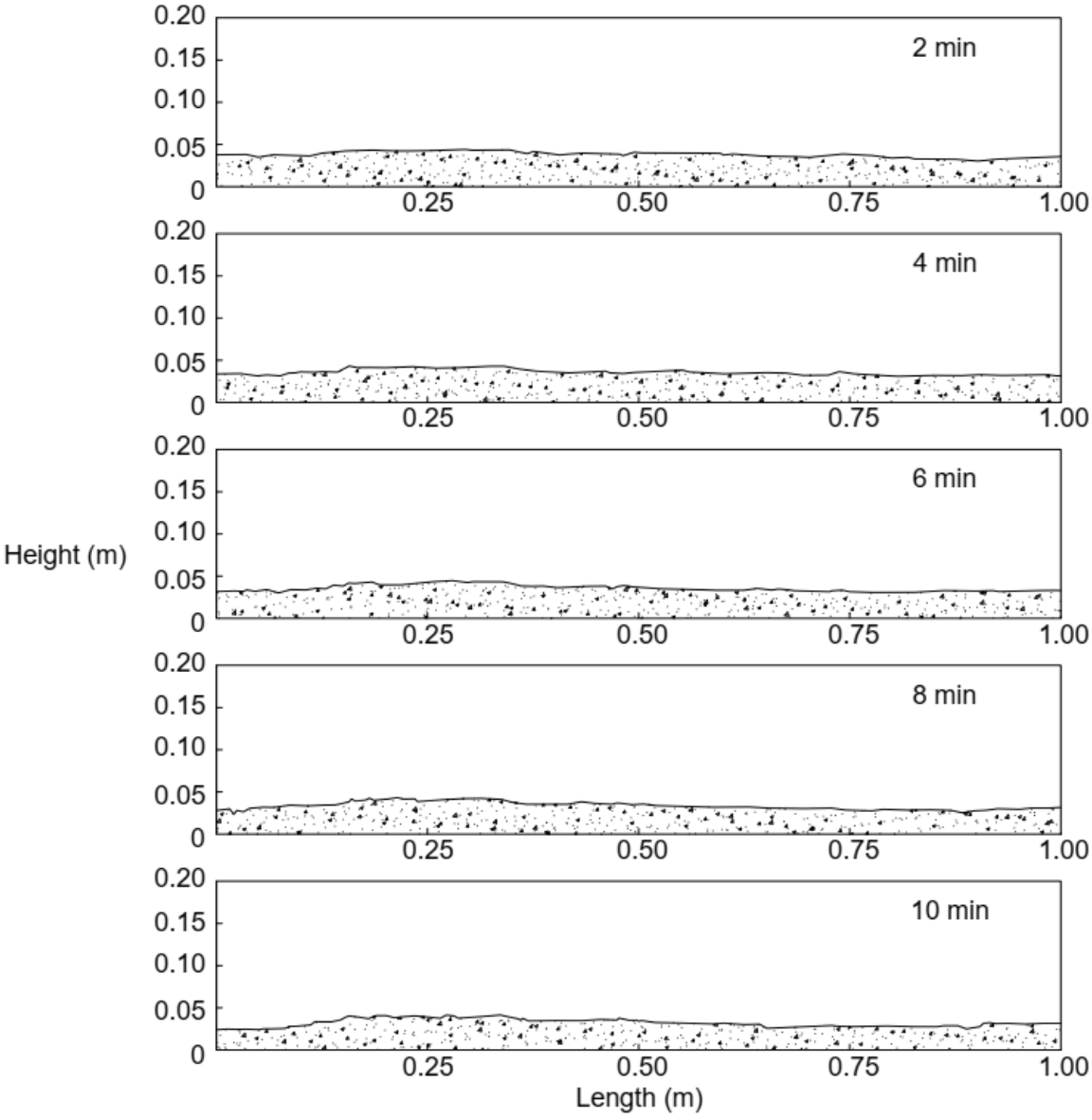

Figure B5. Exp. A-20 at 4 L/s

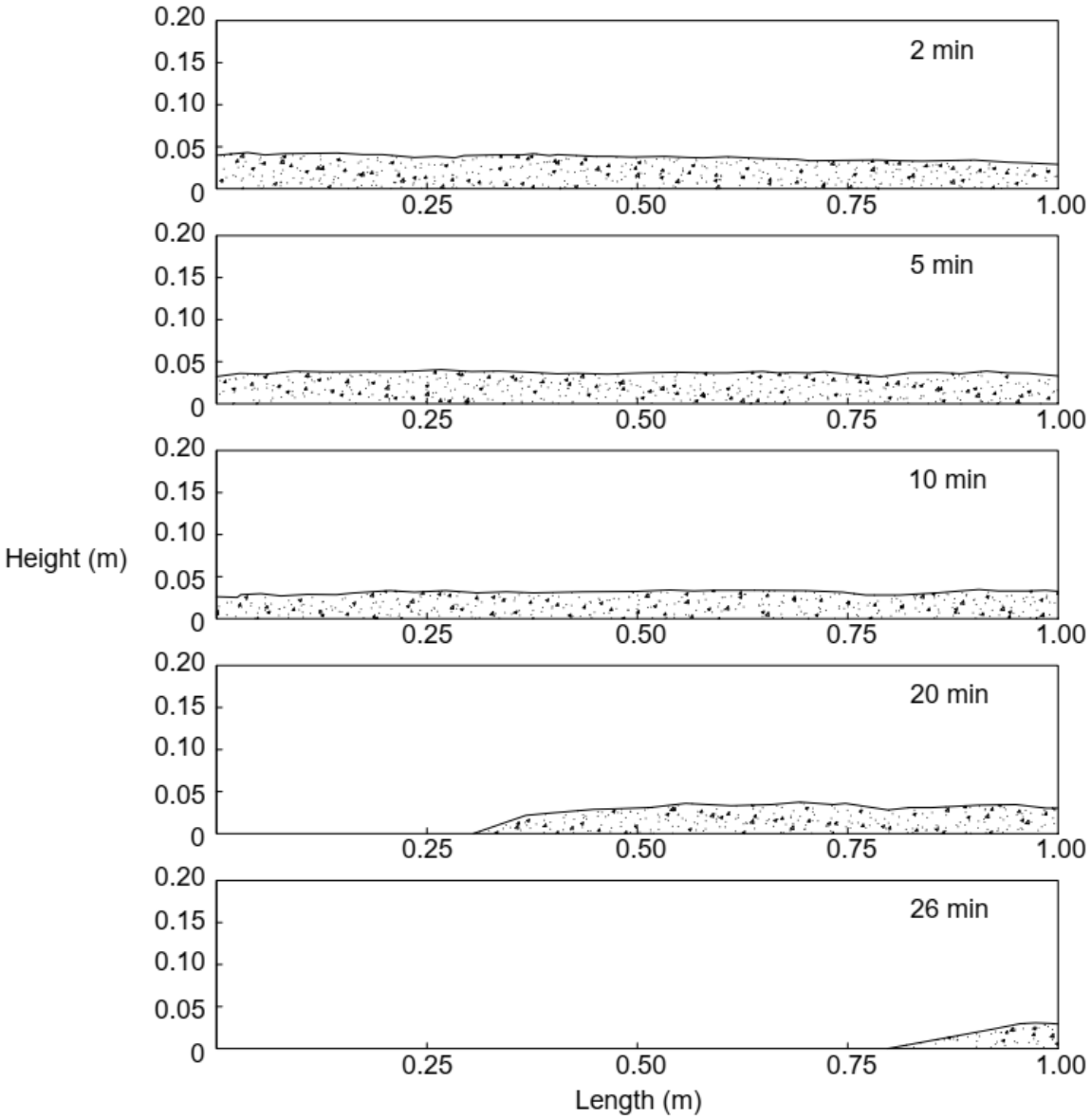

Figure B6. Exp. B-0 at 9 L/s

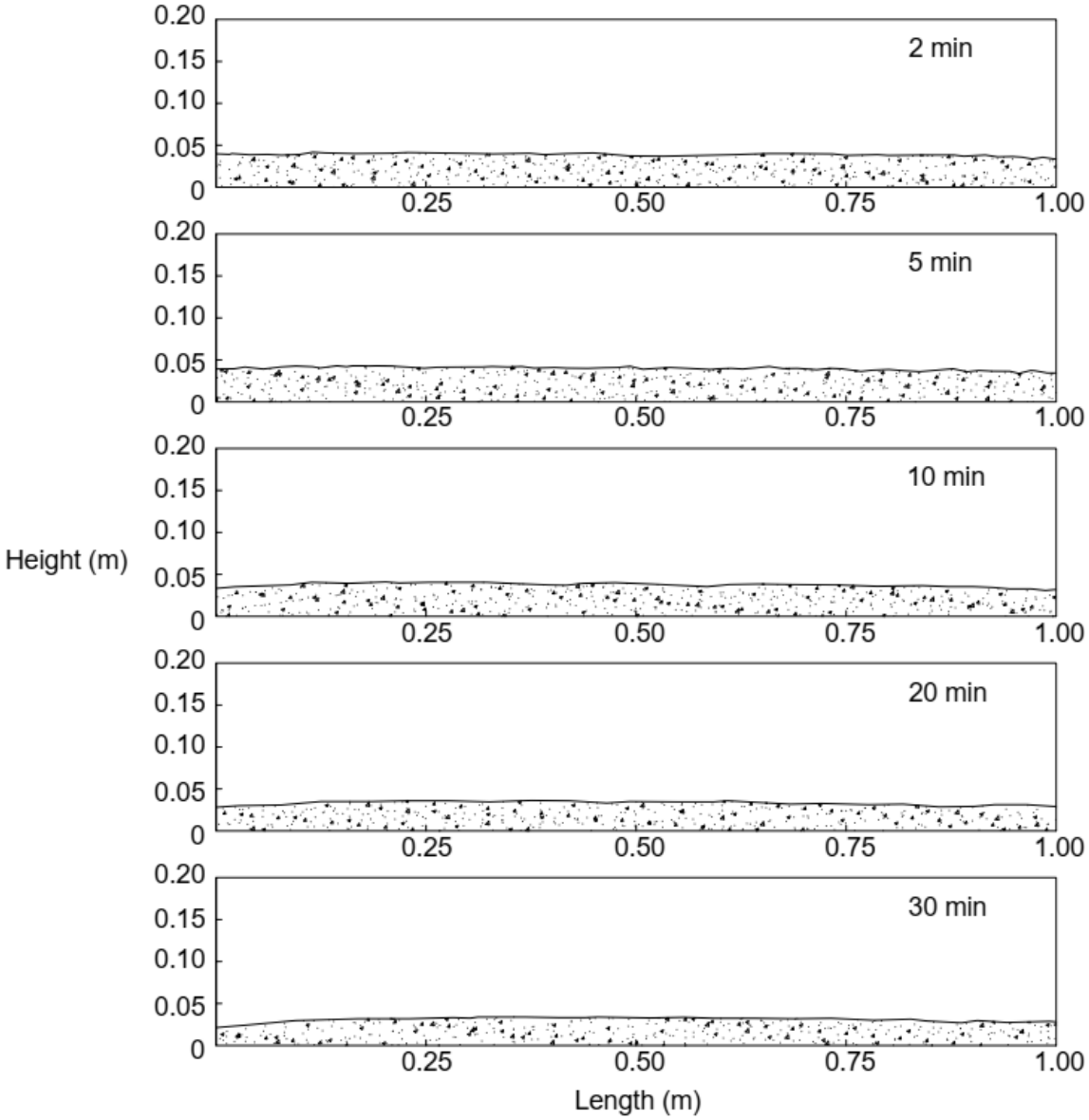

Figure B7. Exp. B-10 at 9 L/s

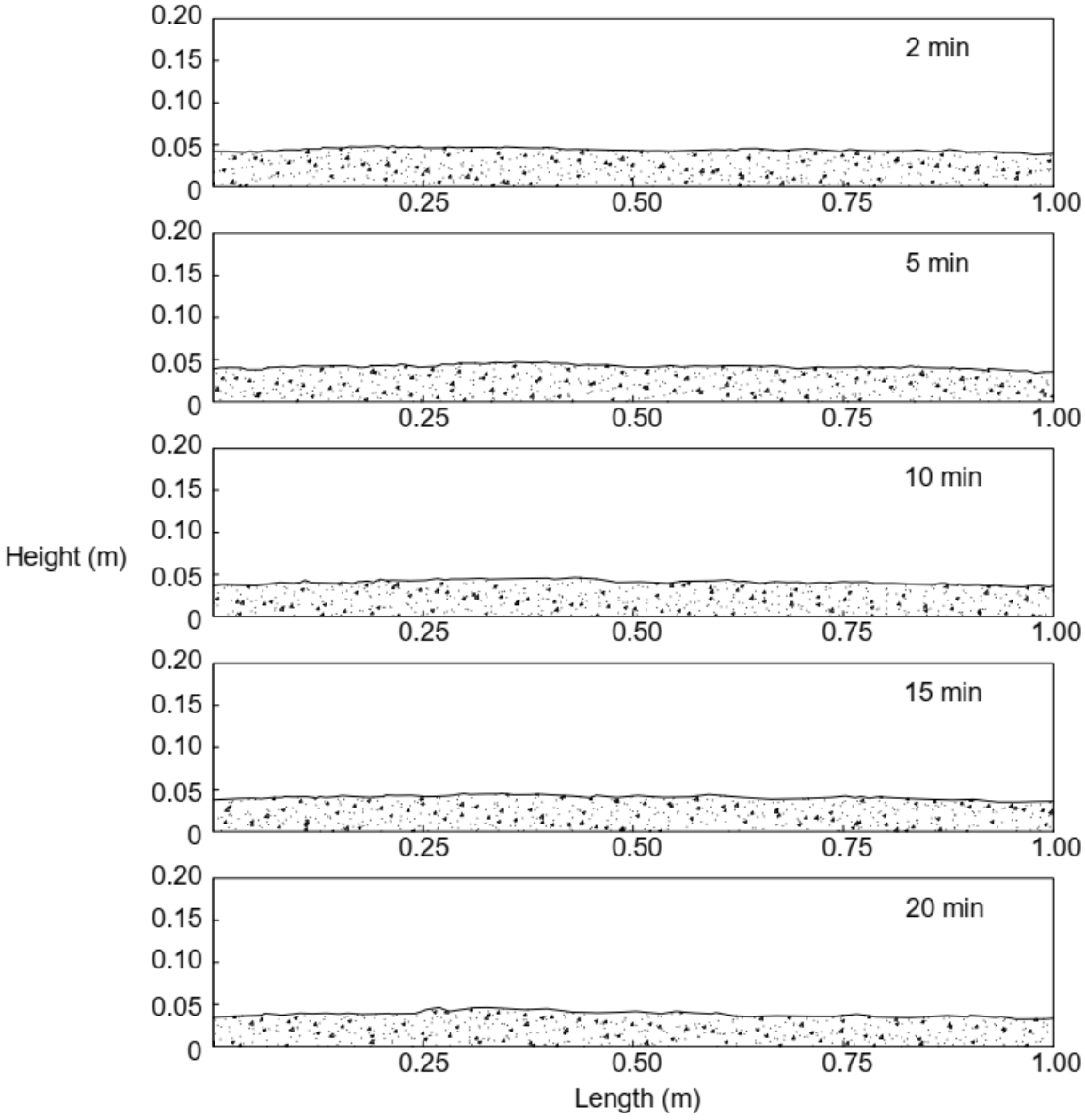

Figure B8. Exp. B-10 at 17 L/s

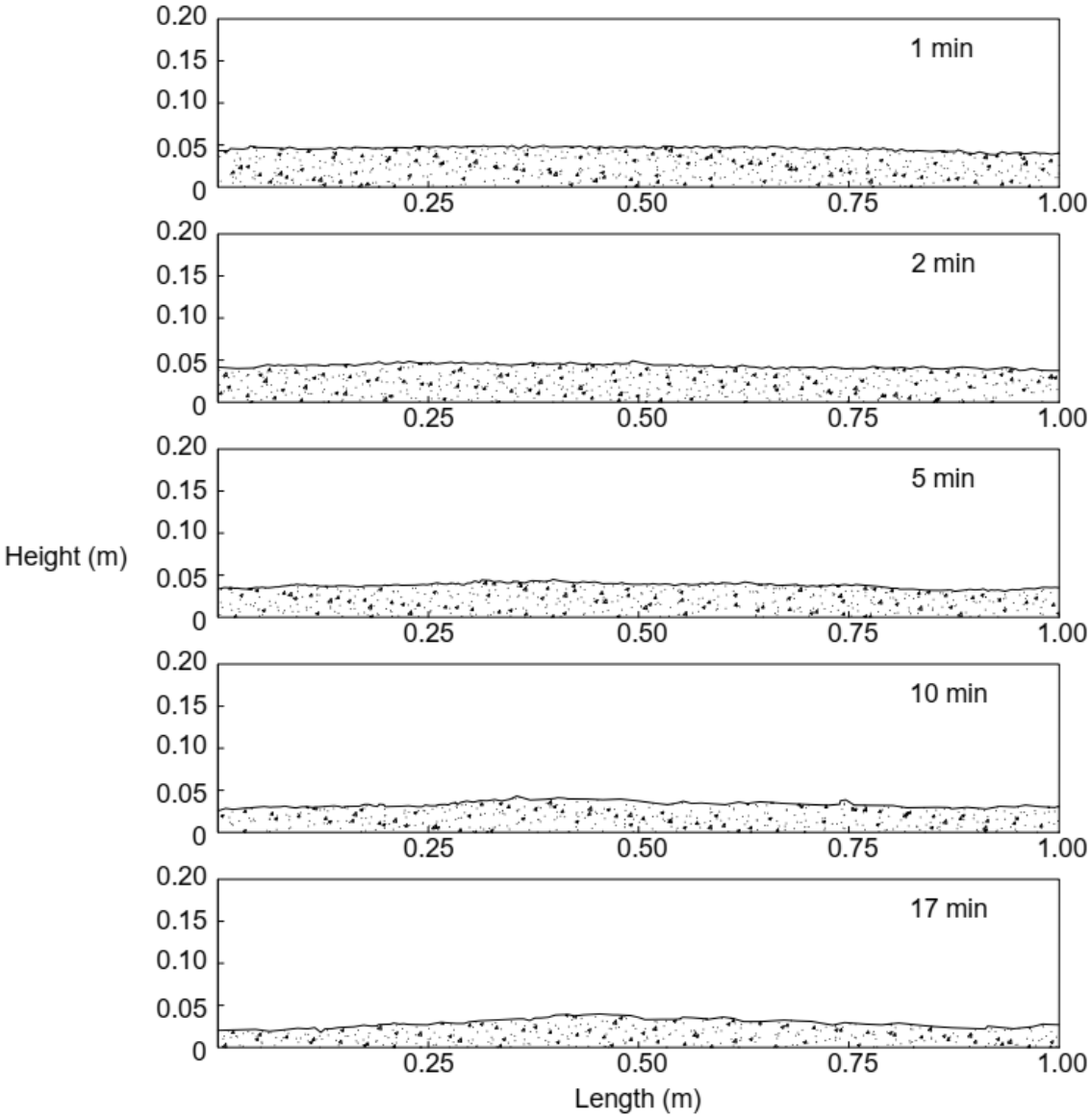

Figure B9. Exp. B-20 at 9.5 L/s

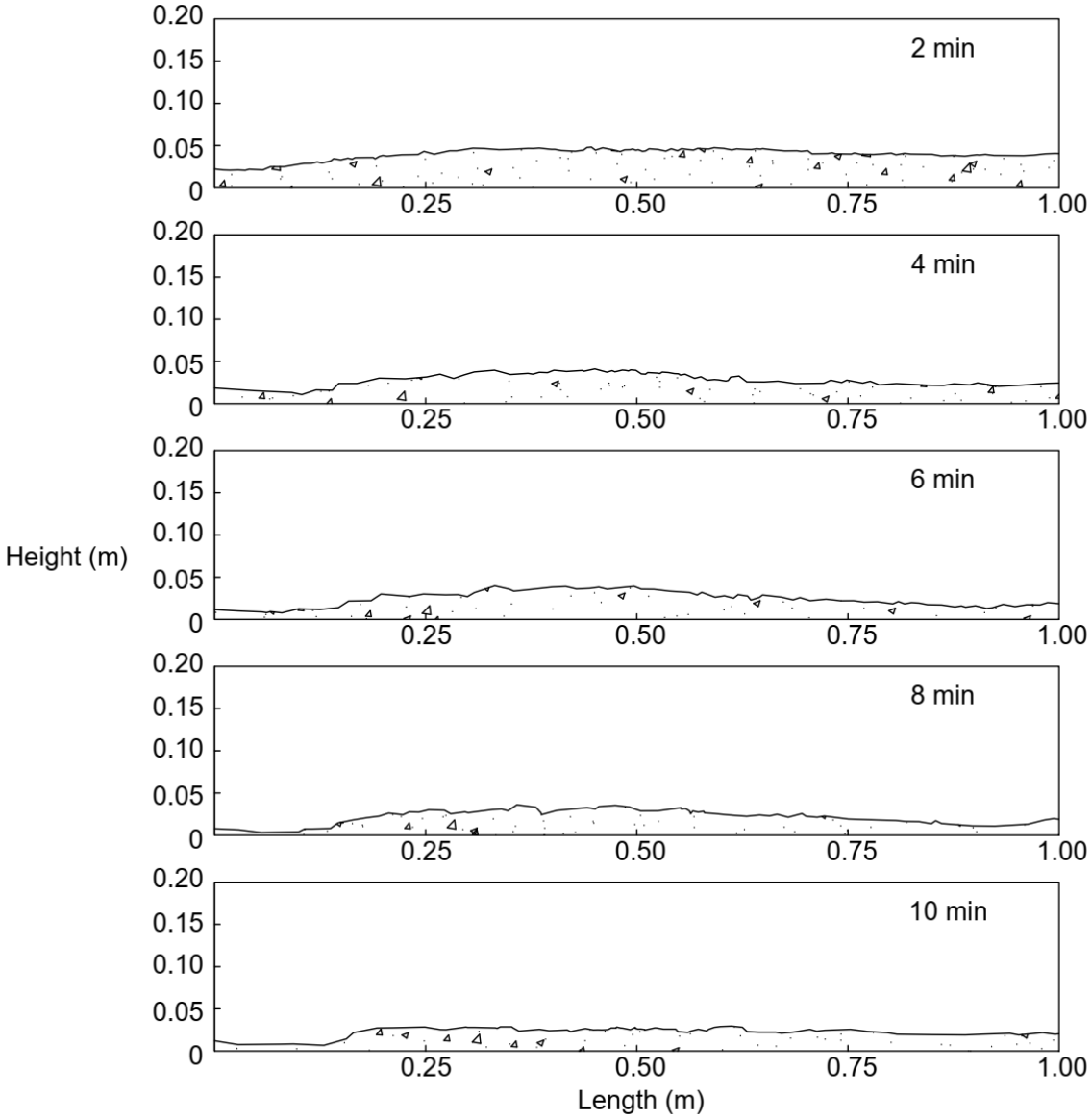

Figure B10. Exp. B-20 at 26 L/s